

A TUNABLE VACUUM ULTRAVIOLET XENON LASER

by

DAVID ROGER HULL B.Sc.

being a thesis submitted to the University
of London for the degree of Doctor of Philosophy

Department of Physics
Imperial College of Science and Technology
University of London

December 1975

ABSTRACT

The molecular fluorescence from high pressure (>1 ktorr) xenon, excited by a 2.5 ns pulse of 0.5 MeV electrons has been investigated and a pressure dependent decay rate was observed.

The design and construction of a coaxial electron beam diode, devised to achieve efficient pumping of high pressure gas lasers is described. Using this diode, laser action from high pressure xenon was observed at a wavelength of 172 nm. Output energies of 12 millijoules were recorded, giving peak powers of the order of 4 MW. The conversion efficiency from electron beam energy to laser energy was 0.3%.

Using a prism as the dispersive element, the laser spectrum narrowed from 1.3 to 0.13 nm and the laser was continuously tunable from 169.2 to 176.5 nm. The peak energy obtained was 3.6 millijoules.

CONTENTS

	Page
Abstract	(i)
List of Plates	(iv)
Chapter 1 Introduction	1
Chapter 2 The Structure and Formation of the Xenon Molecule	4
2.1 The Structure of the Xenon Molecule	4
2.2 The Deposition of Electron Energy	8
2.3 Predictions of the Fluorescence Efficiency	10
2.4 The Formation Processes of Excited Xenon	10
Chapter 3 Experimental Studies of Fluorescence	17
3.1 The Electron Beam Generator	17
3.2 The Experimental Set Up for Fluorescence Measurements	19
3.3 Temporal Studies of Fluorescence	23
3.4 Theoretical Models for Fluorescence from Xenon	30
3.5 Spectral Studies of Fluorescence	34
3.6 The Visible Emissions from Xenon	40
3.7 Measurement of Fluorescence Efficiency	41
Chapter 4 The Design of Coaxial Electron Beam Diodes	45
4.1 Electron Beam Drifting	45
4.2 Calculation of the Coaxial Diode Parameters	53
4.3 Construction of the Diode	58
4.4 Modification of the Diode	63
4.5 Extension of the Blumlein Circuit	66
Chapter 5 The Characteristics of the Xenon Laser	71
5.1 The Coaxial Xenon Laser (Mark 1)	71
5.2 Measurement of the Gain	78

	Page
5.3 The Effects of Gas Heating	84
5.3.1 The Addition of Other Noble Gases to Xenon	89
5.3.2 The Gas Circulating System	94
5.4 The Coaxial Xenon Laser (Mark 2)	96
5.5 Optimisation of the Laser Output	98
5.6 Saturation of the Laser	102
 Chapter 6 Tuning of the Xenon Laser	 106
6.1 The Selection of a Tuning Element	107
6.1.1 Diffraction Gratings	107
6.1.2 Fabry-Perot Etalons	109
6.1.3 Prisms	110
6.2 The Design of a Mount for the Tuning Element	112
6.3 The Output obtained from the Tuned Laser	117
6.4 A Discussion of the Tuning Results	122
 Chapter 7 Conclusions	 126
 Acknowledgements	 133
 References	 134
 Publications	

LIST OF PLATES

PLATES

- 1 Temporal Dependence of the Xenon Fluorescence
- 2 The Xenon Fluorescence Spectrum
- 3 Temporal Dependence of Visible and Vacuum Ultraviolet Radiation at 0.76 ktorr
- 4 Mark 1 Diode
- 5 Mark 1 Diode Illustrating the Radial Arrangement of the Cathode Spikes
- 6 Simulation of Impedance Matching of the Mark 2 Diode
- 7 Charging Voltage of the Blumlein
- 8 Faraday Cup Traces of the Electron Beam Output
- 9 Spectrum of the Laser Output
- 10 Temporal Dependence of the Laser Output
- 11 Output Spectra of the Tuned Laser
- 12 Temporal Dependence of the Tuned Laser

CHAPTER ONE

INTRODUCTION

An investigation has been made of the processes involved in the interaction of relativistic electrons with xenon, and an efficient tunable xenon laser, using a small commercially available electron gun has been developed.

It was recognised by Houtermans ⁽¹⁾ in 1960, that transitions from bound molecular states to loosely bound states could be used to obtain laser action. Specifically, he suggested the use of the alkaline earths, the triplet state of hydrogen, the alkali molecules and the noble gases. A transition from a bound to a dissociative state in diatomic molecules offers two attractive features with regard to laser action. Firstly, if the final state potential is steeply repulsive then this lower state will remain virtually unpopulated as the kinetic energy of the atomic fragments formed in the dissociation may be much greater than the thermal kinetic energy of the unexcited atoms. Secondly a broad band emission results, due to the repulsive final state and this may enable the laser to be tuned over a wide spectral range.

The idea of using xenon to achieve vacuum ultraviolet (VUV) laser action was put forward by Basov ⁽²⁾ in 1966. In xenon, the ground molecular state potential is repulsive (except for a weak van der Waal's attractive force) due to the 'closed shell' structure of the ground state atoms ⁽³⁾. If, however, one atom formed in an excited state collides with a ground state atom, a stable bound molecule may result. Transitions from such bound states to the ground state produce a broad continuous emission spectrum in the wavelength region of 170 nm ⁽⁴⁾. The structure and formation of the xenon molecule are discussed in

Chapter 2. An understanding of some of the processes involved in the interaction of high energy electrons with xenon was gained by studying the fluorescence from high pressure xenon, and these results are reported in Chapter 3.

Some of the difficulties in extending lasers to short wavelengths were discussed by Schawlow and Townes ⁽⁵⁾. One fundamental difficulty they pointed out, was that the spontaneous emitted power increased rapidly with increasing frequency, ν , (decreasing wavelength) with at least a ν^4 dependence. Also, with xenon, the broad band emission spectrum results in a decreased intensity per unit frequency, so that to obtain a high gain, a large inversion is required. Thus a high power pumping source, capable of exciting transitions with energies greater than about 10 eV is required. Basov et al. ⁽⁶⁾ proposed the use of high current beams of relativistic electrons, and using a beam of 1 MeV electrons, with a current density of about 300 A.cm^{-2} in a pulse of 10^{-8} s they obtained the first evidence of laser action in liquid xenon, at 176 nm.

Extensive research effort has been directed recently towards the study of electron beam excited dissociative lasers, particularly with the noble gases. These elements are used in the gaseous state in preference to the liquid state mainly because they exist in the gaseous state at room temperature and also because of the improved optical homogeneity over the liquid state. Electron beams with energies in the range 0.5 to 2 MeV and with total beam energies from less than 10 J to many kilojoules delivered in a pulse of duration of 3 to 100 ns, have been used as excitation sources, most of the work having been carried out with high energy long pulse beams. These have enabled laser action in gaseous xenon ⁽⁷⁾ at 172 nm, krypton ⁽⁸⁾ at 146 nm, argon ⁽⁹⁾ at 126 nm, and in noble gas mixtures ⁽⁸⁾ ⁽¹⁰⁾ to be obtained.

In the work described in this thesis, electron beam energies of the order of 20 joules in pulses of 5 ns were used with electron energies of 0.5 McV. In order to utilize the energy efficiently a coaxial electron beam diode was designed and constructed, as described in Chapter 4. This new pumping arrangement was used instead of the transverse geometry used in other laboratories and enabled a compact tunable xenon laser to be developed. The parameters of such a laser are outlined in Chapters 5 and 6. Optimum pressures and cavity parameters were obtained experimentally and an estimate was made of the peak gain. The effects of gas heating and saturation on limiting the laser output are discussed and methods of reducing the gas temperature were investigated. A prism was inserted in the cavity to act as a dispersive element and the laser energy was extracted over a narrower bandwidth than in the untuned case, and tuning over part of the broad fluorescence spectrum was observed.

In the final chapter, the experimental results which were obtained are discussed and possible uses for the xenon laser are suggested. The feasibility of obtaining higher energies and powers using xenon amplifiers is examined briefly.

CHAPTER TWO

THE STRUCTURE AND FORMATION OF THE XENON MOLECULE

In the search for new light sources for absorption spectroscopy in the VUV (vacuum ultraviolet), many studies have been made of the emissions from the noble gases, and these have contributed to a greater understanding of the structures of the noble gases. Emissions have been observed in xenon and all the lighter noble gases ⁽¹¹⁾ ⁽¹²⁾ and together these provide continuous sources of radiation covering almost the entire range from 60 to 200 nm ⁽¹³⁾.

In this chapter, the form of the fluorescence from xenon is outlined and the structure of the xenon molecule is discussed briefly. The deposition of high energy electrons (energies of the order of MeV) in high pressure xenon (greater than 1 ktorr) is considered, and an estimate made of the distribution of energy between the excited states and the ions. Finally various mechanisms that have been proposed for the formation of excited xenon molecules are examined. Although the following discussion relates specifically to xenon, many of the results are applicable to the other noble gases.

2.1 THE STRUCTURE OF THE XENON MOLECULE

The fluorescence spectrum of xenon is dependent on gas pressure. At pressures of less than 1 torr the two xenon resonance lines at 129.6 and 147.0 nm are observed ⁽¹⁴⁾. When the pressure is increased to a few torr the 129.6 nm line broadens on both sides by less than 1 nm while the 147.0 nm line broadens considerably towards longer wavelengths but only a little towards shorter wavelengths. The broad continuum consists of two parts, known as the first and second continua. The first continuum starts at the 147.0 nm resonance line and falls off gradually

in intensity towards the red, it is dominant at pressures of less than about 50 torr. At higher pressures, the intensity of the second continuum increases, with a broad symmetrical maximum at about 165 nm, with only this second continuum being observed ⁽¹⁵⁾ at pressures of greater than a few hundred torr.

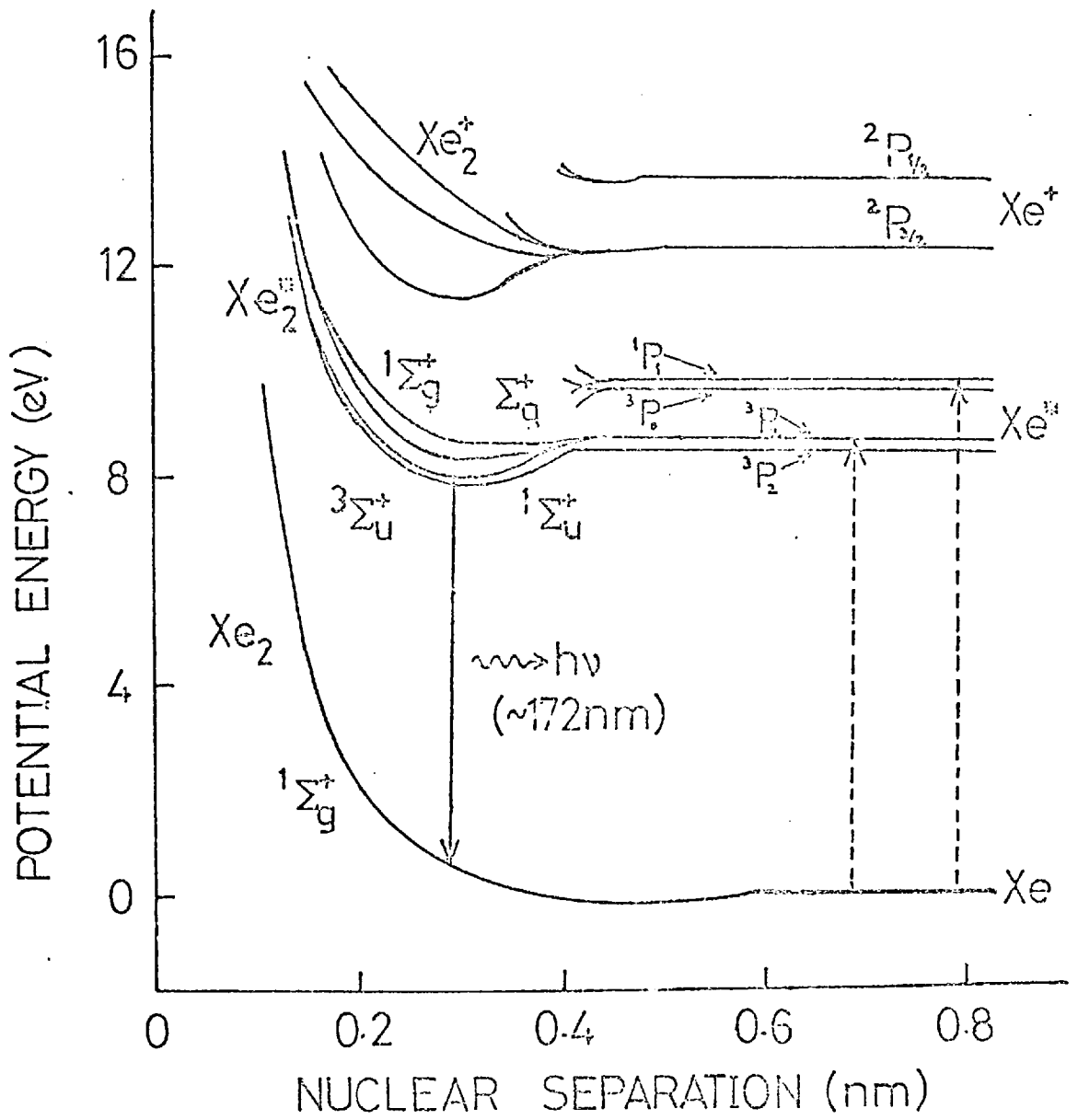
The main features of the radiation may be explained by reference to the analysis of Mulliken ⁽³⁾. Fig 1 shows some of the relevant states of xenon. The ground state of the xenon molecule is repulsive, except for a weak van der Waal's force, as the ground state atoms are characterized by the closed shell structure $(\dots 5s^2 5p^6) ^1S_0$. The excitation of one of the $5p^6$ electrons in the atoms to the first s orbital results in the configuration $\dots 5s^2 5p^5 6s$ which gives rise to four states: 3P_1 , 3P_2 , 1P_1 , and 3P_0 . L-S coupling notation is used, although in xenon the coupling is J-j with the spin-orbit interaction of the five 'p' electrons very large compared with the spin-spin interaction between 6s and $5p^5$. This strong spin-orbit interaction is illustrated by the large separation of the $^2P_{1/2}$ and $^2P_{3/2}$ levels, shown in fig 1 where the energy difference is approximately 1.25 eV.

The 3P_1 and 1P_1 states are the resonance levels which radiate to the 1S_0 ground state with lifetimes of the order of 4 ns ⁽¹⁴⁾, and these are the transitions which correspond to the radiation emitted at 147.0 and 129.6 nm, respectively. The other two levels are metastable, as transitions to the 1S_0 state are forbidden because of the dipole selection rule:

$$\Delta J = 0, \pm 1 \quad \text{and} \quad J = 0 \not\leftrightarrow J = 0$$

The first continuum is due to transitions from the high vibrational levels of the $^1\Sigma_u^+$ and $^3\Sigma_u^+$ states to the $^1\Sigma_g^+$ ground state. The two upper states are formed in the collision of atoms in the 3P_1 and 3P_2 states, respectively, with the ground state atoms. Because of the

POTENTIAL CURVES OF XENON



----- Atomic resonance lines
at 147.0 and 129.6 nm

Fig 1

strong spin-orbit interaction, Hund's case (c) coupling (16) is applicable, so that the selection rule $\Delta S = 0$ is less strictly obeyed and triplet to singlet transitions may occur. Evidence for the formation of the $^3\Sigma_u^+$ state and its subsequent radiating to the $^1\Sigma_g^+$ state is suggested by the results of Tanaka (4). He observed a distinct band emission at 149.1 nm, which was broadened to the red. This corresponds to the forbidden transition 3P_2 to 1S_0 and the broadening is due to transitions from the higher vibrational states of the $^3\Sigma_u^+$ molecules. Timpson et al. (17) also showed that radiation occurred from the $^3\Sigma_u^+$ state and measured the formation rate of the molecular state.

Gedanken et al. (18) showed that the molecular decay time for $^3\Sigma_u^+$ depends strongly on the internuclear separation as the associated atomic state is metastable. The decay times for the $^1\Sigma_u^+$ level should be approximately independent of internuclear separation as both atomic and molecular transitions are strongly allowed.

The second continuum results from transitions from the lower vibrational levels of the excited molecule. This is suggested by the fact that this continuum is favoured at higher pressures so that the molecules which are formed in high vibrational levels are relaxed to lower vibrational levels in collisions with ground state atoms.

As the gas pressures used in the VUV molecular xenon laser were in the range of about 5 to 15 ktorr, only the second continuum was observed. These high pressures were necessary so that the formation and relaxation processes of the excited molecule were fast compared with the fluorescence decay time. As three-body formation processes were also involved, it was clearly necessary to operate at high pressures. This is discussed in more detail in Section 2.4.

2.2 THE DEPOSITION OF ELECTRON ENERGY

In all high pressure xenon lasers reported to date, the gas has been excited by a beam of electrons with energies of the order of MeV and current densities of the order of kA. cm^{-2} . This energy is deposited in a volume smaller than that which would be expected using the CSDA (19) (continuous slowing down approximation). This is due to multiple scattering of the electrons in the gas and in the foil through which the electrons enter the gas, as well as the initial angular distribution of the electrons on leaving the gun. The range was measured for 0.5 MeV electrons by taking pinhole photographs of the fluorescence from xenon excited by electrons from a Febetron 706 electron gun. The range estimated from these pinhole photographs was of the order of one fifth of the CSDA range. (Further details are given in Section 4.5).

The primary electrons produced by the electron gun have sufficient energy to excite and ionize atoms, and to create energetic secondary electrons which may in turn have enough energy to excite and ionize other atoms.

If the electron loses all its energy in the gas, as is the case for high pressure xenon, then the distribution of energy among the excited states, ions and secondary electrons may be determined (20) (21). For an electron with initial energy, E ,

$$E = N_i \bar{E}_i + N_{ex} \bar{E}_{ex} + N_e \bar{E}_e \quad (2.1)$$

where N_i = number of singly charged ions

N_{ex} = number of excited atoms

\bar{E}_i = average energy required to ionize an atom

\bar{E}_{ex} = average energy required to excite an atom

\bar{E}_e = average energy of the electrons with insufficient energy to excite the gas.

The efficiency of ionization is defined as the mean energy, W , required to form an ion pair, so that

$$W = \frac{E}{N_i} \quad (2.2)$$

For the noble gases, it has been found that $\frac{W}{I}$ is approximately constant (20), with a value of about 1.8, where I is the ionization potential, so that

$$\frac{\bar{E}_i}{I} + \frac{N_{ex} \bar{E}_{ex}}{N_i I} + \frac{\bar{E}_e}{I} = \text{constant} \quad (2.3)$$

Each term on the left-hand side of this equation has been evaluated experimentally for helium. The values obtained are considered to be approximately correct for the other noble gases, so that an estimate of N_{ex}/N_i for xenon may be found.

The value of $\bar{E}_i/I = 1.06$ was chosen, being the same as that found for helium. This is greater than 1 as some multiply ionized atoms and molecules are produced. \bar{E}_{ex}/I depends on the distribution of atoms in the excited states, but as these excited states lie close to the ionization limit in xenon, the dependence on the population distribution should not be strong. If it is assumed that the population is distributed evenly among the excited states, then an average value for \bar{E}_{ex} of the order of 10eV may be used. As I is equal to 12.1 eV, then \bar{E}_{ex}/I is approximately equal to 0.83. Again, as for helium, assuming that approximately 18% of the energy goes into creating electrons which have insufficient energy to excite or ionize xenon atoms, then \bar{E}_e/I is approximately equal to 0.31. Substituting these values into equation 2.3 gives $N_{ex}/N_i = 0.51$, so that approximately 66% of the excited species will be in the form of ions.

2.3 PREDICTIONS OF THE FLUORESCENCE EFFICIENCY

It is possible to obtain an estimate of the maximum fluorescence efficiency attainable from high pressure xenon excited by high energy electrons. The system has an inherent efficiency of less than 100% because the energy required to form an ion pair or an excited atom, which eventually form a radiating molecule, is greater than the energy of the photon which is emitted.

It was shown in the previous section, that about 66% of the excited species are in the form of ions with the remaining 34% as excited atoms. The average energy required to form an ion pair is about 16.5 eV which is the sum of the values of \bar{E}_i and \bar{E}_e (see equation 2.1). The average energy required to form an excited atom is about 10 eV so that

$$\text{Maximum fluorescence efficiency} = F_i \frac{h\nu}{\bar{E}_i + \bar{E}_e} + F_{ex} \frac{h\nu}{\bar{E}_{ex}} \quad (2.4)$$

where F_i = the percentage of ions formed

F_{ex} = the percentage of excited atoms formed

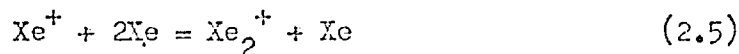
$h\nu$ = the photon energy

Substituting a photon energy of 7.2 eV into equation 2.4 gives an efficiency of about 53%. It should be noted that this is the maximum efficiency which can be obtained as it assumes that each ion and excited atom forms a radiating molecule and all loss mechanisms are ignored.

2.4 THE FORMATION PROCESSES OF EXCITED XENON

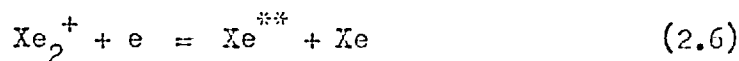
In this section some of the processes involved in the formation of the $^1\Sigma_u^+$ and $^3\Sigma_u^+$ states are discussed; understanding of all the processes involved is still incomplete. The analysis of the interaction

of high energy electrons with high pressure xenon, given in Section 2.3 showed that the majority of the species are formed as ions. The main mechanism for the removal of the atomic ion is the 3-body reaction:



in which the third body is required to conserve energy and momentum. The rate for this reaction was measured by Smith et al. (22) to be $3.6 \times 10^{-31} \text{ cm}^6 \cdot \text{s}^{-1}$ so that at a pressure of about 1 ktorr the formation time of the molecular ion is approximately 2 ns. As it is a 3-body reaction, the formation rate is proportional to the square of the pressure.

The molecular ions produced are removed by the process of dissociative recombination



where Xe^{**} is some excited state of the atom

This process was first proposed by Bates (23) to account for the fast ionic recombination observed in some species. It occurs as a result of a radiationless transition to an unstable state of the molecule in which the constituent atoms move apart and gain kinetic energy under their mutual repulsion so that neutralization is permanent. The reaction is best illustrated by consideration of a typical energy scheme shown in fig 2.

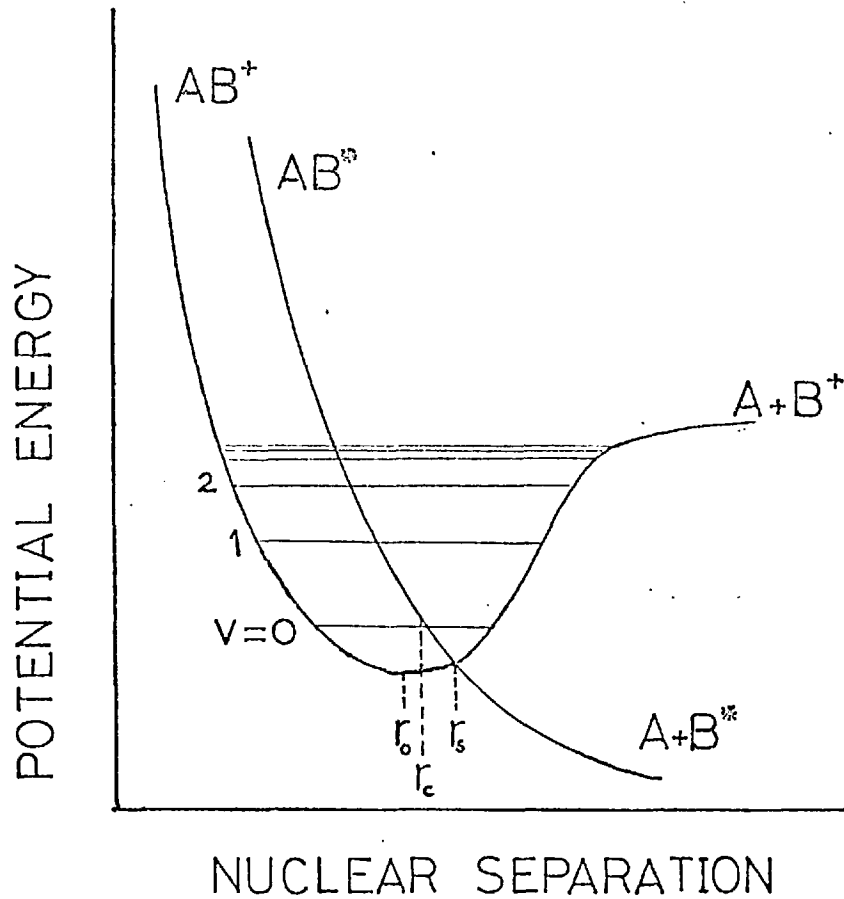


Fig 2

where r_0 = equilibrium separation

r_s = stabilisation point

r_c = separation for which the overlap integral is a maximum

The reaction occurs at a separation, r_c , when

$$V_{AB^*}(r_c) - V_{AB^+}(r_c) = \epsilon \quad (2.7)$$

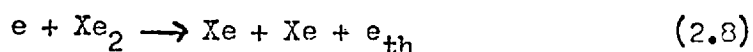
where ϵ = energy of the incident electron

From the energy level diagrams of Mulliken (3), it can be seen that there are a number of unstable states of Xe_2^{**} intersecting the potential energy curves of Xe_2^+ . (Xe_2^{**} denotes a highly excited state of the xenon molecule.)

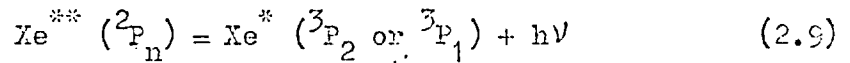
In xenon, the rate for reaction 2.6 has been measured by Lennon et al. (24) and Oskam et al. (25) to be of the order of $2 \times 10^{-6} \text{ cm}^3 \text{ s}^{-1}$ at 300°K . The rate coefficient is electron temperature dependent, the dependence being given theoretically (26) by $T_e^{-0.5}$. A temperature dependence of $T_e^{-0.67}$ for argon has been measured experimentally (27).

The binding energy of Xe_2^+ is about 1eV whereas the average energy of the subexcitation electrons is of the order of 3.8 eV ($E_e/I \approx 0.51$), so that any collision between an electron and a molecular ion results in dissociation of the molecule. For dissociative recombination to occur, the electrons must be thermalized although the optimum electron energy for reaction 2.6 is not known, as it depends on the form of the two potential curves which cross, and on the vibrational temperature of the molecular ion.

Various processes have been proposed for thermalizing the electrons. At the high initial electron densities produced by the excitation source, electron-electron collisions produce a Boltzmann energy distribution. The high energy electron in the tail of the distribution lose energy through inelastic collisions as they have sufficient energy to excite and ionize atoms. At energies of the order of 1 eV, however, elastic cooling in collisions with xenon atoms becomes dominant. Lorents and Olsen (28) calculated the rate of cooling of an electron with an initial energy of 6 eV, by collisions with atoms. They found that the cooling rate was fast down to about 1 eV, due to inelastic collisions dominating, and then decreased at lower electron energies as elastic collisions became the predominant loss mechanism. Davidenko et al. (29) proposed that collisions with van der Waals molecules may also be an important thermalization process in xenon:



Dissociative recombination occurs to excited states of the xenon atom which lie above the 3P_2 and 3P_1 levels which form the radiating molecules. This has been investigated by Frommhold and Biondi (30) in both argon and neon and they found that the 2P_n states were populated by dissociative recombination of Ar_2^+ and Ne_2^+ . Assuming that this is also true for xenon then the 2P_n states are linked radiatively to the 3P_2 and 3P_1 states, so that



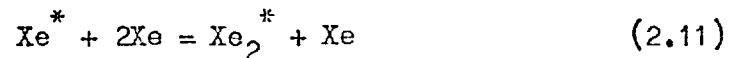
The radiative lifetimes for the transition have been measured by Allen et al. (31) and Verolainen et al. (32) to be of the order of 55 ns.

The destruction of atoms in the highly excited states in collisions with electrons or ground state atoms has been observed by Phelps (33) in neon. The cross-section for the electron-induced decay was about 10^{-13} to 10^{-14} cm², whereas for collisions with atoms, the cross-sections were of the order of 10^6 smaller. The electron induced reactions were incorporated in the models of George et al. (34) and Fournier et al. (35) to account for the behaviour of the fluorescence from high pressure xenon.

Only the levels which lie below the bottom of the molecular ion well, will be effectively populated by dissociative recombination, as any levels which lie above will be re-ionized by the Hornbeck-Molnar process (36):



The two molecular states, $^1\Sigma_u^+$ and $^3\Sigma_u^+$ are formed in the 3-body reaction



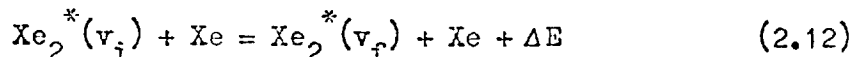
As discussed in section 2.2, both states can radiate to the $^1\Sigma_g^+$ ground state as there is strong spin-orbit coupling so that the selection rule $\Delta S = 0$ holds less strictly.

There is still some debate about the role of these two states. The

early studies on the interaction of high energy electrons with xenon, assumed only a single radiative decay rate (37) (38) and formation rate. Recent results indicate that two separate radiating levels may be important in explaining the experimental results (39) (40).

Different formation rates for the molecule have been measured. Freeman et al. (41) obtained a value of $(1.5 \pm 0.7) \times 10^{-32} \text{ cm}^6 \cdot \text{s}^{-1}$ whilst Timpson et al. (17) measured a rate of $7.2 \times 10^{-32} \text{ cm}^6 \cdot \text{s}^{-1}$. The latter result was for the $3 \sum_u^+$ level whereas the origin of the radiation observed in the experiment of Freeman et al. is uncertain. Since they excited the gas by using the 147.0 nm line of xenon, it is probable that the radiation emitted was due to transitions from the $1 \sum_u^+$ level. Bouciqué et al. (42) measured the formation rate of Xe_2^* to be $2.5 \times 10^{-32} \text{ cm}^6 \cdot \text{s}^{-1}$. From the experimental results obtained in the research reported here (see Chapter 3) a value of $(3.0 \pm 0.3) \times 10^{-32} \text{ cm}^6 \cdot \text{s}^{-1}$ was derived. In both these cases, no account was taken of the formation of two levels.

The xenon molecules are formed in high vibrational levels and at high pressures are relaxed quickly to lower vibrational states by collision with ground state atoms:

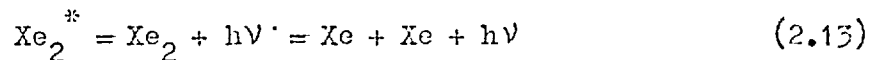


where $\text{Xe}_2^*(v_i)$ and $\text{Xe}_2^*(v_f)$ denote the molecules in the initial and final vibrational states, respectively.

ΔE is the energy carried away by the ground state atom.

From the results of Fink et al. (43), the rate constant for vibrational relaxation out of the initial levels is approximately $6.6 \times 10^{-10} \tau_f^{-1} \text{ cm}^3 \cdot \text{s}^{-1}$. For a lifetime of the order of 10 ns, and at a pressure of 10 ktorr, this corresponds to a vibrational relaxation time of about 40 ps. The excited

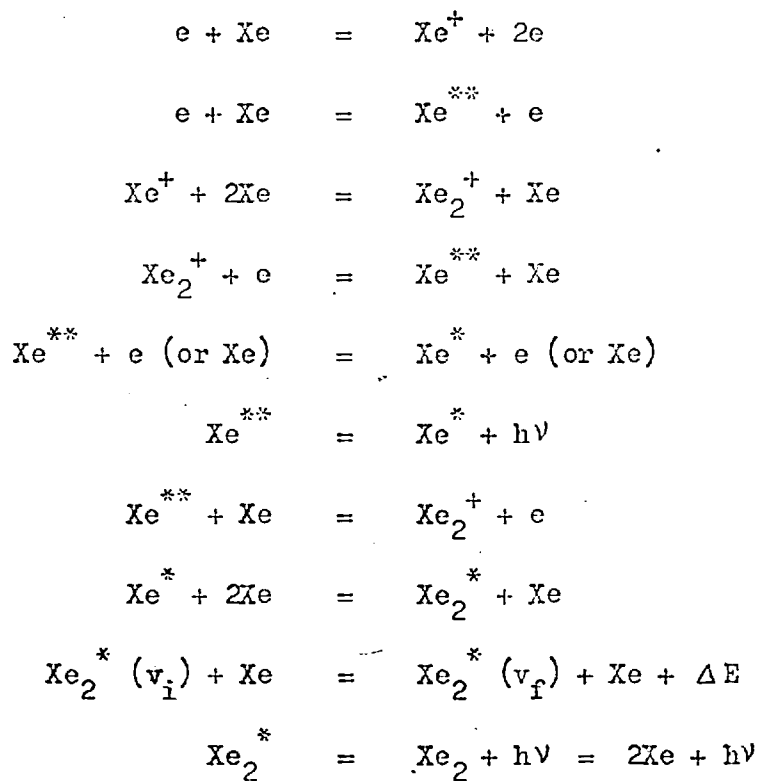
molecule then decays to the ground state with the emission of a photon. Owing to the repulsive nature of the ground state, the 'quasi molecule' quickly dissociates to form two ground state atoms:



The reactions discussed in this section are summarized in Table 2.1

TABLE 2.1

FORMATION MECHANISMS OF XENON



CHAPTER THREE

EXPERIMENTAL STUDIES OF FLUORESCENCE

Most of the early studies in xenon were carried out to obtain a vacuum ultraviolet source and were concerned only with the spectral analysis of the output radiation from discharges at subatmospheric pressures (4) (11). More recently the temporal dependence of the radiation from xenon at pressures up to about 25 ktorr with a time resolution of the order of nanoseconds, has been investigated. This has led to a greater understanding of the reaction mechanisms, and together with the availability of reliable electron beam sources, with electron energies of the order of an MeV and pulses with durations of nanoseconds, has resulted in the production of efficient VUV lasers (7) (44).

In this chapter, experimental results from the fluorescence studies of high pressure xenon are presented. The dependence of the time behaviour with pressure was investigated, and estimates of the 3-body formation rate and the fluorescence decay time of the excited state molecule were made. The variation in results obtained at different laboratories is discussed together with some of the theoretical models designed to account for the discrepancies.

3.1 THE ELECTRON BEAM GENERATOR

The excitation source used in the fluorescence studies and in subsequent studies on the laser, was a Febetron 706 (45). This is a commercially available electron gun which produces a 2.5 ns (FWHM) pulse of electrons with a mean energy of 0.5 MeV and a total beam energy of about 10 joules. The basic circuit consisted of a Marx generator and an additional pulse forming circuit, known as a Blumlein circuit. The electron beam generation and acceleration occurred in a diode which was energised by the pulse-forming network.

The Marx generator consisted of 15 capacitors (modules) which were d.c. charged in parallel to 30 kV, and then discharged in series by triggered breakdown of the spark gaps which were connected across each capacitor. Breakdown of the gaps was initiated by applying a 17.5 kV trigger pulse to the first gap (the trigger gap), which caused the remaining gaps to breakdown in series by overvolting. The spark gaps were pressurized using dry air and the pressure adjusted so that the system did not fire before the trigger pulse was applied. For a 30 kV charging voltage the spark gap pressure (module chamber pressure) was about 3.5 ktorr.

As the Marx erected, a spark gap (series gap) between the output corona knob of the Marx and the intermediate conductor of the Blumlein circuit, broke down. Part of the energy stored in the Marx was transferred to the Blumlein circuit ⁽⁴⁶⁾. This circuit consists of two transmission lines with the same impedance, Z , which for the Febetron 706 was 30 ohms. The Blumlein discharges when the radial spark gaps breakdown, and for a two way transit time the circuit acts like a generator of twice the charging voltage, with an internal impedance, $2Z$ ⁽⁴⁷⁾. (The construction of the Blumlein is described in Chapter 4). The output voltage appeared across a load (the field emission diode) which had an impedance, Z_L , equal to $2Z$. The cathode of the Febetron 5510 diode, which was used in the fluorescence experiments, consisted of an array of sharp spikes. When the -600 kV pulse was applied to these spikes, electrons were produced by the process of field emission. These electrons were accelerated towards and passed through a 0.025 mm titanium anode foil which was maintained at earth potential. The electrons had a peak energy of 600 keV and a mean energy of about 500 keV.

The operator was protected from ionising radiation by placing 2 mm of lead and 2 mm of aluminium between the operator and the electron diode, and by operating at a minimum distance of 5 metres from the electron source.

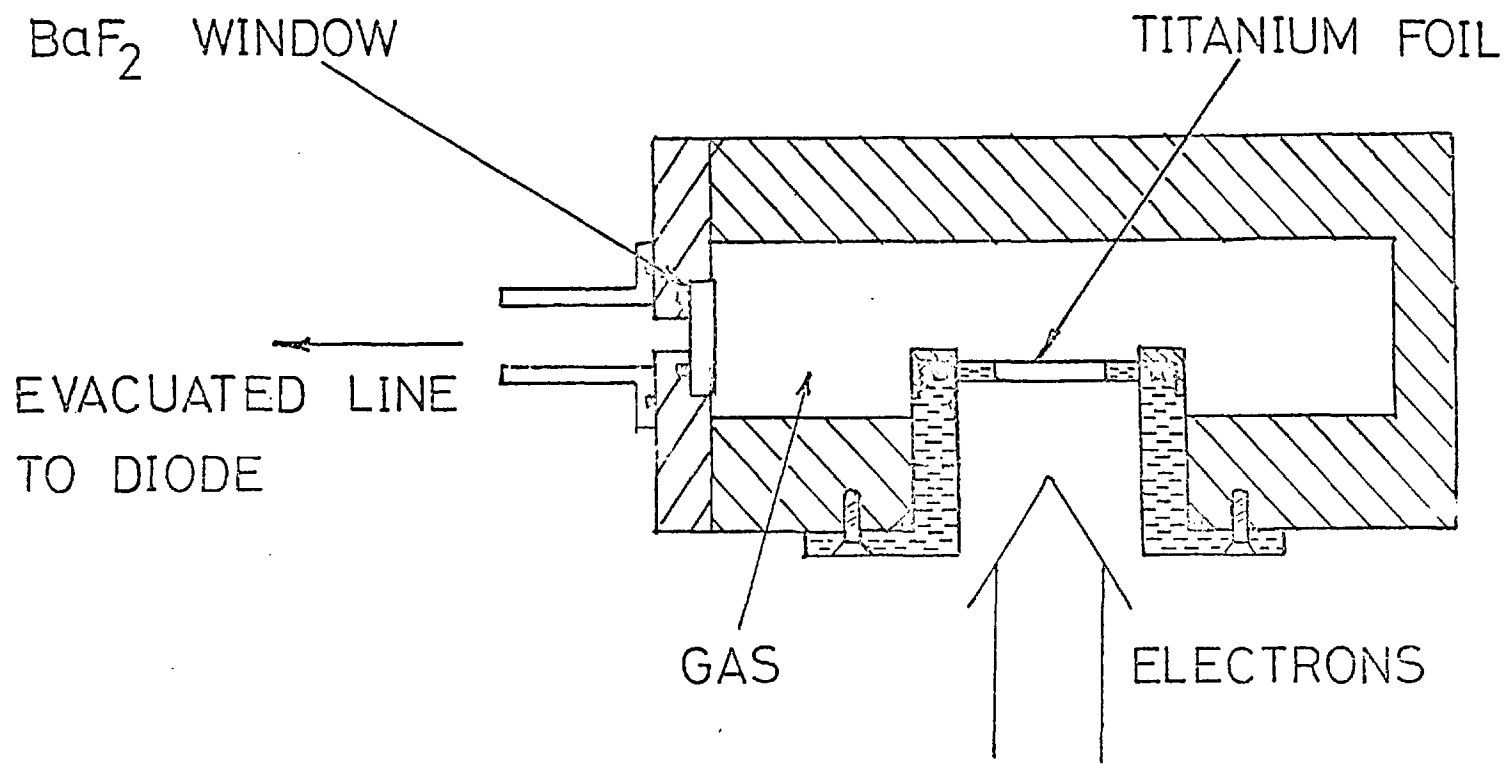
The maximum radiation dose that the operator was subjected to under these conditions, was well within the required safety standards.

3.2 THE EXPERIMENTAL SET UP FOR FLUORESCENCE MEASUREMENTS

In order to study the fluorescence from xenon, it was necessary to design a cavity and gas handling system which could be evacuated and then filled to pressures up to 20 ktorr. (1 ktorr = 1.32 atmospheres = 19.3 psi). The cavity which was constructed for this purpose, is shown in fig 3. The 500 keV electrons entered the gas through a thin titanium foil. Foil thicknesses in the range 0.025 to 0.075 mm were used (foils were supplied by Goodfellow Metals). Titanium was chosen because it satisfied the requirements for both a low electron stopping power and a high mechanical strength. The foil was fixed to a stainless steel supporting ring, using Araldite epoxy resin, and was cured by baking at 150°C for 1 hour. It was then supported on the side open to the atmosphere by a stainless steel plate in which a 30 mm by 6 mm slot was cut, to allow electrons to enter the cell. The foil supporting ring was held firmly against a silicone O-ring, in order to make a seal. The system was tested for leaks and strength, to at least 50% above the maximum working pressure, using compressed air. The maximum safe working pressure under the prevailing experimental conditions was found to be about 15 ktorr for 0.025 mm thick foils, and 40 ktorr for 0.075 mm thick foils.

The gas handling system is shown in fig 4. Stainless steel pipes were used throughout and connections were made either by brazing these pipes, or by using high pressure stainless steel gas connectors (Ermeto couplings). Narrow bore pipes with an internal diameter of 0.32 mm and wall thickness of 0.16 mm, were used to reduce the volume of gas required. This did however increase the time required to evacuate the system.

/// ALUMINIUM
▨ STAINLESS STEEL



HIGH PRESSURE CAVITY

Fig 3

GAS HANDLING SYSTEM

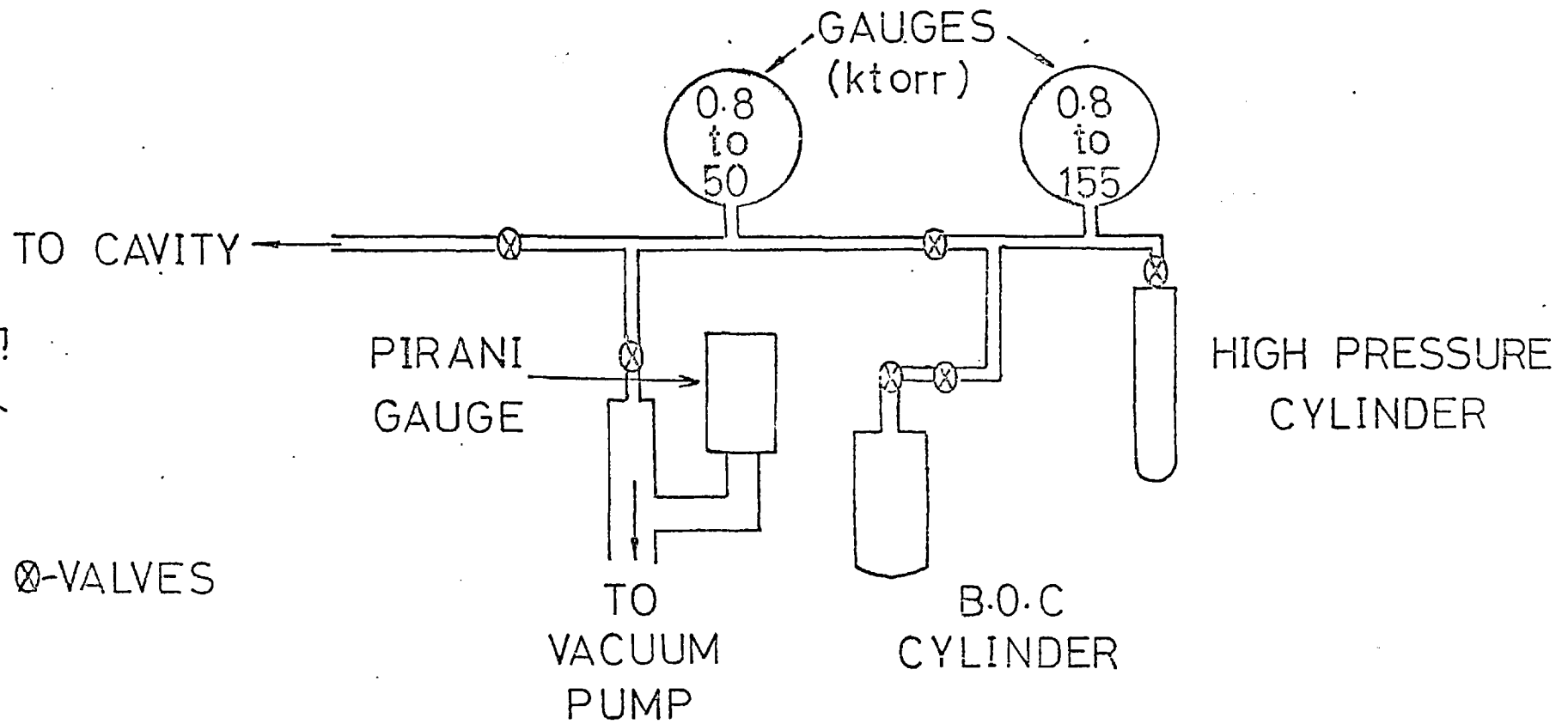


Fig4
21

The gas pressure was measured to an accuracy of ± 0.2 ktorr, using a gauge, which was calibrated in the range 0.8 to 50 ktorr. The pressure of the xenon in the cylinders, supplied by The British Oxygen Company, was approximately 10 ktorr in a volume of about 1.5 litres, so in order to fill the system to pressures greater than the cylinder pressure, the gas was transferred to an evacuated high pressure cylinder of volume 100 mls (Hone instruments) which had been tested by the manufacturers to 260 ktorr. This latter cylinder was surrounded by liquid nitrogen, so that when the B.O.C. cylinder was connected and opened, the gas was transferred to, and frozen in the high pressure bomb (liquid nitrogen temperature: 77°K , freezing point of xenon: 161°K). This technique of freezing the gas was also used to recover the gas from the cavity. While the xenon was frozen, volatile contaminants such as oxygen and nitrogen were removed by evacuating the system with the high pressure cylinder valve open. Repeated re-distillation of the gas further purified the 99.997% Grade-X xenon and also allowed the same gas to be recycled many times. The 0.8 to 155 ktorr gauge was used to monitor the pressure inside the high pressure cylinder.

The cavity was pumped to about 10^{-2} torr, using a rotary pump (Edwards High Vacuum ED 50), and then purged with xenon. The pressure was monitored on a Pirani gauge (Edwards High Vacuum M5C-2). The xenon was then slowly leaked into the system from the high pressure gas cylinder and the pressure read from the 0.8 to 50 ktorr gauge.

The electron beam from the 5510 diode travelled 3 cm through the air at atmospheric pressure before entering the cavity through the titanium foil. From the manufacturer's data, the current density on entering the gas was about $1 \text{ kA} \cdot \text{cm}^{-2}$ compared with the current density close to the anode foil of about $5 \text{ kA} \cdot \text{cm}^{-2}$.

Because of both the distortion of the foil at pressures greater than 760 torr (1 atmosphere) and the thickness of the plate used to retain the foil, the line of sight for viewing the fluorescence was about 2 mm from the input foil. At high pressures, where the electron range was a few millimetres, the region of maximum excitation was not observed.

Barium fluoride (supplied by Harshaw Chemical Company) was selected as the material for the output window. It was chosen for its high transmittance at 170 nm, and its resistance to damage by ionising radiation (48). The window was 3 mm thick and 1.3 cm in diameter, and it was clamped near its edge, between 2 Viton O-rings, giving a useful diameter of 8 mm. The ratio of the thickness to the open diameter was 0.375, so that the safe working pressure, as given in the Harshaw Catalogue (49), was about 15 ktorr, with a safety factor of 4.

3.3 TEMPORAL STUDIES OF FLUORESCENCE.

The barium fluoride window was connected by an evacuated pipe to a fast photodiode (supplied by Instrument Technology Ltd). The photodiode had an S.20 photocathode and a quartz window of high transmission at the wavelength of interest. It was calibrated at 280 nm using the second harmonic of a laser-pumped dye laser and with an anode potential of 5 kV, it was found that a current of 2 A could be drawn from the photodiode without saturation; in practice a maximum current of 1.6 A was employed. The fluorescence intensity profiles were recorded on a Tektronix 519 oscilloscope giving a combined instrumental resolution of about 0.5 ns.

Oscillograms were recorded for xenon pressures in the range 1.3 to 11 ktorr, and for pressures greater than 2.3 ktorr the VUV signal incident on the photodiode was reduced by half, using an aperture to prevent diode saturation. The photodiode output signal was then reduced, using

calibrated electrical attenuators (Tektronix 125 ohm attenuators). When the photodiode line was open to the atmosphere no signal was recorded, indicating that the signal was in the vacuum ultraviolet. This was confirmed by recording the fluorescence spectra, as reported in Section 3.5.

Three oscillograms of the output fluorescence are shown in plate 1 and it is evident that both the decay time and the rise time are pressure dependent. The decay times were measured by enlarging the polaroid traces and plotting a graph of $\log I(t)$ against t , where $I(t)$ is the signal intensity at time, t . In the range of pressures studied, a linear relationship was found, see fig 5; thus the fluorescence decay may be described by the equation

$$I(t) = I(0) \exp \frac{-t}{\tau_p} \quad (3.1)$$

where τ_p is the fluorescence decay time at pressure, p . The error in measuring $I(t)$ increases as t increases due to the uncertainty in defining zero intensity and also because of the finite thickness of the lines on the polaroid traces. The fluorescence decay time, τ_p , was then measured from the slope of the graph. The variation of the decay rate, $\frac{1}{\tau_p}$, with pressure, is shown graphically in fig 6. The graph is divided into two sections, the division occurring at about 3.1 ktorr. The overall temporal shape of the fluorescence depends on both the rate of formation of Xe_2^* and its rate of decay. In order for the true decay to be measured, the formation rate should be fast compared with the decay.

The low pressure region of fig 6 may be explained by the slow creation of Xe_2^* . In plate 1a it is evident that the build up of the fluorescence was slower than in the high pressure cases. The build up time, defined as the time for the fluorescence to increase from 10 to 90%

PLATE 1

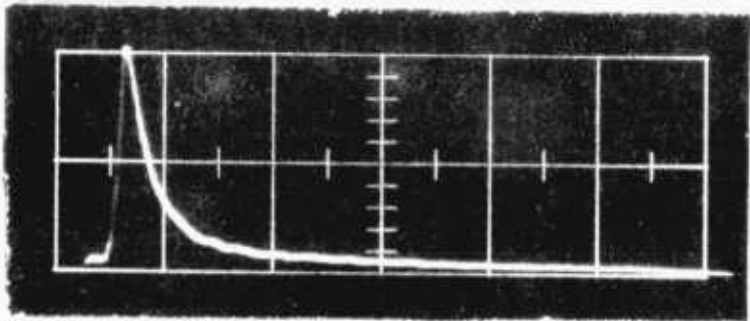
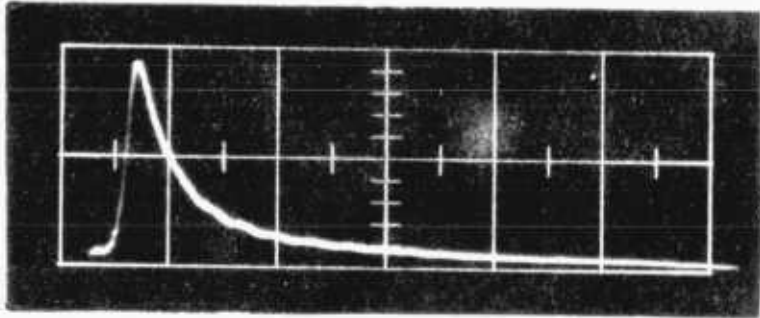
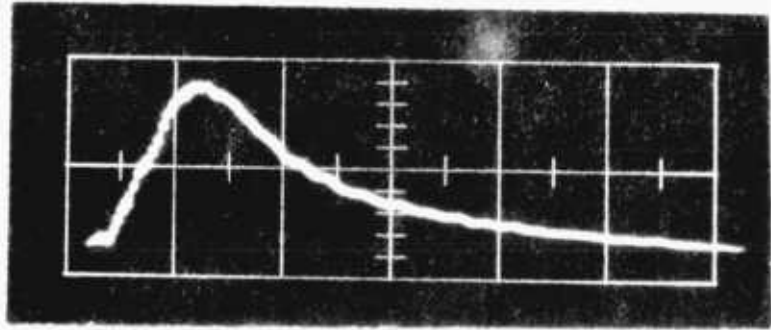
Temporal Dependence of the Xenon Fluorescence
at following Xenon Pressures

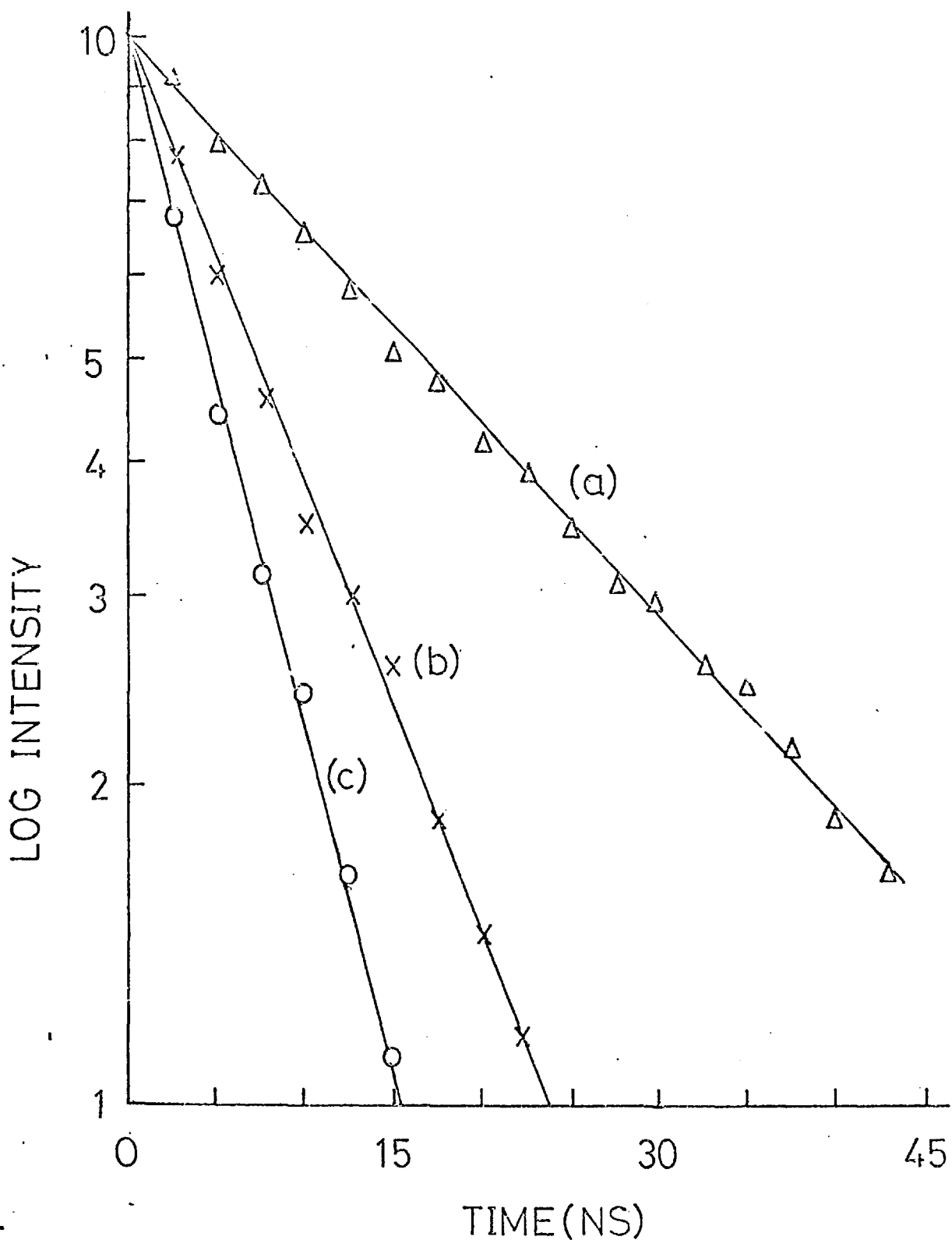
(a) 1.5 ktorr

(b) 4.7 ktorr

(c) 10.0 ktorr

timescale : 20 ns per major division





- (a) 1.5 ktorr xenon
- (b) 4.6 ktorr xenon
- (c) 10 ktorr xenon

Fig 5
25

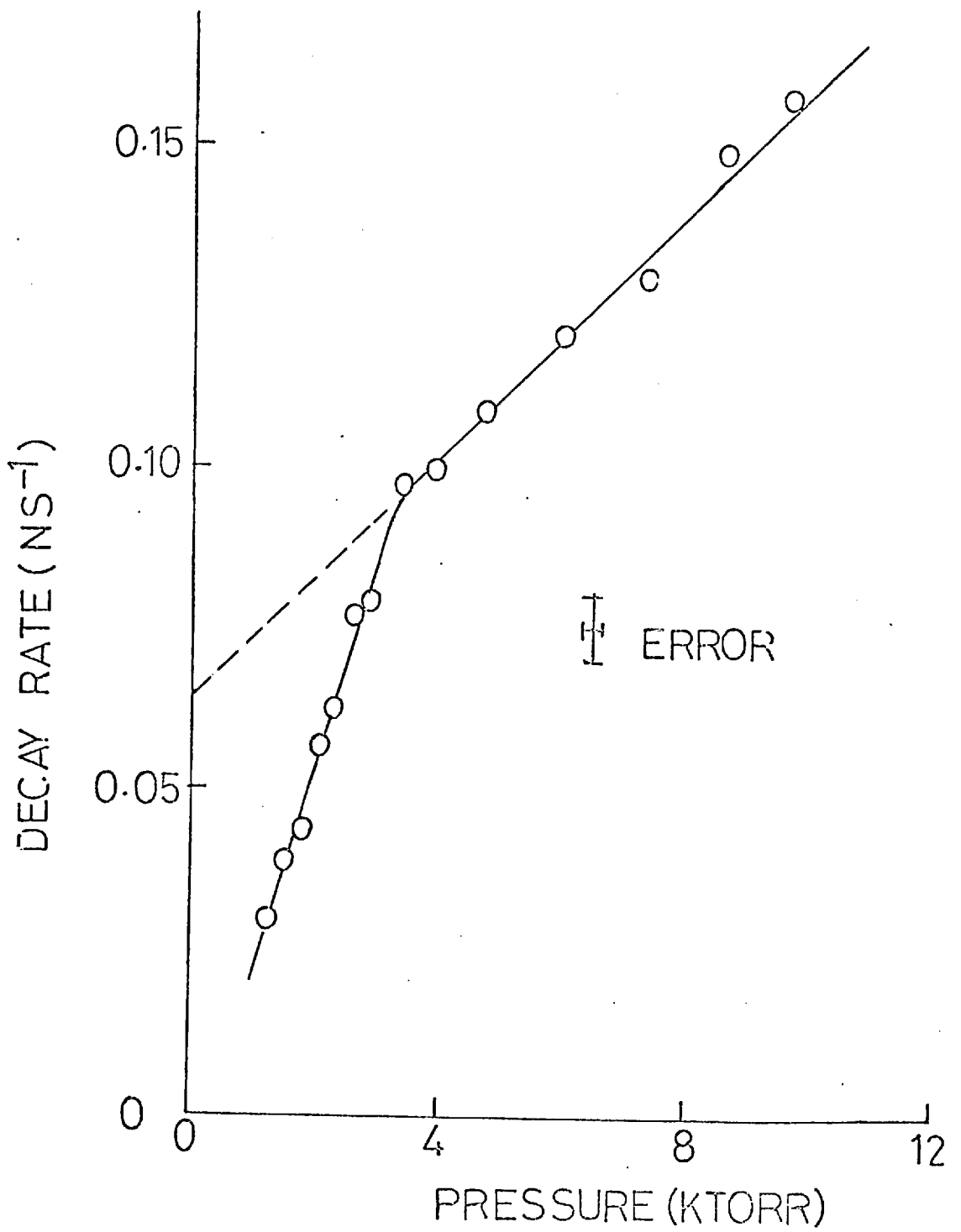


Fig 6

of its peak value, was measured for a number of fluorescence results in the pressure range 0.6 to 3.1 ktorr. As the formation of excited molecules occurs by the 3-body reaction (equation 2.11), the rate is proportional to (pressure)². The pressure dependence of the fluorescence build up, which is a measure of the formation rate of Xe₂^{*}, is shown graphically in fig 7. It was necessary to make a correction to the measured risetime, t_m, to account for the electron pulse duration, t_p, which was approximately 2.5 ns. The risetime, t_r, was determined from

$$t_r^2 = t_m^2 - t_p^2 \quad (3.2)$$

Clearly, values found at low pressures, where t_m ≫ t_p were more accurate than those at higher pressures.

At pressures of greater than 3.1 ktorr, the measured risetime of the pulse was about 3 ns and was thus governed by the pulse duration of the electron beam, (equation 3.2). The formation rate, determined from the slope of the graph, was found to be (3.0 ± 0.3) × 10⁻³² cm⁶.s⁻¹. This result compares well with values obtained by other workers (17) (41).

If there are 2 distinct radiating levels with different formation rates, then this value will be the weighted mean of the 2 formation rates. At low pressures where the build up time is greater than the electron beam pulse, the excitation energy will be stored through resonance trapping (50)(51). Imprisonment of resonance radiation in gases is due to selective absorption by ground state atoms. At these pressures a resonance quantum emitted in the excited volume has a small chance of escaping so that transitions which are strongly allowed at very low pressures (eg the lifetimes for ¹P₁ and ³P₁ are approximately 4 ns (14)) appear to become metastable as the pressure increases. Resonance trapping is evident as the atomic resonance lines at 147 and 129.6 nm were not observed.

At xenon pressures greater than 3.1 ktorr the rate of decay was found

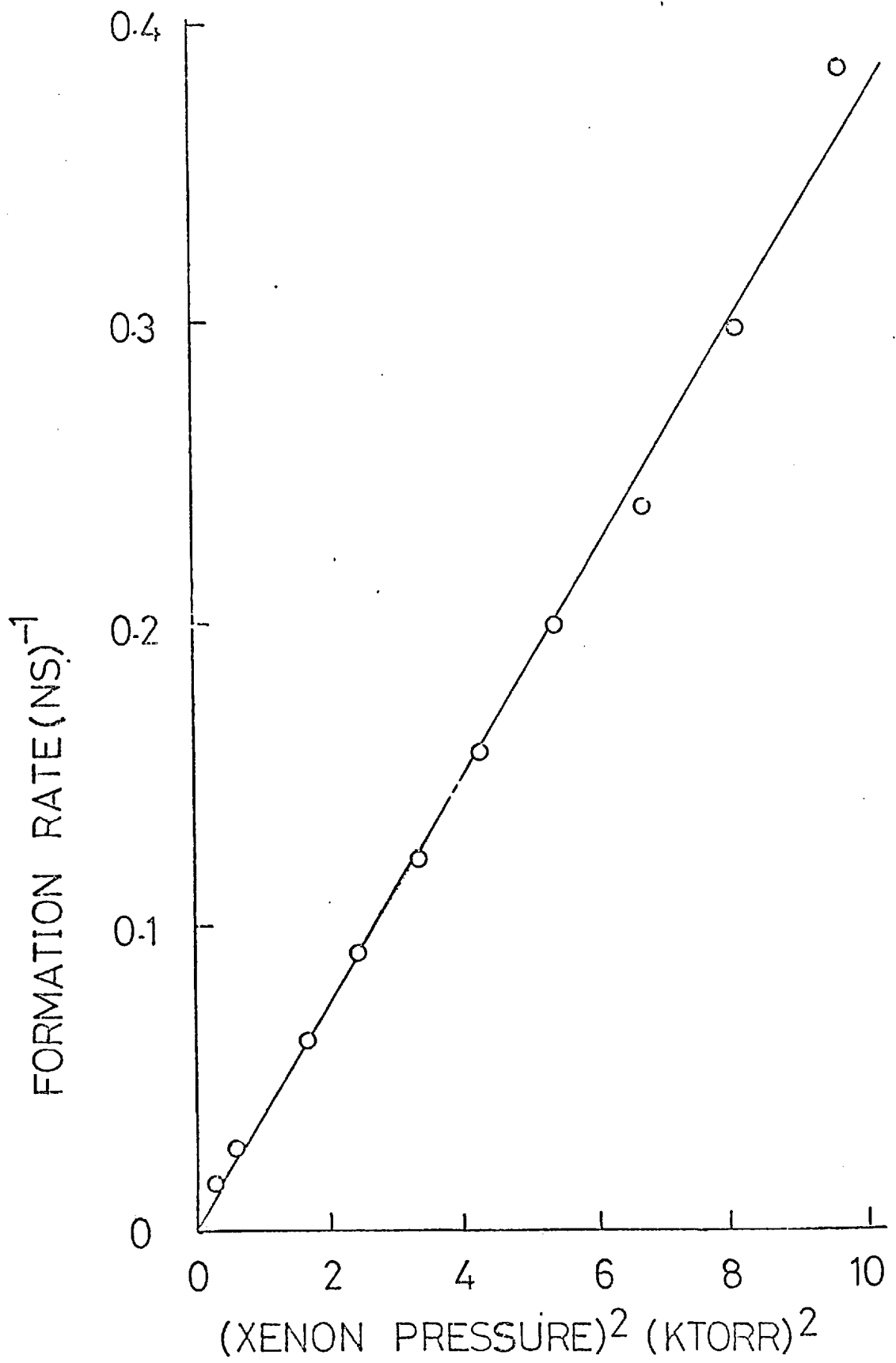


Fig 7

to increase linearly with pressure (fig 6). In order to account for the removal of Xe_2^* , the existence of a quenching process in addition to the radiative decay was proposed by Bradley et al. (37).

$$\text{Xe}_2^* + \text{Xe} = 3\text{Xe} \quad (3.3)$$

(A similar process was suggested by Dolgoshein⁽⁵²⁾.) The rate equation for the population density of Xe_2^* then becomes

$$\frac{dN^*}{dt} = k_1 n^2 n^* - \frac{N^*}{\tau_f} - k_2 n N^* \quad (3.4)$$

where n , n^* and N^* are the number densities of the ground state atoms, the excited atoms, and the excited molecules, respectively.

τ_f is the radiative decay time

k_1 is the 3-body formation rate of Xe_2^*

k_2 is the rate coefficient for the quenching process

The measured decay time, τ_p , may then be written

$$\frac{1}{\tau_p} = \frac{1}{\tau_f} + k_1 n \quad (3.5)$$

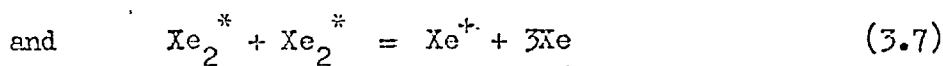
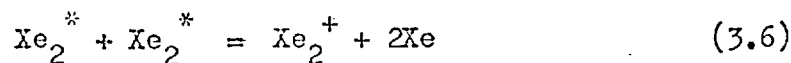
The graph of $\frac{1}{\tau_p}$ against p gives the following results

$$\tau_f = (16 \pm 2) \text{ ns}, \quad k_1 = (2.7 \pm 0.3) \times 10^{-13} \text{ cm}^3 \cdot \text{s}^{-1}$$

from the intercept and slope respectively.

Other groups have supported this theory of quenching of the excited dimer by ground state atoms. Wallace et al. (38) repeated the experiments and also observed a linear relationship between decay rate and pressure, but they obtained a fluorescence decay time of (130 ± 20) ns and a quenching coefficient of $5.1 \times 10^{-13} \text{ cm}^3 \cdot \text{s}^{-1}$. Johnson et al. (53) measured the fluorescence decay time to be 50 ns and found a quenching coefficient of $6.6 \times 10^{-13} \text{ cm}^3 \cdot \text{s}^{-1}$. This latter group, suggested a

further loss mechanism, Penning (or mutual) ionization:



The corresponding rate equation for the decay was given by

$$\frac{dN^*}{dt} = -\left(\frac{N^*}{\tau_p}\right) - k_3 N^{*2} \quad (3.8)$$

where N^* is the number density of excited molecules

τ_p is the measured decay time

k_3 is the rate coefficient for Penning ionization

so that

$$N^* = \frac{\exp\left(\frac{-t}{\tau_p}\right)}{\frac{1}{N_0^*} + k_3 \tau_p \left[1 - \exp\left(\frac{-t}{\tau_p}\right)\right]} \quad (3.9)$$

They obtained a value of $(3.5 \pm 1.4) \times 10^{-10} \text{ cm}^3 \text{ s}^{-1}$ for k_3 , by fitting equation 3.9 to the fluorescence results. In Penning ionization, one excimer is deactivated and either an atomic or molecular ion formed; the ejected electron carries away the excess reaction energy. The rate of this reaction increases as the concentration of Xe_2^* increases, so that it becomes a more significant loss with high current density electron beams. This is an important consideration in designing a laser as this mechanism puts an upper limit on the useful inversion.

Although all three sets of experimental results were carried out using a Febetron 706 as the excitation source and over a similar pressure range, the measured lifetimes varied from about 16 to 130 ns.

3.4 THEORETICAL MODELS FOR FLUORESCENCE FROM XENON

In xenon and other noble gases there are two states, $1\sum_u^+$ and $3\sum_u^+$, which can radiate to the ground state, $1\sum_g^+$. These states are

closely spaced and as the repulsive ground state is steep, the radiation appears as a single continuous band (see fig 1). The results given in the previous section only considered one radiating state with a single lifetime.

Lorents et al. (54) suggested that the two states have different lifetimes and that the variation of lifetime with pressure is due to electron mixing of the states and to Penning ionization. The pressure dependent radiative lifetimes were then explained by an electron density dependent lifetime and the variation found in the measurements made of lifetime was attributed to the use of different pumping geometries and current densities.

Koehler et al. (39) obtained time constants for the build up and decay of the VUV continuum intensity, $I(t)$, by fitting fluorescence results to a sum of exponential terms:

$$I(t) = \sum_i A_i \exp\left(\frac{-t}{\tau_i}\right) \quad (3.10)$$

where A_i is the amplitude

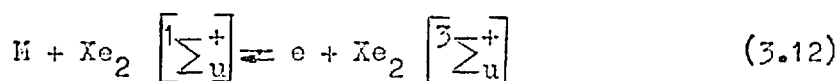
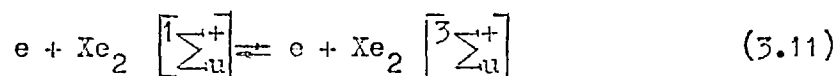
τ_i is the build up or decay time

They found that for pressures in the range 11 to 40 ktorr, the decay could be represented by two exponential terms with lifetimes, τ_i , of 4 and 16 ns. These decay times were attributed to transitions from the $1\Sigma_u^+$ and $3\Sigma_u^+$ states to the $1\Sigma_g^+$ ground state, respectively.

After reanalysing Koehler's results, Werner et al. (55) reported that values of 5 and 40 ns for the lifetimes of the singlet and triplet states, respectively, also represented the decay results satisfactorily. Using these two values, Werner et al. developed a model similar to that

of Lorents et al. to explain the behaviour of the xenon laser. This model was an extension of earlier theoretical work ⁽³⁴⁾ on reactions involved in the production and decay of the excited xenon molecule, in which a single level was assumed to radiate. In the later model, contributions from both the $^1\sum_u^+$ and $^3\sum_u^+$ were incorporated.

The following two processes were assumed to occur in the mixing of the singlet and triplet levels:



where M is a heavy particle such as Xe.

The mean electron energy (about 5eV) is greater than the singlet triplet spacing, so that reaction 3.11 tends to equalise the populations of the 2 levels. On the other hand reaction 3.12 tends to favour relaxation to the triplet level as the energy of the xenon atoms is less than the singlet triplet spacing at normal temperatures. Werner assumed that the gain cross-section for the triplet level was less than for the singlet level, so that at pressures where reaction 3.12 becomes more dominant than reaction 3.11, the gain would be reduced. As dissociative recombination is the dominant electron loss mechanism, the rate of reaction 3.11 will increase approximately as the square root of the gas pressure, whereas the rate of reaction 3.12 will increase linearly with pressure such that it becomes the dominant reaction at high pressures. The model predicted the temporal shape of the laser pulse, the relative intensities of the laser and fluorescence, the spectral red shift and the spectral half width of the laser spectra. By choosing values for the rates of the reactions Werner found a reasonable agreement between the experimental results and the theory, for the high pressure xenon laser.

The results predicted by this model were inconsistent with some of the experimental results obtained by Gerardo and Johnson (56), who showed that the laser terminated while the measured gain was larger than the pre-lasing losses of the resonator. They postulated that the termination was due to a time dependent loss which was independent of the laser medium, a characteristic which was not incorporated in Werner's model.

A model which was developed by Fournier (55) to describe the temporal behaviour of the fluorescence from xenon excited by a Eebetron 706, assumes values of 4 and 16 ns for the lifetimes of the two radiating levels, as calculated by Koehler. The distinguishing feature of his model is the use of two different formation rates for the singlet and triplet states. Fournier made a number of assumptions. Firstly that the number of channels open to triplet formation is three times that of the singlet, so that a faster triplet formation rate can be expected. Also, that the dissociative recombination terminates in a cascade level which is linked radiatively and by electron induced transitions to the relevant resonance and metastable levels. This cascade level is incorporated to account for the properties of the levels to which dissociative recombination occurs. At low pressures the electron density is low so that the decay of the cascade level into the atomic states which form Xe_2^* occurs radiatively with lifetimes of the order of tens of nanoseconds. The population is stored in the cascade level and so the measured fluorescence decay is governed by the decay rate of this level. As the pressure increases the number of electrons deposited per unit volume increases so that electron induced transitions become more important in depopulating the cascade level. Only when the decay rate of this cascade level is greater than the fluorescence decay rate, will the true fluorescence decay time be measured so that at high pressures the measured decay times should reach an asymptotic value.

This is consistent with the experimental results obtained by Koehler et al..

As in other models, the pressure dependent decay is attributed by Fournier to an electron density dependent decay. In an attempt to observe the electron density dependence, fluorescence profiles were obtained, using a higher current density electron beam source than that employed earlier. A Febetron 5516 X diode was used, and with the beam travelling a few millimetres through air before entering the cavity, the current density was estimated to be about 4 kA.cm^{-2} on entering the cavity. The fluorescence decay rate showed a small increase in the higher current density case, consistent with the prediction of Fournier's model. The increased decay rate is illustrated in fig 8 which shows a comparison of two sets of experimental results at two different current densities; the curves have been normalised at peak intensity. This increased decay rate with current density was also observed by Johnson et al. (53), who attributed it to the Penning ionization reaction.

3.5 SPECTRAL STUDIES OF FLUORESCENCE

Before obtaining meaningful spectral results, the characteristics of the VUV film used were determined for the prevailing experimental conditions. Kodak SC7 film was chosen for the detection of VUV radiation as it is the most sensitive of the ultraviolet films over most of the wavelength range 100 to 250 nm⁽⁵⁷⁾ and also because the film γ is constant over a large density range at a given wavelength. The γ of a film is defined by

$$D = \gamma \log E \quad (3.13)$$

where D = film density

E = energy density of the radiation incident on the film

Spectra of the fluorescence were recorded using a 1 m normal incidence

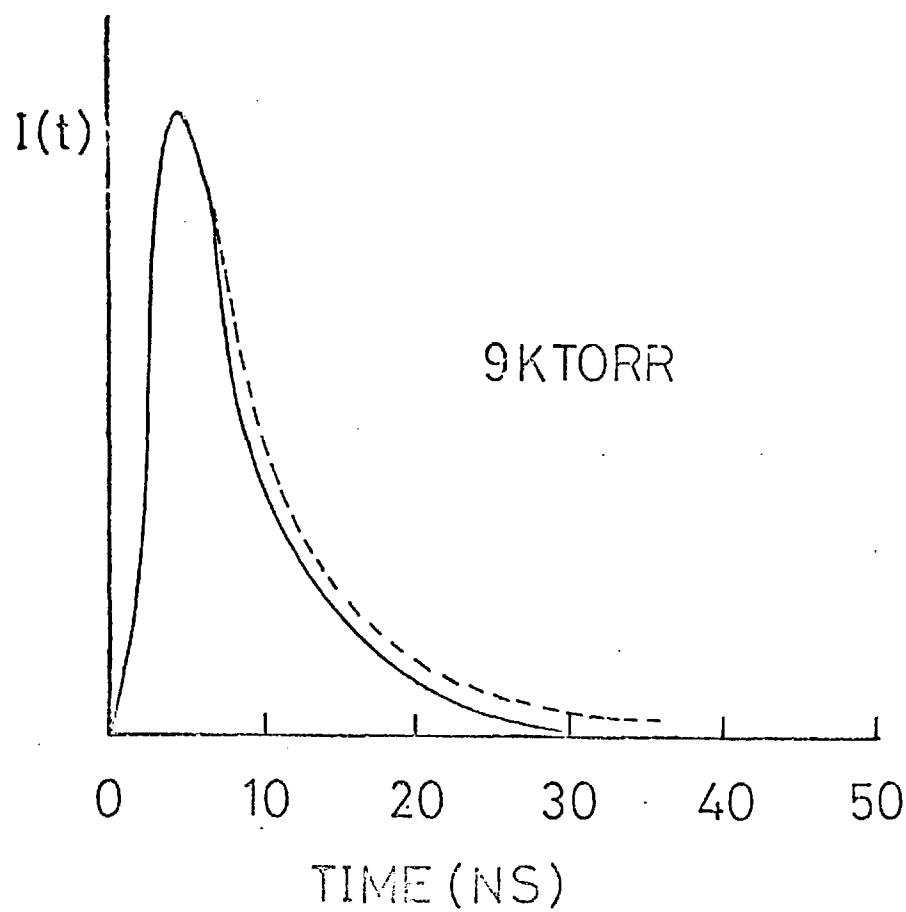
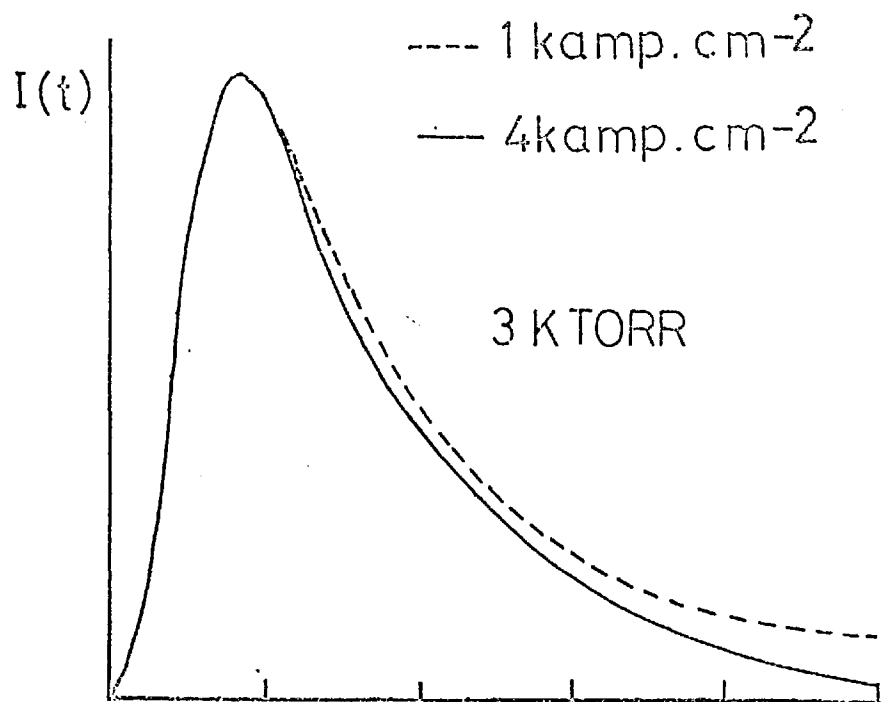


Fig 8

vacuum spectrograph, with a 600 line mm^{-1} grating, centred at 170 nm. The arrangement used was the same as that shown in fig 3, but with the diode replaced by the spectrograph. The spectrograph was evacuated to less than 10^{-5} torr using a mercury diffusion pump, backed by a rotary pump, both of which had liquid nitrogen cold traps.

Two spectra were recorded on each piece of film, one having twice the intensity of the other, the result of superimposing twice the number of shots on one spectra than on the other. Because the output fluorescence energy was found to be reproducible to within $\pm 5\%$ at a given pressure, it was assumed that the intensity of the radiation was proportional to the number of shots superimposed. After exposure, the film was developed in accordance with the manufacturer's instructions.

Densitometer traces of the two spectra were recorded using a Joyce Loebel microdensitometer and the half width was measured directly. Plate 2 shows 2 spectra taken at a xenon pressure of 4.6 ktorr and the densitometer traces are shown in fig 9.

The density at the half width, $D_{\frac{1}{2}}$, is defined such that if D_1 , the recorded peak density is equal to $\gamma \log E$ then

$$D_{\frac{1}{2}} = \gamma \log \frac{E}{2} \quad (3.14)$$

For a microdensitometer with a calibrated reference density wedge of slope $W \text{ cm}^{-1}$

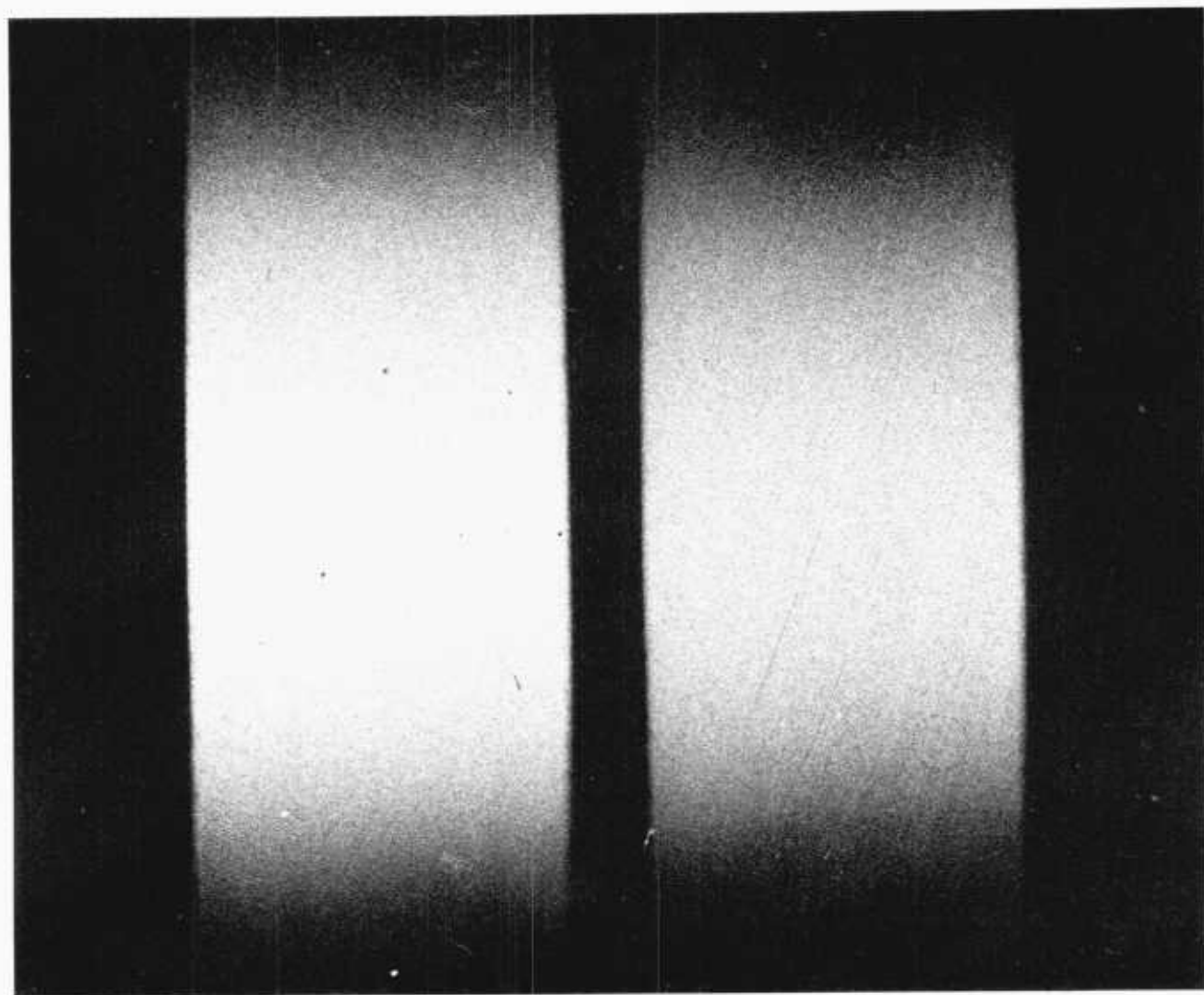
$$D_{\frac{1}{2}} = D_1 - \frac{\gamma}{W} \log 2 \quad (3.15)$$

γ was found to be equal to 1.1 ± 0.3 for densities, D_1 , in the range 0.7 to 1.4. The observed variation in γ may be accounted for by the variation in incident intensity, because in order to get sufficient exposure it was necessary to superimpose between 2 and 12 shots for a spectrograph slit width of 1 mm.

PLATE 2

The Xenon Fluorescence Spectrum
at Xenon Pressure of 4.6 ktorr

Spectrum (a) is twice the intensity of spectrum (b)



FLUORESCENCE SPECTRA

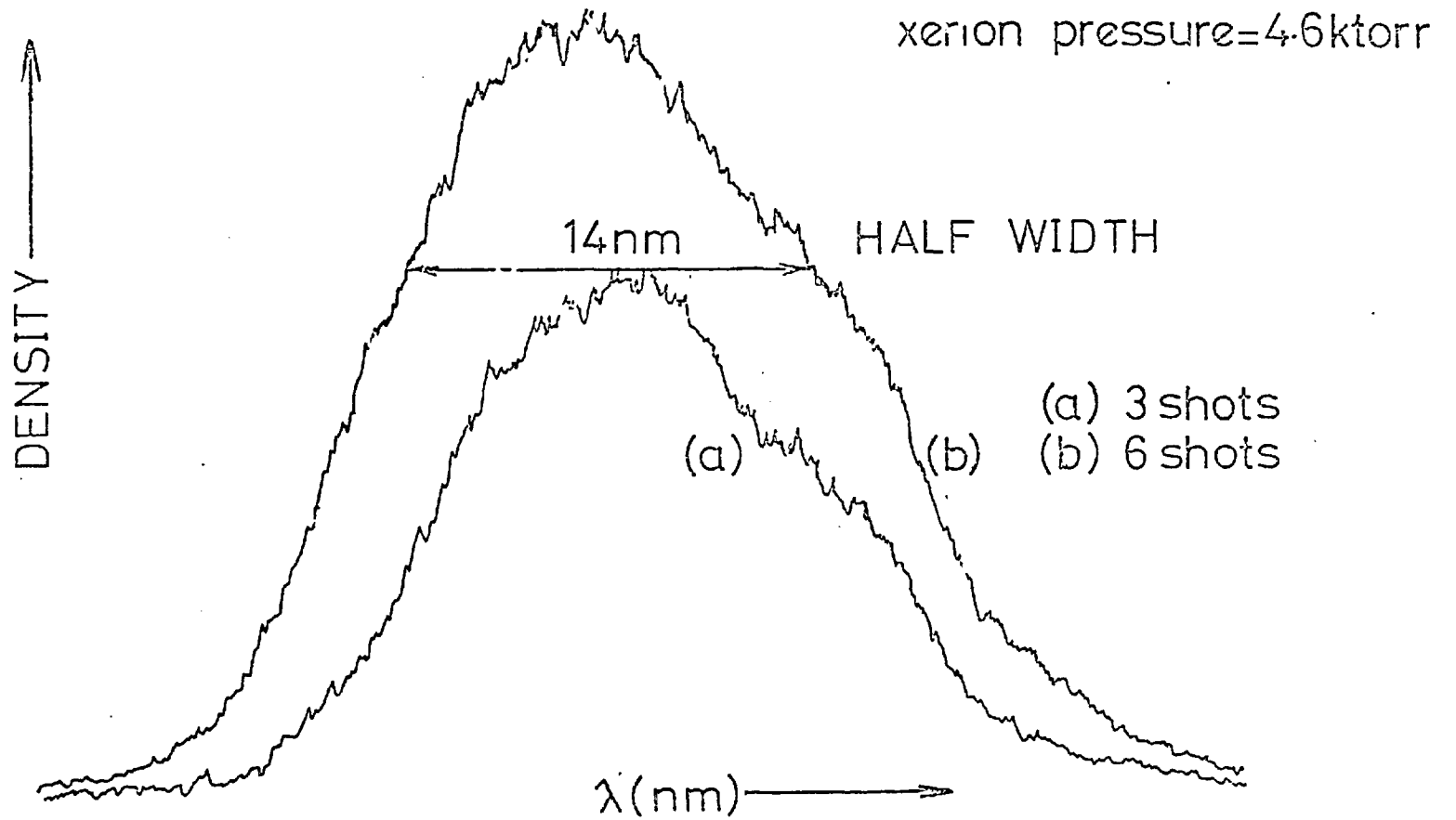


Fig 9

The mean value of γ is in good agreement with that observed by Burton et al. (57) who, using a noble gas microwave discharge as the calibration source and film exposure times between 1 and 120 s, found that at 174.5 nm the film γ was constant at 1.0 for film densities in the range of 0.3 to 2.0. This agreement indicates that the film is not subject to reciprocity failure even though the duration of the exposure is of the order of nanoseconds. A value of $\gamma = 1$ was used to measure the spectral half width, and errors quoted to allow for both spectral resolution and variation in γ . It has been suggested by Fowler et al. (58) and also by Burton et al. (57) that there may be a large variation in film sensitivity between different batches of film (greater than a factor of 2), so absolute measurements of energy were not estimated from spectral results.

The film holder was modified so that one edge of the film could be calibrated and the calibration was carried out using a hydrogen discharge lamp. Spectra were recorded at different xenon pressures, and in all cases a broad structureless continuum was observed with a half width of (13.5 ± 1.5) nm. A variation of the half width of the spectra with pressure has been reported (39) (55). Whilst it was not possible in this experiment to measure the variation accurately, owing to the uncertainty in the film γ and to the low spectral resolution (1.7 nm), it was observed that for pressures greater than 7.5 ktorr, the half widths were consistently less than those for pressures of less than 7.5 ktorr.

The position of the peak wavelength was also measured at different pressures, and the variation with pressure is shown in fig 10. The peak shifted towards the red as the pressure increased, and this is consistent with results reported by other groups (39) (59).

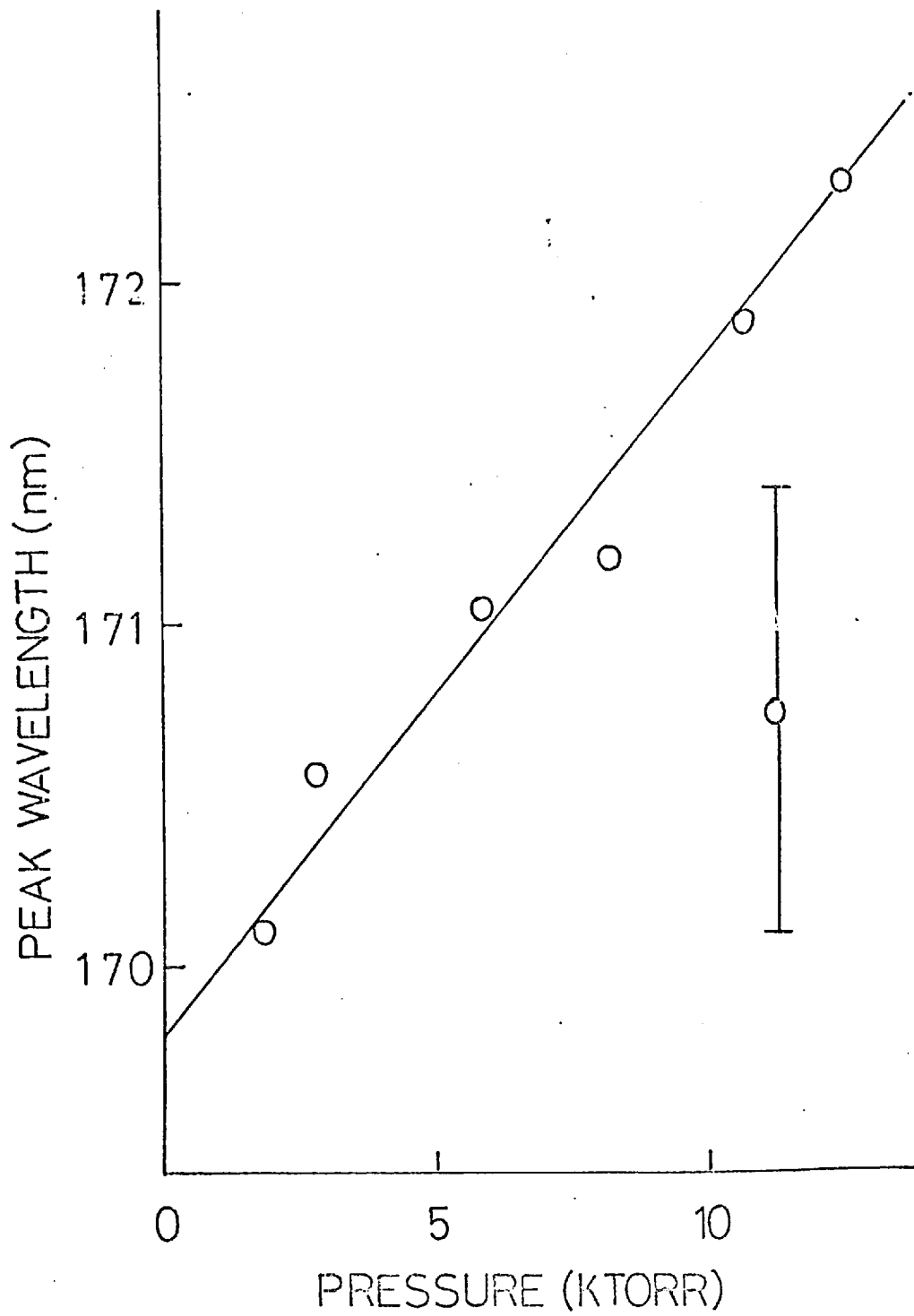


Fig 10

Various explanations have been proposed for this result. Both Koehler et al. (39) and Gerardo et al. (60) suggested that the narrowing and peak shifts are due to increasing absorption from the ground state molecules. If the absorption is stronger at shorter wavelengths then the shorter wavelength region will be eroded more quickly, so that the peak will shift to the red and the spectrum will narrow. A similar result will be caused by absorption due to an impurity in the xenon gas, such as oxygen, whose absorption coefficient increases as the wavelength decreases. It is also possible that the spectral shift and narrowing is due to the distribution of population in the upper state (61) which is determined by vibrational relaxation in collisions with ground state atoms (43). At low pressures, radiation will occur from higher vibrational levels than those observed at higher pressures. Depending on the shape of the potentials of the upper radiating states and repulsive ground state, spectral narrowing and a shift to the red may occur as the pressure increases.

3.6 THE VISIBLE EMISSIONS FROM XENON

For xenon pressures of greater than 1 ktorr, the complete spectral range from 140 to 700 nm was scanned and no emissions other than those in the wavelength region of 170 nm, were observed. The S-20 diode which was used to detect the VUV fluorescence, was sensitive to radiation up to 700 nm and when the photodiode line was at atmospheric pressure no signal was observed, indicating that there was no appreciable signal at wavelengths greater than 200 nm. This was confirmed spectrally using a Monospek 600 spectrograph and Polaroid 3000 ASA Film. The wavelength range from 140 to 200 nm was scanned spectrally using a 1 m normal incidence spectrograph and Kodak SC7 film.

At pressures of less than 0.8 ktorr, however, radiation at a wavelength greater than 170 nm was observed. This was detected by the S-20 diode.

The output signal observed when the photodiode line was evacuated, was made up of two signals (see plate 3); a fast signal with duration of about 15 ns and the slower VUV signal. If the diode line was at atmospheric pressure the VUV signal disappeared while the other remained unchanged. This radiation was found to occur at approximately 310 nm. To obtain the spectrum, a spectrograph slit width of 1 mm was used, which gave a resolution of the order of 1 nm and several shots were superimposed. Since the measured spectral width was of the order of 1 nm it appeared that the emission was line radiation. The origin of this radiation is still uncertain but it may be due to radiative recombination of the xenon atomic ion (62).



As the xenon pressure increases the removal of the atomic ions by 3-body recombination increases, so that the number of ions which can undergo radiative recombination decreases. The rate of reaction 3.16 is not known but from values for other atoms, the rate is of the order of $10^{-12} \text{ cm}^3 \text{ s}^{-1}$ (62).

3.7 MEASUREMENT OF FLUORESCENCE EFFICIENCY

The total fluorescence efficiency from high pressure xenon was determined experimentally, where efficiency was defined as the percentage of the electron energy deposited in the gas, which was converted to VUV photons. The photodiode was placed 25 cms from the excited volume and the viewing aperture was 1 cm in diameter. Assuming that the photons were radiated into 4π , then approximately 0.01% of the total signal was incident on the diode. The signal measured by the photodiode at a pressure of 8.5 ktorr, after correction for attenuation, was approximately 200 Watts and thus the total power radiated from the cell was of the order of 2 MW in a pulse of 10 ns (FWHM).

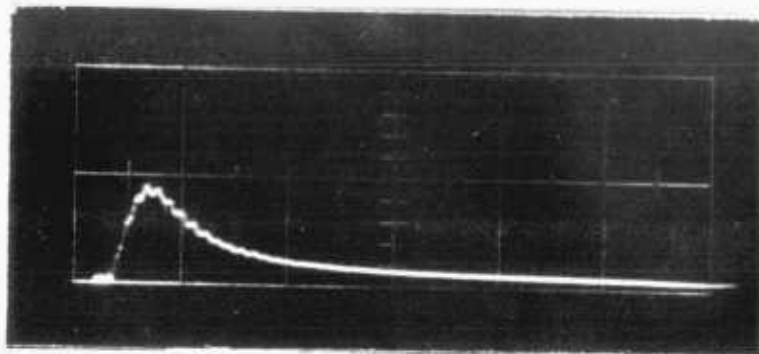
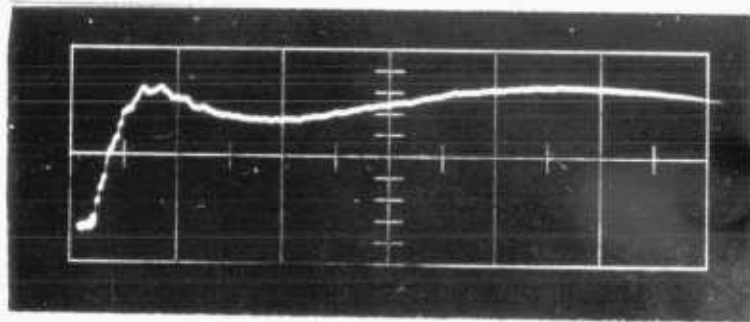
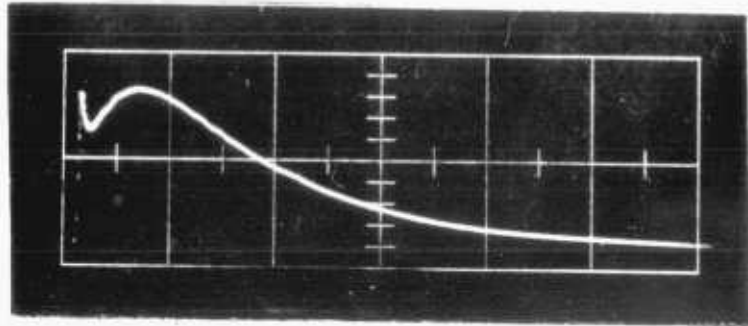
PLATE 3

Temporal Dependence of Visible and Vacuum Ultraviolet Radiation
at 0.76 ktorr

- (a) the fast component is due to visible radiation and the slow component is due to VUV radiation
timescale : 50 ns per major division

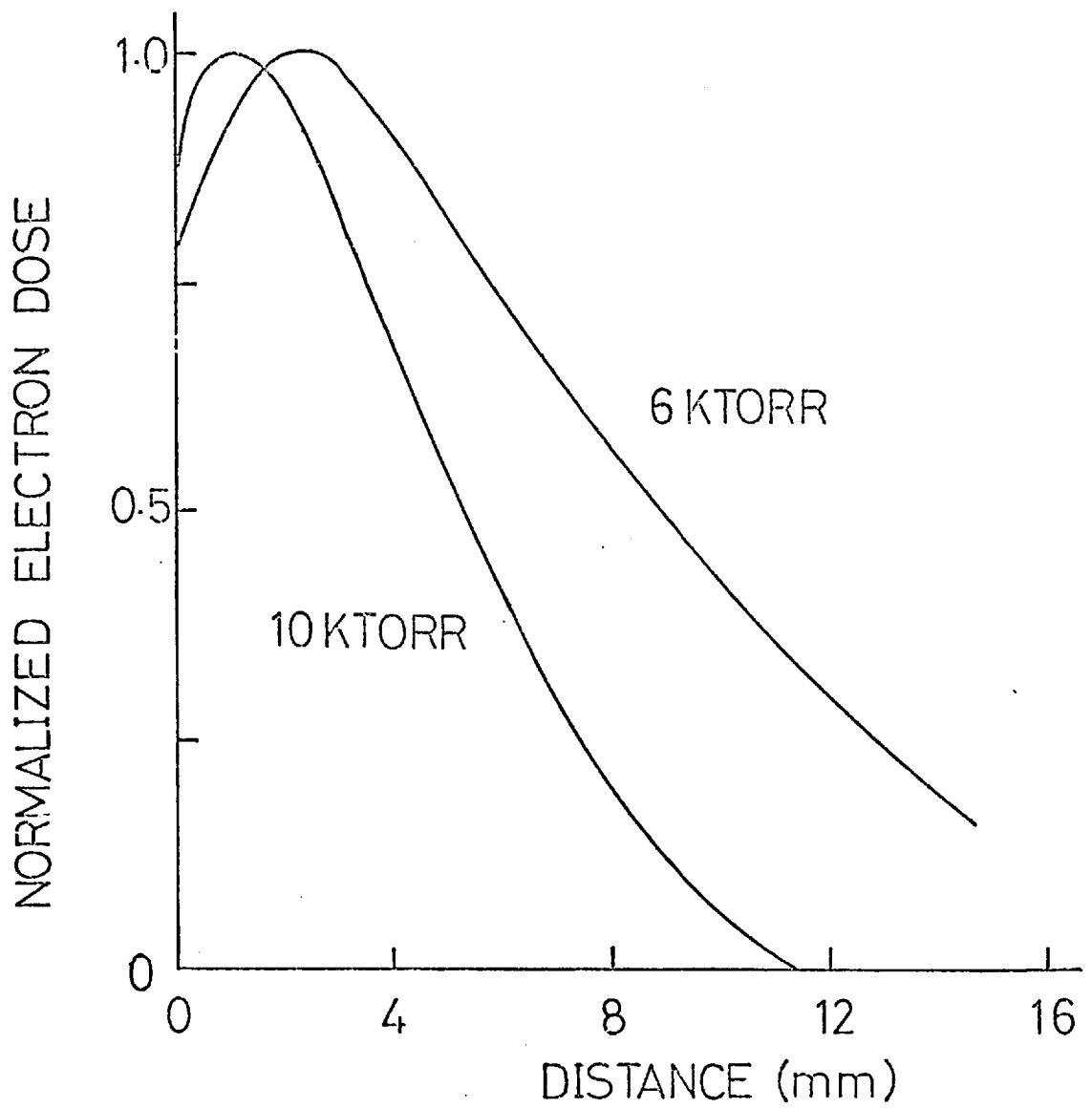
- (b) as (a) but with
timescale : 10 ns per major division

- (c) visible component only, VUV component attenuated by air
timescale : 20 ns per major division



The total energy deposited in the gas, within the field of view of the diode, was estimated to be 0.3J . This was obtained using the graphs supplied by Field Emission, for the variation of the beam current density, with the distance from the diode output foil, the area of the slot through which the electrons passed and the electron deposition obtained from pinhole photographs (see fig 11). An efficiency of about 7% was found which compares well with the 10% measured by Koehler et al. (39) and 6% obtained by Johnson et al. (60). Both these latter results were obtained using a Febetron 705 excitation source which gave a 50 ns pulse of electrons. The variation of fluorescence efficiency with pressure was not measured, as it was difficult to determine accurately the fraction of radiation within the field of view of the diode, over a range of pressures.

Some of the loss mechanisms were discussed in Chapter 2 and also earlier in this chapter. Additional loss mechanisms were suggested by Fournier (35), whose model predicts a fluorescence efficiency of 12%. The maximum theoretical efficiency which can be obtained by relativistic electron excitation of high pressure xenon is about 53% (derived in Section 2.3). Fournier suggests that this is further reduced by about 50% as only half the levels in the cascade manifold decay to the levels which form the excited molecule, due to the selection rule: $\Delta J = 0, \pm 1$ (16). Furthermore he suggests that the energy will be partitioned between the $3\Sigma_g^+$ and the $1\Sigma_g^+$ levels, in addition to the $3\Sigma_u^+$ and $1\Sigma_u^+$ levels. The former two states cannot radiate to the $1\Sigma_g^+$ ground state owing to the selection rule $g \leftrightarrow g$. Transitions $1\Sigma_g^+$ to $1\Sigma_u^+$ and $3\Sigma_g^+$ to $3\Sigma_u^+$ can occur, and Fournier attributed the 96 ns lifetime of Keto et al. (40) and the 500 ns lifetime of Boucique et al. (42) to be the lifetimes of these transitions, respectively. At times long compared with the fluorescence decay time the feedrate from these levels then controls the radiative decay of Xe_2^* . In the experimental



Electron dose measured from pin-hole photographs of the fluorescence from xenon.

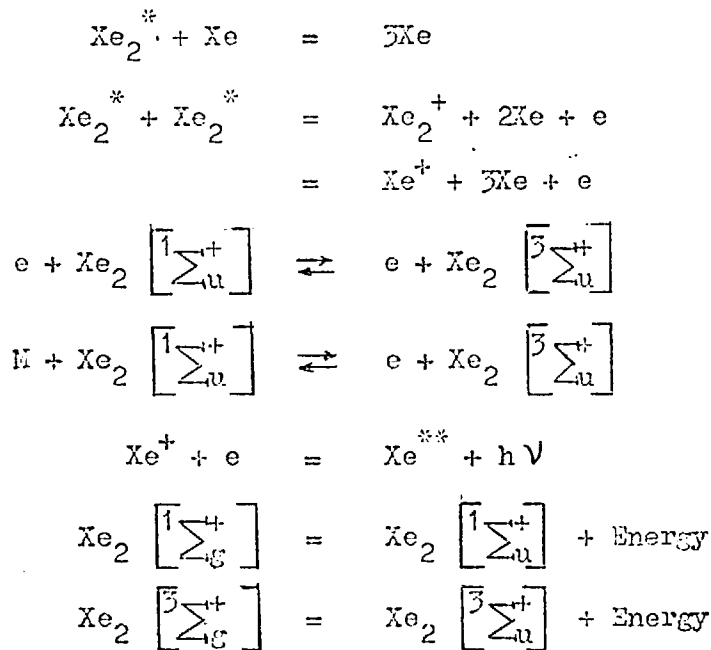
Fig 11

measurements of efficiency, only the energy emitted in the initial pulse is considered, the contribution from the tail being ignored, so that the energy deposited in the $1\sum_g^{++}$ and $3\sum_g^{++}$ levels, is not included.

The reactions which have been discussed in this chapter are summarised in Table 3.1 below.

TABLE 3.1

SUMMARY OF REACTIONS.



THE DESIGN OF COAXIAL ELECTRON BEAM DIODES

A prerequisite of any efficient laser is an efficient utilisation of the pumping energy. It has been shown that the maximum theoretical efficiency obtainable from pure xenon excited by relativistic electrons, is 53%, compared with an experimentally observed value of 10%. This efficiency is defined as the ratio of the total fluorescence output to the energy deposited within the line of sight of the detection system. The overall efficiency was low as only a small percentage of the total energy entered the gas and was used for excitation.

Two methods to achieve efficient coupling of electrons into the gas were investigated. In the first, electrons were drifted through a tapered copper cone which was maintained at a pressure of a few torr. This method has been used successfully for pulses with durations of tens of nanoseconds but very little data is available for pulses of less than 10 ns. Secondly a novel coaxial electron beam diode was designed and constructed which gave an efficient and reproducible coupling of electrons into the high pressure gas. This diode was modified and improved to provide a compact and reliable pumping source for the xenon laser. The reproducibility of the electron beam output was important, as it enabled an accurate determination of some of the laser parameters to be made.

4.1 ELECTRON BEAM DRIFTING

The efficient transport of an intense beam of relativistic electrons, by injection into a metallic guide tube filled with a neutral gas, has become important in electron beam technology. Beams can be focussed using a gently tapering cone so that high current densities can be achieved without the application of large magnetic fields. This enables

experiments, such as target and X-ray studies, to be carried out well away from the diode, thus reducing the risk of damage to the emitting cathode. Most of the experimental work reported has been performed using electron beams with pulse durations of the order of tens of nanoseconds and with total energies in the range of hundreds of joules. There is little data available on short pulse, low energy beams.

The mechanism of cone focussing is complex and many theoretical explanations have been put forward ⁽⁶³⁾. A simple explanation is outlined here ⁽⁶⁴⁾. Consider a relativistic electron beam in vacuum. The total force, F , acting on an electron at the surface of the beam, is given by the Lorentz equation:

$$\underline{F} = e (\underline{E} + \underline{v} \times \underline{B}) \quad (4.1)$$

$$= \underline{F}_e + \underline{F}_m \quad (4.2)$$

where \underline{E} is the electric field

\underline{B} is the magnetic field

\underline{v} is the velocity of the electron

\underline{F}_e is the electric component of the force

\underline{F}_m is the magnetic component of the force

The magnetic field appears in the "laboratory" frame because of the application of a relativistic transformation to the electric force from a frame moving with velocity \underline{v} . In this frame the charge is stationary and hence creates an electric field according to Coulomb's law.

It can be shown ⁽⁶⁵⁾ that

$$\underline{F}_m = - \underline{F}_e \beta^2 \quad (4.3)$$

$$\text{where } \beta = \frac{v}{c}$$

c = velocity of light

$$\text{so that } \underline{F} = \underline{F}_e (1 - \beta^2) \quad (4.4)$$

and since the electric force is repulsive, the net force is also repulsive because $\beta^2 < 1$.

As the pressure is increased, ionization of the gas occurs in the beam. These secondary electrons are repelled to the walls and thus leave a surplus of positive ions which tend to neutralize the beam. The ions then set up an electric field opposite to that of the field of the electrons so that

$$\underline{F} = \underline{F}_e (1 - \beta^2) - \underline{F}_i \quad (4.5)$$

where \underline{F}_i = component of the force due to the ions
 If $\underline{F}_e (1 - \beta^2)$ equals \underline{F}_i , then there is no net force on the beam so that the beam should travel unchanged, but if \underline{F}_i is greater than $\underline{F}_e (1 - \beta^2)$, then focussing occurs. Before neutralization or focussing can occur it is necessary to create ions and, for a short pulse, the time required to form them may be significant compared with the pulse duration. The ionization time may be estimated using the following analysis.

Assume that the pulse of electrons has a linear risetime, t_0 , so that the current density, $J(t)$, is given by

$$\begin{aligned} J(t) &= \frac{j_0 t}{t_0} \\ &= n_b e v \end{aligned} \quad (4.6)$$

where j_0 = peak beam current density

n_b = electron flux

e = charge

v = velocity

then

$$n_b = \frac{j_0 t}{t_0 e v} \quad (4.7)$$

Now

$$n_e = \int_0^t n_b \sigma N v dt \quad (4.8)$$

where n_e = number of electrons formed by ionization

σ = ionization cross section

N = number of atoms per unit volume

Substituting for n_b and integrating equation 4.8, gives

$$n_e = \frac{j_o \sigma N t^2}{2t_o e} \quad (4.9)$$

So at time, $t = \frac{2}{\sigma N v}$,

the number of electrons formed by ionization, n_e , and hence the number of positive ions, equals the electron flux n_b .

Substituting the approximate experimental values:

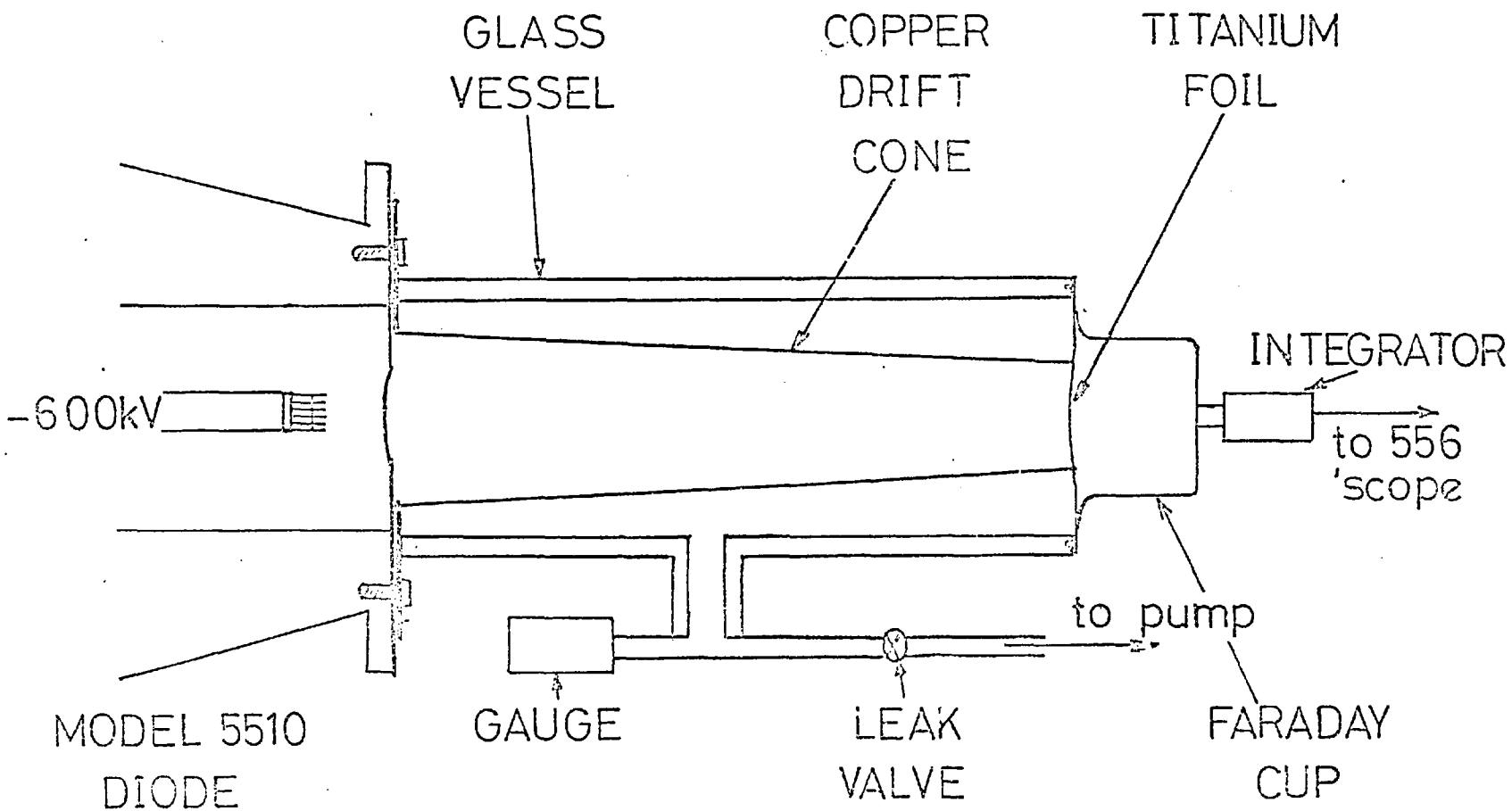
$$\sigma = 2 \times 10^{-18} \text{ cm}^2 \quad (66), \quad N = 10^{17} \text{ cm}^{-3}, \quad v = 2.5 \times 10^{10} \text{ cm.s}^{-1}$$

then $t = 0.4 \text{ ns}$

This indicates that the drifted pulse duration should be about 0.4 ns less than the undrifted pulse.

An experiment was designed to measure the optimum pressure and the overall efficiency, and to investigate the reproducibility for drifting and focussing electrons from a model 5510 commercial electron beam diode. The experimental set up is shown in fig.12. The copper cone was 128 mm long and tapered from 40 mm at the input end to 25 mm at the output. A copper flange was soldered to the cone and this was held firmly in contact with the Febetron to provide a path to earth for the return current. The cone was enclosed in a glass vessel which was evacuated using a rotary pump. A leak valve was then used to increase the air pressure inside the cone and this pressure was read on a McLeod gauge, accurate in the range 0.1 to 10 torr. The total beam current was measured using a Faraday cup and integrating circuit, and feeding the signal into a Tektronix 556 oscilloscope. Electrons from the diode drifted through the cone and passed through an earthed 0.025 mm titanium foil before being collected. This signal was then compared with that obtained when the Faraday cup was placed close to the diode with the cone removed; a 0.025 mm foil was placed in front of the Faraday cup so as to keep the collection geometry the same. Fig 13 shows how the efficiency varied with air pressure in

EXPERIMENTAL ARRANGEMENT FOR DRIFTING



4.9
Fig 12

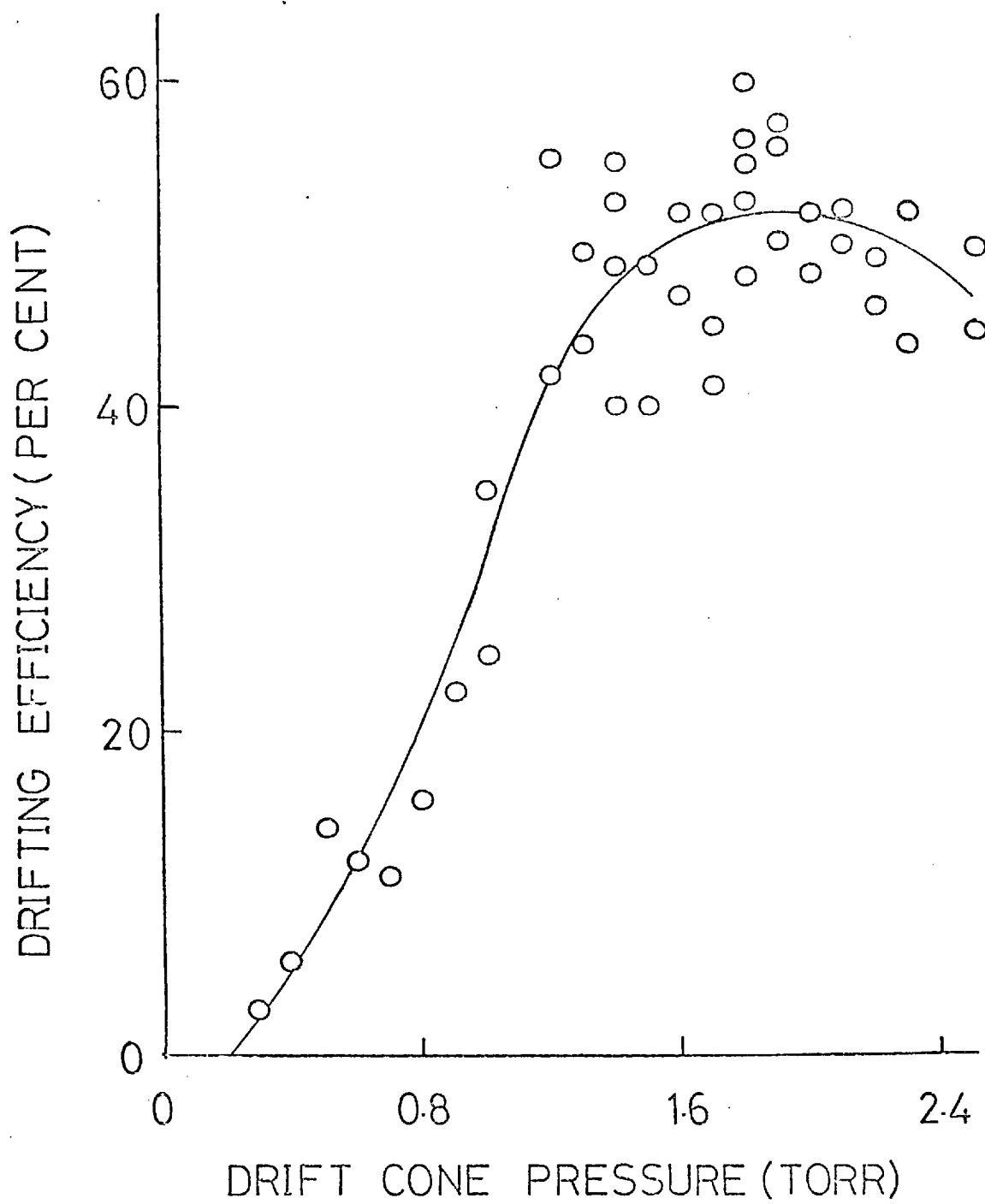


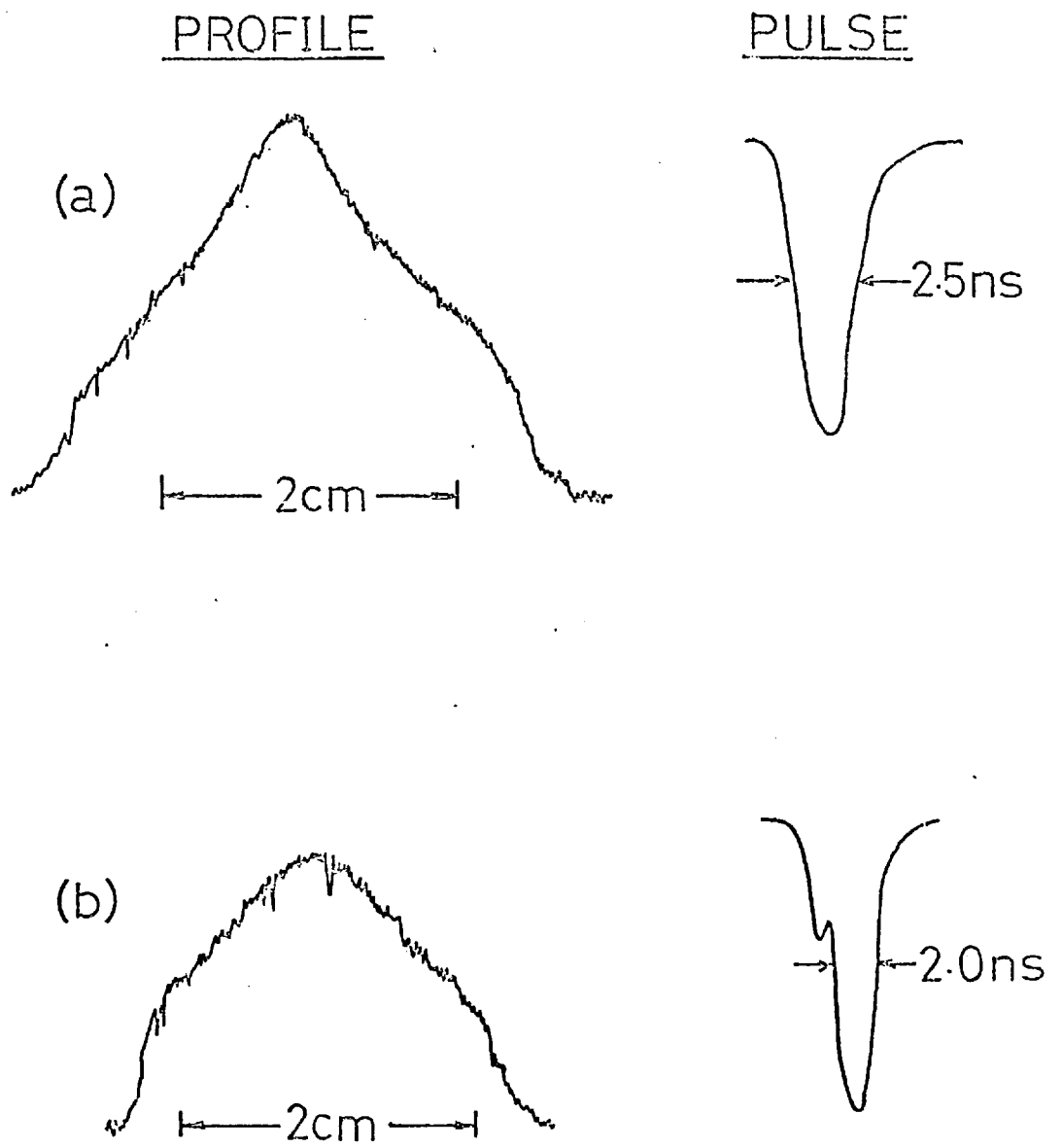
Fig 13

the cone. The highest efficiency achieved was about 60%, this was recorded at a pressure of approximately 1.8 torr. Efficiency increased rapidly in the pressure range 0.2 to 1.8 and then fell off slowly at higher pressures.

The pulse duration (FWHM) was determined by aperturing the Faraday cup and monitoring the signal on a Tektronix 519 oscilloscope with a time resolution of about 0.5 ns. A value of about 2 ns was obtained for the drifted beam compared with 2.5 ns for the undrifted beam, as shown in fig 14. This difference is consistent with the calculated value of 0.4 ns so that the change in pulse duration may be attributed mainly to the finite time required to create ions to neutralize the beam.

The beam profile was measured by bleaching Avisco 1950HS Light Blue Cellophane. The dose was determined by taking a densitometer trace at the wavelength 655 nm and then comparing with the calibration curve of dose against density, as provided for this material (68). Fig 14 shows the beam profile with and without the cone. The overall shape of the focussed and unfocussed beams is similar, with the diameter of the focussed beam being reduced to that of the output aperture of the cone.

From these results, it was concluded that electron beam drifting was not a satisfactory method for efficiently coupling electrons into the gas. For a given gas pressure in the cone, the shot to shot variation was of the order of 20% which would make quantitative work on the laser very difficult. As transverse pumping is still used, a thin foil separating the low pressure drift cone region and the high pressure gas is required, so that it would be necessary to devise a method to minimise the effect of foil distortion.



(a) Undrifted e-beam

(b) Drifted e-beam

Fig14

4.2 CALCULATION OF THE COAXIAL DIODE PARAMETERS

In order to overcome many of the difficulties associated with efficiently pumping high pressure gases with relatively low energy electrons, a completely new coaxial electron beam diode was designed and constructed (67). It consisted of a thin walled stainless steel anode tube, maintained at earth potential, and a field emitting cathode, surrounding the anode, which was pulse charged to -- 600 kV. The electrons emitted from the cathode were accelerated towards the anode and they penetrated the tube wall before exciting the high pressure gas which was contained in the anode tube. As these electrons entered the gas from all sides, the penetration depth was effectively increased, allowing a larger volume to be excited uniformly than was possible with a transverse pumping geometry. Also the total excited volume was in the line of sight of the laser mirrors. The total electron energy was distributed more evenly over a longer length than was achievable with the commercial diodes. This enabled the ratio of the excited length of the gas to mirror separation to be reduced.

The dimensions of the coaxial diode were calculated from the equations for space charge limited flow of current between concentric cylinders. Space charge effects must be considered because of the high current densities in these field emission devices. Consider the case of a cylindrical anode surrounded by an electron emitting cylindrical cathode (69). Assume that electrons escape without initial velocity, therefore the potential, V , at any point is given by

$$\frac{1}{2}mv^2 = Ve \quad (4.10)$$

where m = electron mass

v = velocity

e = charge

The Child-Langmuir law holds under these conditions, so current density,

J is given by

$$J = kV^{\frac{3}{2}} \quad (4.11)$$

where k is a constant.

Assume also a radial electron flow between the cathode and the anode, so that only one co-ordinate, r, is involved, then the Poisson equation is of the form:

$$\frac{d^2 V}{dr^2} + \frac{1}{r} \frac{dV}{dr} = -4\pi\eta \quad (4.12)$$

$$\text{where space charge, } \eta, \text{ is equal to } \frac{J}{v} \quad (4.13)$$

Eliminating v in equation (4.10) and substituting into equation (4.12) gives

$$\frac{d^2 V}{dr^2} + \frac{1}{r} \frac{dV}{dr} = 2(2)^{\frac{1}{2}} \left(\frac{m}{e}\right)^{\frac{1}{2}} Jv^{-\frac{1}{2}} \quad (4.14)$$

Define two new variables a and b such that

$$a = \ln \frac{r}{r_0} \quad (4.15)$$

where r_0 is the cathode radius

$$\text{and} \quad J = \frac{1}{9\pi} \left(\frac{2e}{m}\right)^{\frac{1}{2}} \frac{v^{\frac{3}{2}}}{r^2 b^2} \quad (4.16)$$

By eliminating J and r in equation (4.13), then

$$\frac{d^2 V}{da^2} + \frac{dV}{da} = \frac{4}{9b^2} V \quad (4.17)$$

The current, I, flowing between the cathode and the anode is independent of r so that the current density is inversely proportional to r and hence is proportional to e^{-a}

$$\therefore \frac{dJ}{da} = -J \quad (4.18)$$

$$\text{so using (4.16)} \quad \frac{3dV}{da} = 2V + \frac{4V}{b} \frac{db}{da} \quad (4.19)$$

Differentiation of this equation gives an expression for $\frac{d^2 V}{da^2}$ and

substituting into equation 4.17 gives

$$3b \frac{d^2 b}{da^2} + \left(\frac{db}{da} \right)^2 + 4b \frac{db}{da} + b^2 = 1 \quad (4.20)$$

Integration of this equation with the boundary conditions

$$V = \frac{dV}{da} = 0 \text{ at } r = 0 \quad (\text{ie } a = 0)$$

has a solution (70)
$$b = a - c_1 a^2 + c_2 a^3 - c_3 a^4 + \dots \quad (4.21)$$

where c_1, c_2, \dots are known constants.

For $\frac{r_0}{r}$ large, the solution simplifies to

$$b^2 = 4.7612 \frac{r_0}{r} \left[\log_{10} \left(\frac{r_0}{1.4142r} \right) \right]^{3/2} \quad (4.22)$$

For concentric cylinders the current, I , is given by

$$I = 2\pi r_0 L J = \frac{2}{9} \left| \frac{2e}{m} \right|^{1/2} \frac{LV^{3/2}}{rb^2} \quad (4.23)$$

where r = anode radius

L = length of the cathode

Substituting for $\frac{e}{m}$ gives

$$I = \frac{14.66 \times 10^{-6} LV^{3/2}}{rb^2} \text{ A} \quad (4.24)$$

For the Febetron 706

$V = 600 \text{ kV}$

$I = 10 \text{ kA}$

L chosen (see later)

r chosen for optimum electron deposition

r_0 calculated from 4.22 and 4.24

In order to obtain a value for the anode radius, r , it was necessary to look at the variation of electron beam deposition with xenon pressure. Other groups (60) calculated the deposition using Monte Carlo computer routines, but as these were not available this was measured experimentally. It was assumed that the fluorescence intensity

was proportional to the deposition so by taking pin hole photographs of the fluorescence an estimate was obtained for electron dose at different distances into the gas. The transverse pumping geometry was used and electrons from a 5516X diode passed through a 6 mm by 6 mm aperture before entering the gas through a 0.025 mm titanium foil. The aperture was used so that only a small section of the gas was excited resulting in an improved camera resolution. The photographs were recorded on Kodak SC7 film and then densitometered.

Fig 11 shows typical electron beam depositions at 7 ktorr and 10 ktorr. The intensity increased to a peak and then decreased approximately exponentially so that the fall off in deposition could be approximated by

$$E = E_0 \exp(-\alpha l) \quad (4.25)$$

where α = absorption coefficient

l = length

E_0 = peak intensity

The absorption coefficient was found to increase linearly with pressure as shown in fig 15.

In order to calculate the tube dimensions for uniform deposition two assumptions were made:

(i) equation 4.25 was valid

and (ii) the number density of electrons was inversely proportional to the radius

so that the number density at any radius R is given by

$$N = N_0 \frac{r}{R} \exp - \alpha (r-R) \quad (4.26)$$

where r = anode tube radius

By making allowance for the fact that the wall thickness of the stainless

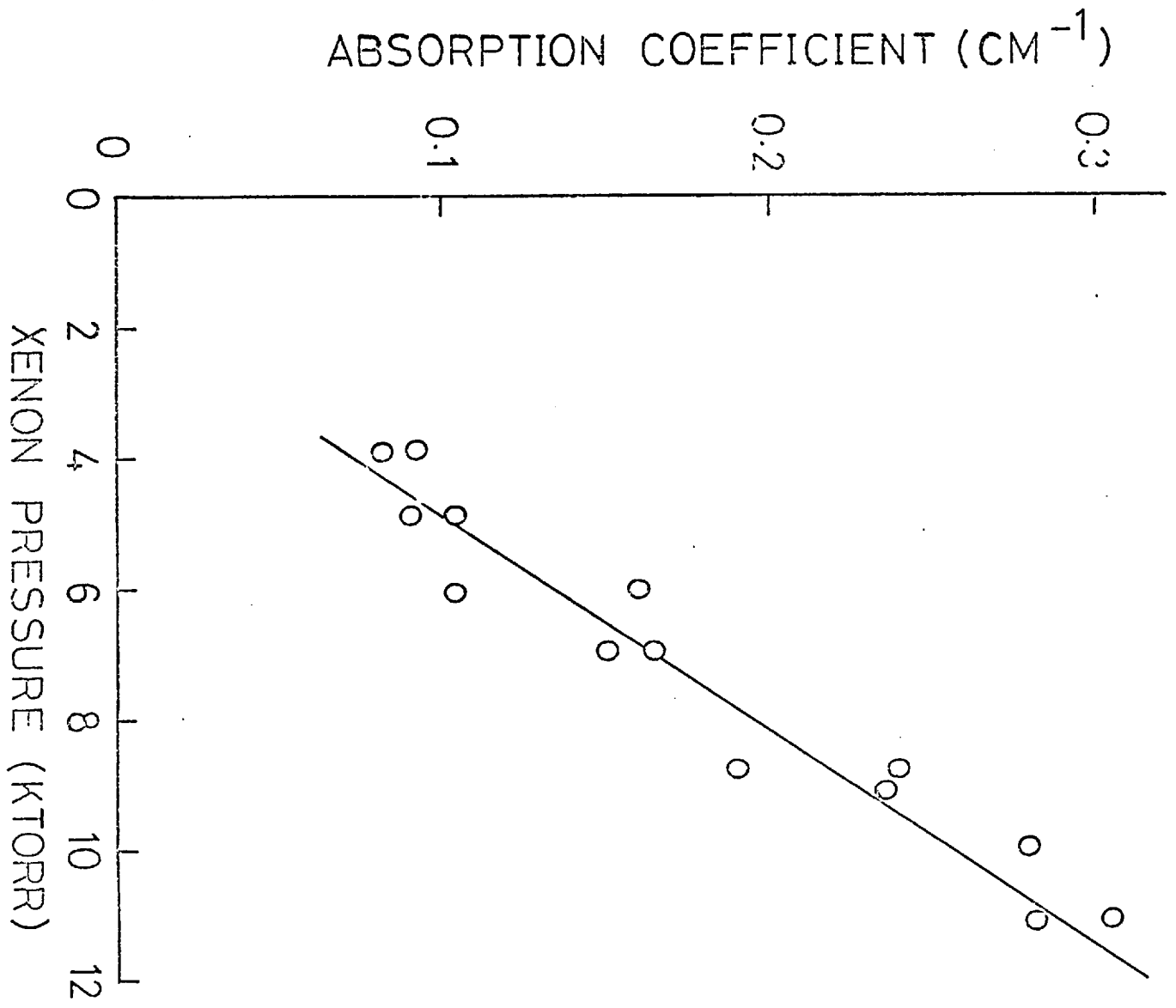


Fig15

steel tube was approximately 0.06 mm compared with the 0.025 mm titanium foil used in the calculation of α , the optimum tube radius was calculated to be approximately 2.2 mm for a xenon pressure of 10 ktorr. From fig 11, it was estimated that about 60% of the electrons which penetrated the tube walls, were deposited in the gas.

4.3 CONSTRUCTION OF THE DIODE

The first coaxial diode (Mark 1), was constructed by modifying a commercial diode so that it could be fitted easily into the existing Blumlein structure, see plate 4 and fig 16. This did, however, put some constraints on the choice of dimensions. In order to prevent breakdown, the cathode conductor was kept a minimum distance of 2.5 cm, (twice the distance between the anode and the cathode), away from other metal surfaces. This condition was satisfied for a cathode conductor of length 7 cm. With an anode radius of 2.2 mm the cathode radius was calculated from equation 4.24 to be 14.65 mm for a diode impedance of 60 ohms. All edges were smoothed and rounded to reduce field intensities and so reduce the possibility of emission from them.

The anode was a 20 cm long stainless steel tube with a wall thickness of 0.15 mm which was machined to a thickness of about 0.06 mm over a length of 14 cm from one end. This end was thin, so that the 500 keV electrons could penetrate the walls with sufficient energy to excite the gas, but still had sufficient strength to withstand high pressures. (A 25 cm stainless steel tube machined to 0.06 mm over 14 cm was static tested to 50 ktorr with no evidence of damage.) From the curves of electron dose against thickness of absorbing medium (supplied by the Field Emission Corporation) it was estimated that about 50% of the electrons penetrate the walls. The kinetic energy lost per electron was calculated from the Bethe Bloch equation⁽⁷¹⁾

PLATE 4

Mark 1 Diode



MARK 1 COAXIAL DIODE

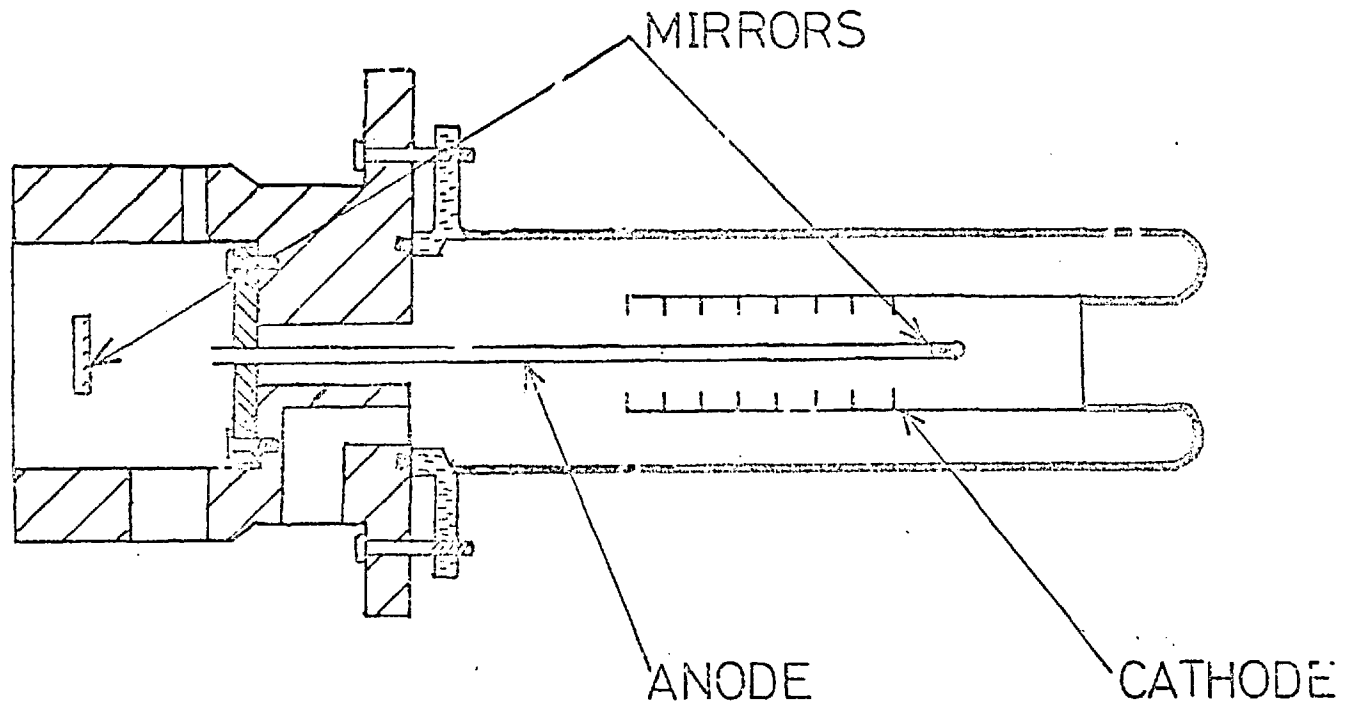


Fig 16

$$\frac{dE}{dx} = 0.153 \varphi \cdot \frac{Z}{A} \beta^{-2} \left[\ln \frac{E(E + mc^2)^2 \beta^2}{2I^2 mc^2} + (1 - \beta^2) \right] - (2 \sqrt{1 - \beta^2} - 1 + \beta^2) \ln 2 + \frac{1}{8} (1 - \sqrt{1 - \beta^2})^2 \Big] \text{keV} \cdot \text{g}^{-1} \cdot \text{cm}^2 \quad (4.27)$$

where E = kinetic energy of incident electron

Z = atomic number

A = atomic weight

φ = density

I = mean atomic excitation potential

$\beta = \frac{v}{c}$

For 500 keV electrons passing through 0.06 mm stainless steel, the energy loss is approximately 50 keV.

The thin end of the tube was sealed using a stainless steel plug which was soldered in position. The unmachined end was pushed through a hole in a stainless steel plate, making sure that there was good electrical contact between the plate and the tube, and then fixed to the plate using Araldite epoxy resin. This plate was bolted to the inside of the cavity with the anode tube passing through a hole in the base of the cavity and concentric with the cathode. A seal between the high pressure cavity and the evacuated diode region was achieved by means of a "Viton" O-ring, so that the retaining bolts also acted as an earth return path for the electrons.

The first type of cathode used, was granulated carbon (Poco Graphite Inc.) which has been designed for field emission devices. The cathode had an internal radius of 14.65 mm and length of 7 cm as explained earlier, and was inserted inside the cathode conductor. The diode was continuously pumped to approximately 10^{-4} torr using a mercury diffusion pump. No change in dose was observed for pressures in the range 10^{-3} to 10^{-5} torr for any of the cathodes which were tested. Electron dose was measured

using Avisco cellophane and then densitometered at 655 nm. These measurements were not used to give quantitative results but only to give an indication of the uniformity of deposition. The energy was measured directly using a calibrated copper-constantan thermocouple and the output was recorded using a pen recorder (Smith's Servoscribe). One end of the thermocouple was in contact with a 2 cm long stainless steel cylinder with wall thickness 0.15 mm which was inserted inside the anode tube. The 0.15 mm walls ensured that all electrons which penetrated the anode tube were stopped in the cylinder. The cylinder was well insulated from the anode tube walls, so that the true deposited energy was measured. By placing the cylinder at various positions along the tube the total electron energy entering the tube was measured. The total electron energy obtained from the carbon was only about 1 J and so was abandoned due to low efficiency.

A new type of cathode was constructed by perforating a 0.075 mm sheet of titanium foil so as to produce a series of sharp points. The cathode was then rolled into a cylinder and slipped inside the cathode conductor with the spikes arranged radially. This is illustrated in plate 5. The optimum number of spikes per unit area was determined experimentally and turned out to be about 5 cm^{-2} . If fewer spikes per sq cm were used, the electron deposition was not uniform, and increasing the number of spikes gave no improvement in performance. Fig 17 shows 2 densitometer traces of the deposition, measured using Avisco cellophane. In (b) the separation of the peaks is equal to the spike separation, whereas in (a) with $5 \text{ spikes} \cdot \text{cm}^{-2}$ the periodic variation is less pronounced. The random variations can be accounted for by the non-uniformity in the wall thickness of the anode tube and the variation in the length of the spikes on the cathode. The circumferential variation was similar to that observed longitudinally. The total energy which penetrated the anode tube was about 5 J, distributed as

PLATE 5

Mark 1 Diode Illustrating the Radial Arrangement of the
Cathode Spikes

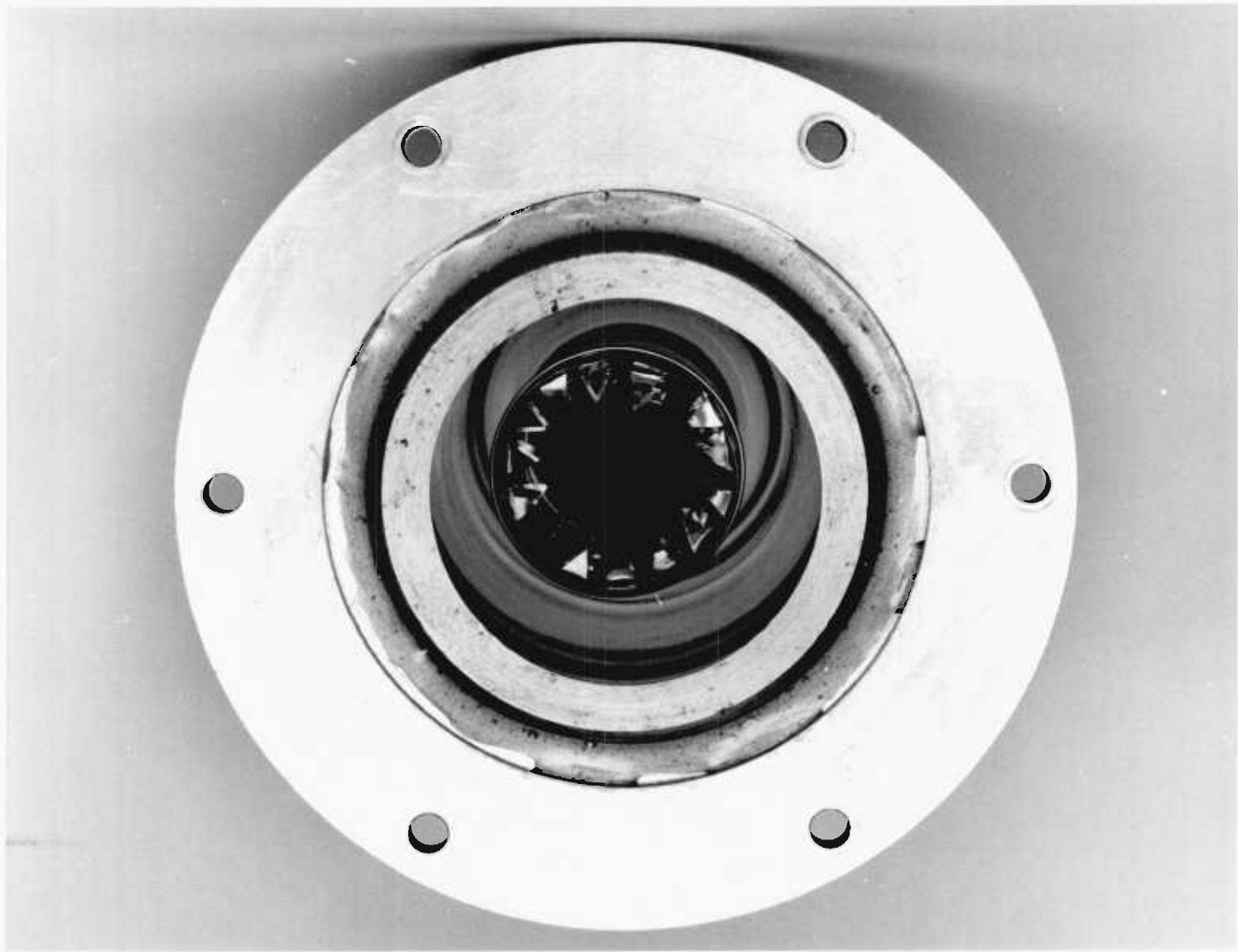
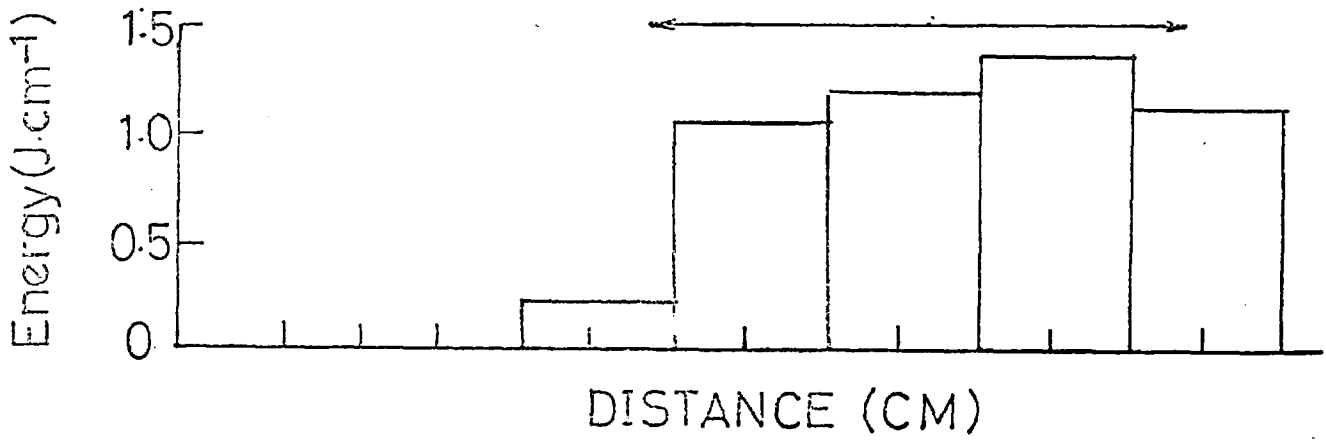
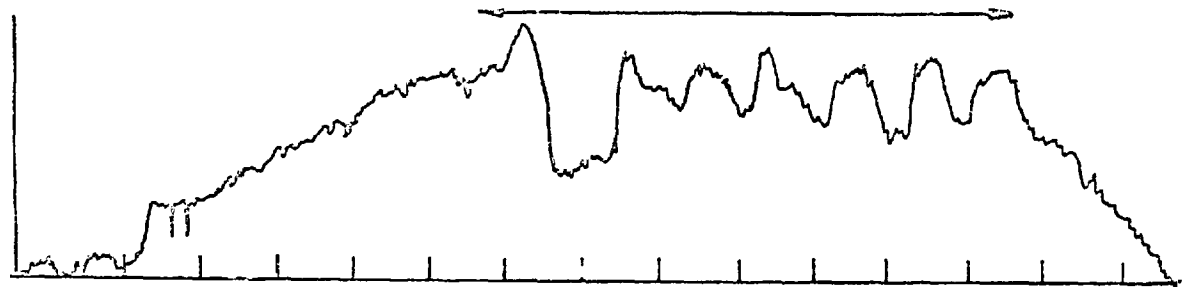
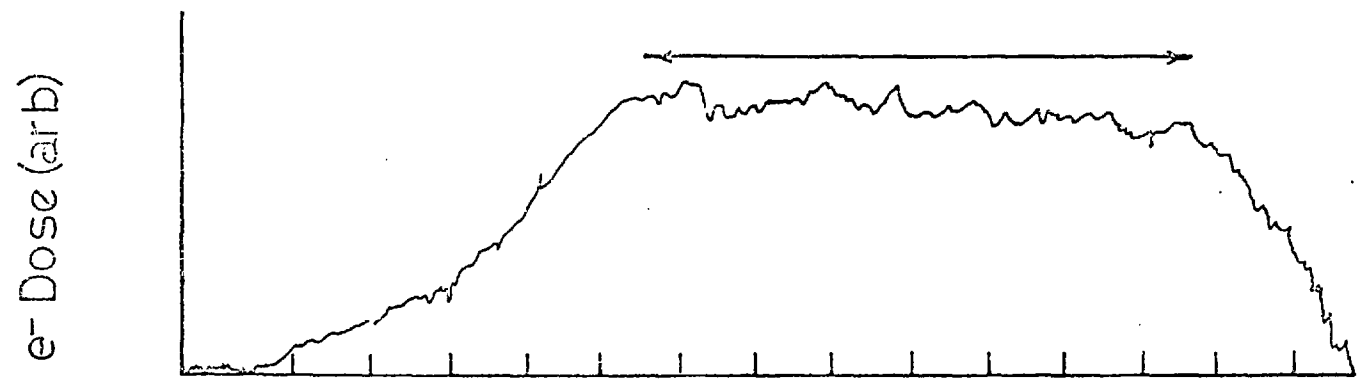


Fig 17



(a)

arrow indicates cathode position

(b)

results for MK1 diode

(c)

shown in fig 17c. This deposition profile was obtained using the calibrated thermocouple. The excited length was about 8.5 cm compared with a cathode length of 7 cm, this was due to end effects on the cathode and also to electron scattering in the tube walls. Using this arrangement, laser action from high pressure xenon with powers of about 1 MW, was achieved (see Chapter 5).

4.4 MODIFICATION OF THE DIODE

The diode (Mark 1) described in the previous section had the serious disadvantage that one end was inaccessible when the system was evacuated or under pressure. This meant that one of the laser mirrors had to be aligned before assembling the system. It was necessary, too, for the reflector, which was sealed in one end of the narrow bore tube, to have an overall diameter of less than 4 mm. If this reflector was damaged the complete system had to be dismantled. It was also difficult to design an arrangement for tuning the laser.

A new coaxial diode (Mark 2) was designed and constructed to overcome the above difficulties by allowing access to both ends of the anode tube. The experimental arrangement is shown in fig 18. The anode radius was the same as that for the Mark 1 diode (2.2 mm) and the tube was machined to approximately 0.06 mm over a length of 8 cm either side of the centre. The overall length of the anode tube was 22.5 cm. The cathode length was increased to 10 cm, so for a diode impedance of 60 ohm, the cathode radius was calculated to be 1.9 cm, using equations 4.22 and 4.24. In practice, a cathode of radius 1.75 cm was used to give optimum deposition, corresponding to an impedance of about 56 ohm. The impedance was changed by varying the length of the spikes on the cathode, and over the range of 50 to 65 ohm, a change of less than 10%, averaged over about 20 shots, was observed in the output.

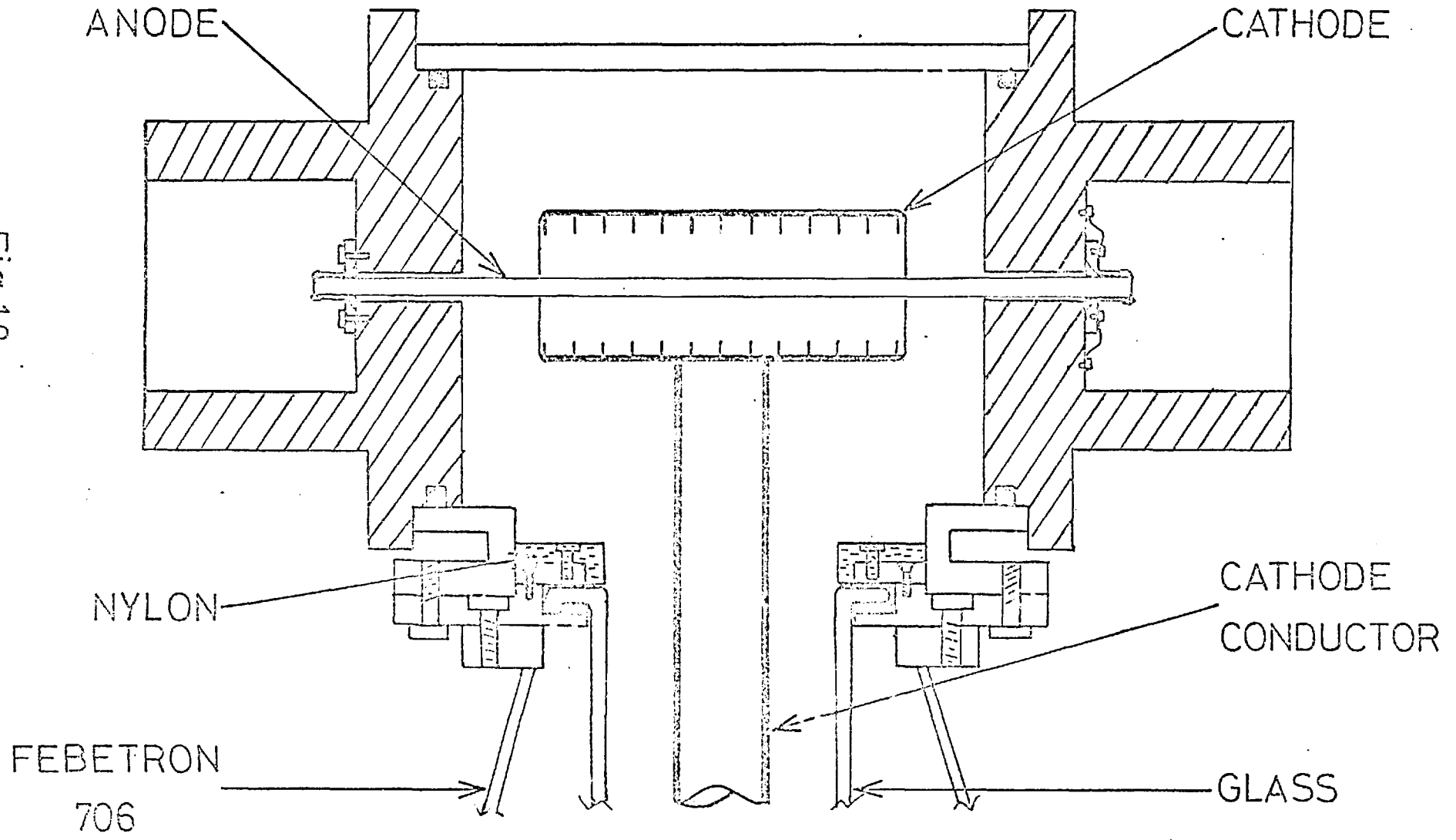


Fig 18
64

The cathode was made, as described earlier, from a 0.075 mm thick sheet of titanium foil. This cathode was inserted inside a cylinder which was fixed at right angles to the cathode conductor. A nylon cover was placed over all components where breakdown was likely to occur, and care was taken to round off all metallic edges.

In order to check the pulse propagation along the cathode conductor and also the impedance matching, a model was constructed to simulate the diode conditions. The dimensions of the model were selected to give a characteristic impedance of 50 ohm, so that the signal could be monitored directly on a Tektronix 7904 oscilloscope. The cathode impedance was approximated by eight 400 ohm carbon resistors, connected in parallel between the anode and cathode.

A 4 ns pulse from a Type 1 pulse generator (impedance 50 ohm), was fed into the 7904 oscilloscope via a matched T-piece. The other arm of the T-piece was then terminated by various methods. Plate 6 shows the signal under 3 conditions:

- (i) signal terminated in 50 ohm
- (ii) signal terminated by the diode
- (iii) signal not terminated

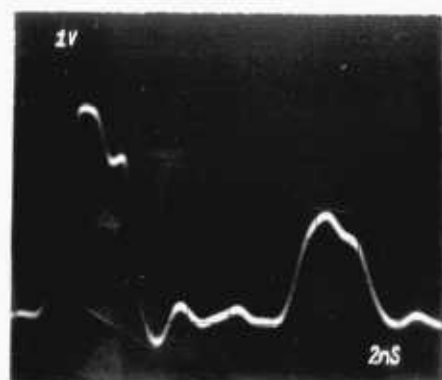
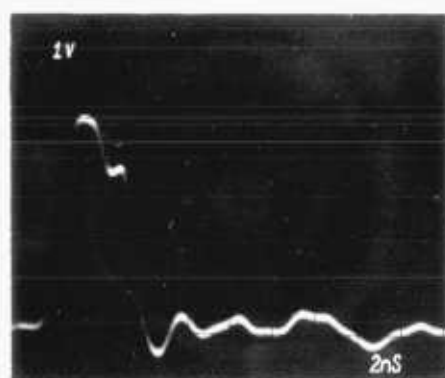
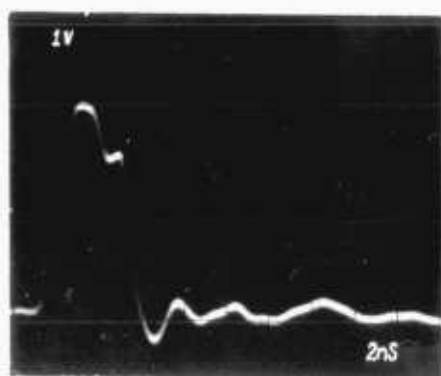
In case (iii) with no termination (open circuit), a reflected pulse is evident, whereas in (i) and (ii) there is negligible reflection. If the diode impedance was altered by inserting a dielectric, the reflected signal increased indicating that the system was mismatched. This simple model appeared to confirm the principle of construction.

In the Mark 1 diode the anode tube was free to expand when it was heated, as the result of absorption of the electrons. When 10 J are absorbed in the stainless steel tube, the temperature rises by about 30°C, so that over a length of 12 cm, the expansion is approximately 0.04 mm.

PLATE 6

Simulation of Impedance Matching of the Mark 2 Diode

- (a) signal terminated in 50 ohms
- (b) signal terminated by diode
- (c) signal unterminated (open circuit)



An expansion of this order was confirmed by placing a Verdict Dial Gauge against the end of the anode tube and noting the deflection when the electron gun was fired.

It was necessary to devise a technique which allowed the tube to expand and at the same time isolate the high pressure gas region from the evacuated diode. First the anode tube was placed in position so that it was concentric with the cathode. One end of the anode tube was then soldered onto a plate which was bolted to one of the cavities, the seal being made using a "Viton" O-ring. This method of sealing is illustrated in fig 18. A similar plate was bolted to the other cavity, with the O-ring seal in position, before soldering the tube to it. The plate retaining bolts were then removed and copper tabs fixed to the plate and the cavity, in order to provide a path to earth for the return current. This technique of sealing proved highly successful; no leaks were detected from the high pressure region into the evacuated diode, and no distortion of the anode tubes occurred.

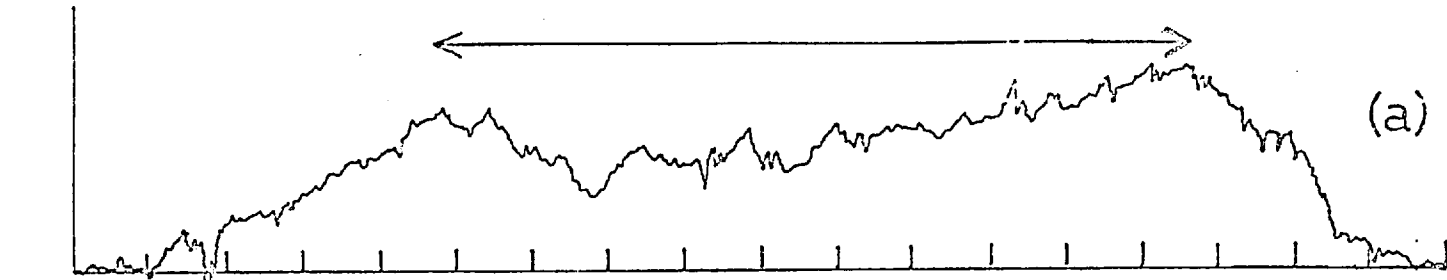
The total energy deposited in the tube was measured using a copper-constantan thermocouple (as described earlier) and the uniformity of deposition was determined by bleaching Avisco cellophane. The total energy deposited in the tube was 5 J and was distributed as shown in fig 19. The excited length was increased to about 12 cm, but the uniformity of deposition was not as good as that obtained using the Mark 1 system.

4.5 EXTENSION OF THE BLUMLEIN CIRCUIT

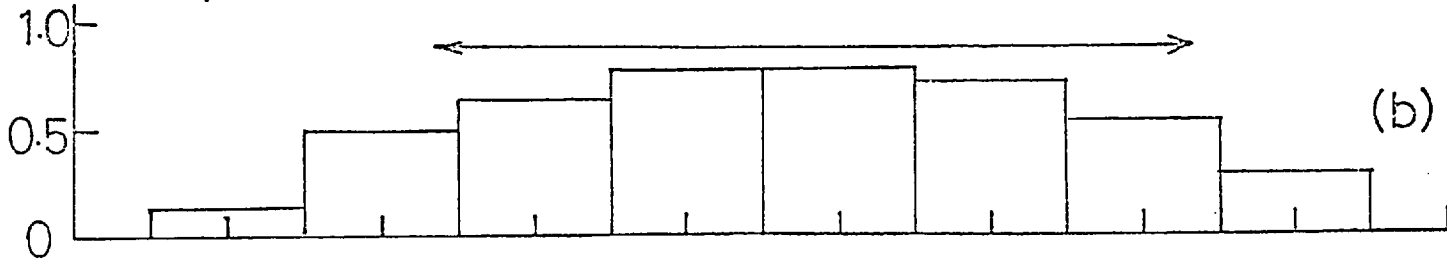
When the Mark 2 diode was used in place of the Mark 1 diode, there was no increase in laser output, as the energy deposited in the gas and the pumping pulse duration were unaltered. In order to try and increase both energy and pulse duration, the Blumlein circuit was modified.

RESULTS FOR MARK 2 DIODE

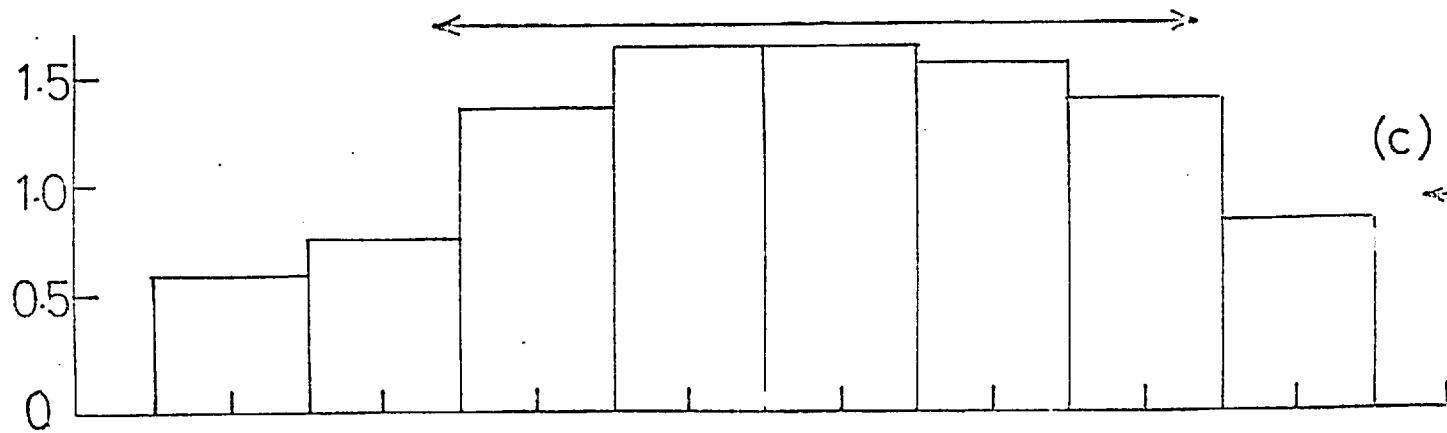
e^- DOSE (arb)



arrow indicates cathode position



ENERGY ($J \cdot CM^{-1}$)



extended Blumlein

DISTANCE (CM)

Fig 19
67

Fig 20 shows a schematic diagram of the Blumlein circuit; this circuit was devised by A. D. Blumlein ⁽⁴⁰⁾. In the Febetron 706 the Blumlein circuit is made up of two coaxial lines of equal impedance. The load impedance, Z_L , is the impedance of the field emission diode. The pulse duration is equal to twice the transit time of the Blumlein ⁽⁴⁰⁾, so in order to increase the pulse duration the two transmission lines were extended linearly. The impedance was maintained by keeping the ratio of the radii of the conductors which made up the Blumlein circuit, constant. In practice, the impedance was reduced to about 28 ohm because of the thickness of the materials used in extending the conductors. The outer, intermediate and inner conductors were each extended linearly by 15 cm as shown in fig 20. (Further details on the construction of the Blumlein circuit are given in "The Febetron 706 Handbook" ⁽⁴⁵⁾, where it is referred to as the "Model 2677 Shortpulse Adapter".)

As the charging conditions of the Blumlein circuit were altered, the spacing of the radial spark gaps was increased to obtain a reproducible signal. The Blumlein circuit was charged from the Marx Generator, and the charging voltage was monitored from the capacitive pick-off connector on the outer conductor of the Febetron 706. The signal was recorded using a Tektronix 519 oscilloscope and the traces which were obtained are shown in plate 7. For comparison, a trace obtained from the unmodified Blumlein is also shown. Sometimes the radial spark gaps broke down before the Blumlein circuit was fully charged, and this is illustrated in plate 7c. The premature firing was corrected by increasing the air pressure in the radial spark gaps or by decreasing the charging voltage of the Marx generator.

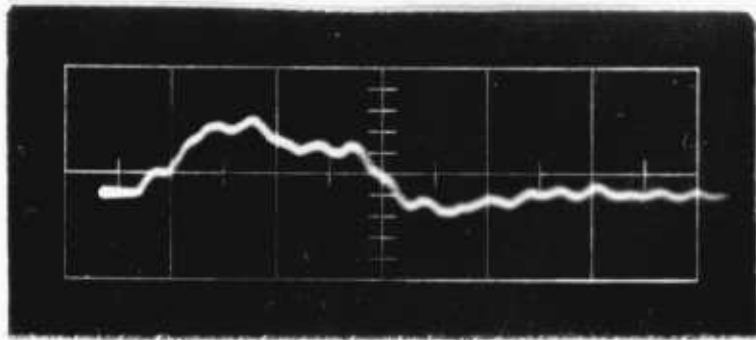
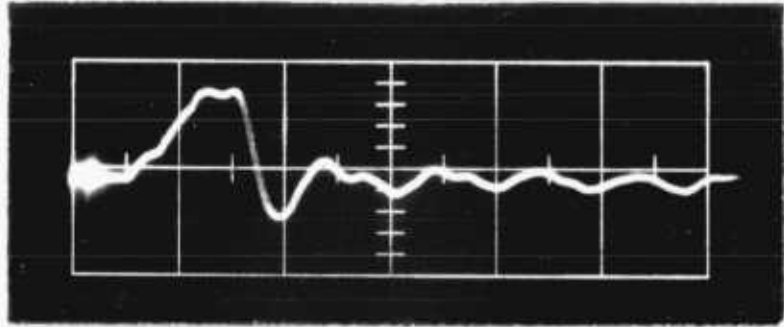
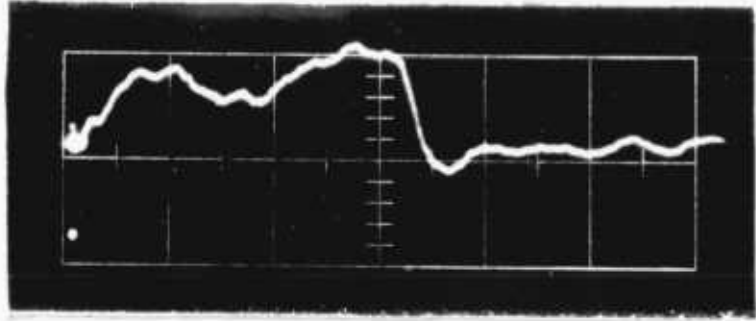
The electron beam pulse duration was measured by observing the

PLATE 7

Charging Voltage of the Blumlein

- (a) extended Blumlein
- (b) unmodified Blumlein
- (c) extended Blumlein illustrating
premature breakdown of the radial
spark gaps.

timescale : 10 ns per major division



(a), (b) and (c) are the inner, intermediate and outer conductors, respectively.

-----Indicates modification

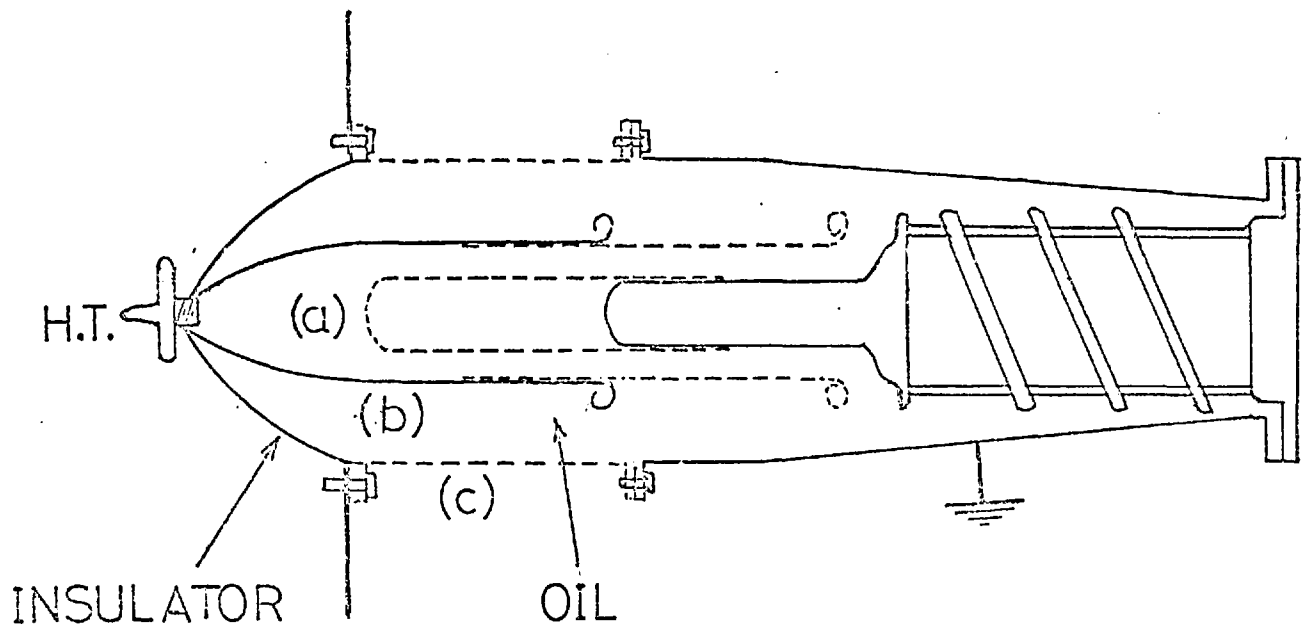


Fig 20

output from a 5516X diode using a Faraday cup. The pulse length increased to approximately 5 ns (FWHM) as shown in plate 8. When this diode was replaced by the Mark 2, the total energy deposited in the anode tube was about 10 J, fig 19, and dye dosimetry indicated that the deposition profile was similar to that obtained using the shorter pulse, although with increased dose. In the case where the radial spark gaps broke down prematurely, the total energy deposited in the tube was about 1 J. In order to check the reproducibility of the system under optimum working conditions, 30 consecutive shots were taken and the energy deposited in the tube was recorded using a thermocouple. 80% of the results were constant to better than 5%, with 50% giving the same reading. The remaining 20% were within 15% of the mean value.

The coaxial electron beam diodes have proved to be compact and reliable pumping sources for the VUV xenon laser, and were used in all future studies of the laser parameters.

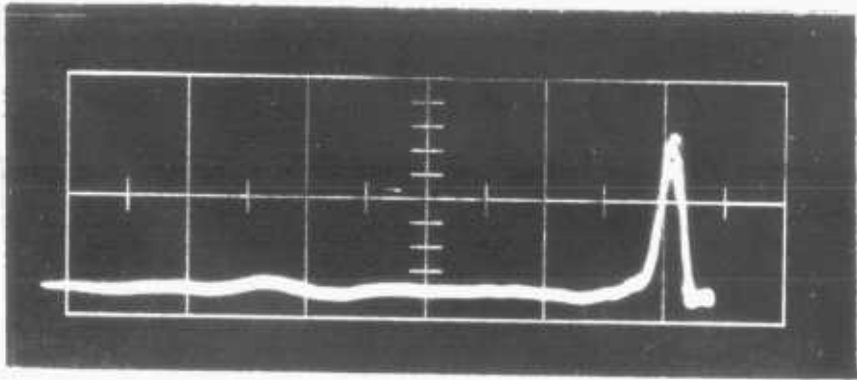
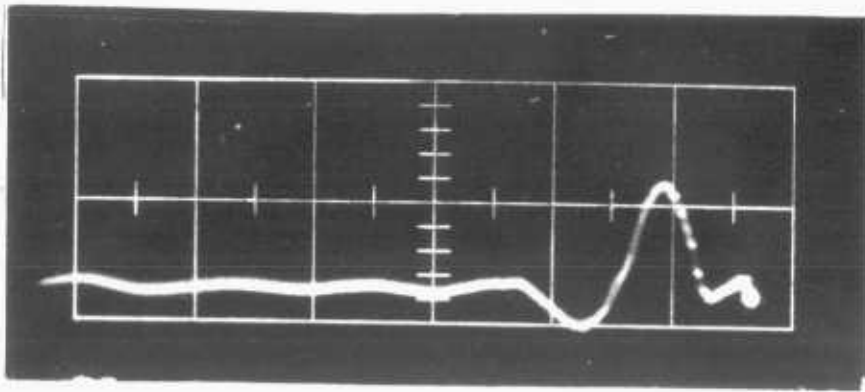
PLATE 8

Faraday Cup Traces of the Electron Beam Output

(a) unmodified Blumlein

(b) extended Blumlein

timescale : 10ns per major division



THE CHARACTERISTICS OF THE XENON LASER

Early attempts to obtain laser action using a transverse pumping geometry and a commercial electron beam diode were not successful. The commercial diode used was a 5516X, which gave a rectangular beam of electrons with dimensions 30 mm by 6 mm and a peak current density of about 10 kA.cm^{-2} . The distribution of current was not uniform over the cathode area so that the gas was not uniformly excited. In one attempt to achieve efficient coupling of electrons into the gas, a cavity was designed with the anode foil of the diode placed about 2 mm from the input titanium foil of the cavity; however the construction of the electron gun imposed a constraint of a 30 cm separation between the mirrors which made up the resonator, and as a result, the number of passes through the active region was small for a 2.5 ns excitation pulse. An alternative method investigated was drifting the electrons through a copper cone, which has been described in Section 4.1. As the efficiency of transportation was not reproducible and was only of the order of 50%, this technique was not used.

The coaxial diode design, described in the previous chapter, overcame the difficulties encountered with the commercial diode and also gave uniform pumping over a longer length with the total volume of excited gas in the line of sight of the mirrors. This coaxial pumping geometry was used in all subsequent laser experiments.

5.1 THE COAXIAL XENON LASER (MARK 1)

The arrangement of the laser is shown in fig 16. The cavity was pumped to less than 10^{-4} torr using an oil diffusion pump (Edwards Speedivac EM2) backed by a rotary pump (Edwards E.D.50), both of which

had liquid nitrogen cold-traps to prevent contamination of the system by hydrocarbons from the pumps. The low pressures were read from a Pirani gauge (Edwards H5C2) which was accurately calibrated in the range 10^{-1} to 10^{-4} torr. The system was then filled to a pressure of 10 ktorr with xenon.

Spectra were obtained without a resonator and the spectral half width was 8.6 ± 0.5 nm, see fig 21. This was narrower than the fluorescence spectra which were obtained at this pressure (half width of approximately 14.0 nm) and this narrowing was taken as evidence of stimulated emission.

The first laser resonator used, consisted of a 90° "roof-top" calcium fluoride prism and a plane aluminium mirror overcoated with magnesium fluoride. The radiation was coupled out through a 0.25 mm radius hole, drilled in the centre of the mirror.

It was necessary to carry out alignment of the prism before the anode tube was fixed in position, and it had to remain aligned after the tube was first evacuated and then filled to the working pressure. The prism was securely fixed to a mount that was screwed into the plug which was used to seal off the inner end of the anode tube. The plug was adjusted until a helium-neon laser beam, aligned along the tube axis, was reflected back along its own path and then soldered into position. A 0.125 mm stainless steel cylinder was placed around the prism to prevent damage to it by the electron beam (48).

The anode was fixed in position in the cavity and the helium-neon laser beam realigned so that it was parallel to the tube axis. The output mirror was then firmly attached to a kinematic mount which was fixed to the end plate. This end plate was bolted to the cavity and the high pressure/vacuum seal was made with an O-ring. The mirror was

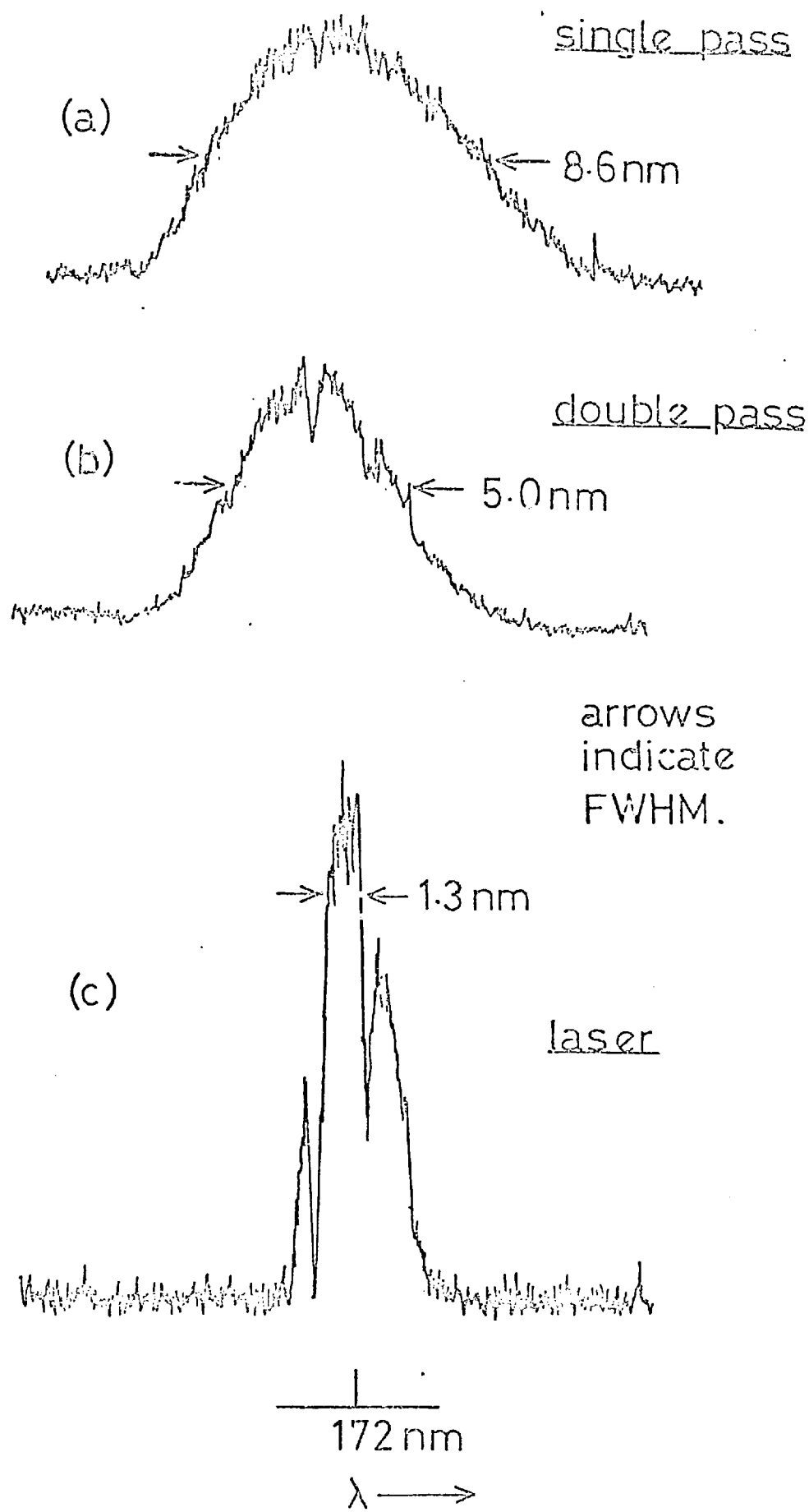


Fig 21

aligned by observing the reflection from the back of the aluminium coating. Final adjustment of the mirror was made while the system was filled with xenon, the adjustment being made through seals which were designed to operate at high pressures and under vacuum.

The output radiation was monitored using a 1 metre normal incidence spectrograph. With the same slit width (0.1 mm) as that which was used to obtain the amplified spontaneous emission, shown in fig 21, the film was over-exposed indicating an increase in light intensity. Also the slit was not uniformly illuminated, as an intense spot surrounded by scattered light of lower intensity was observed. In order to obtain a correctly exposed spectrum the light was attenuated using 10 torr of oxygen and the slit width was reduced to 0.065 mm. The spectrum is shown in plate 9 and the half width was measured from the microdensitometer trace to be (1.3 ± 0.1) nm, see fig 21. Two absorption lines were apparent at wavelengths of about 171.2 and 172.9 nm. They were considered to be due to CO (carbon monoxide) ⁽⁹²⁾, and could not be removed by redistillation of the gas. The CO may be formed by the reaction of the carbon in the stainless steel and the oxygen in the cell, when they are bombarded by high energy electrons. These lines were observed in all the work on the xenon laser.

Oxygen was used to attenuate the radiation because of its strong absorption in the region of 172 nm. The absorption coefficient has been measured accurately by Watanabe ⁽⁷³⁾, who found that in the wavelength range 171 to 173 nm, the absorption coefficient increased approximately linearly from about 12 to 18 cm^{-1} at atmospheric pressure. The oxygen was contained in a 14cm long cell, which was sealed by two barium fluoride windows. The cell was pumped to less than 10^{-1} torr and flushed with oxygen before being filled to the required pressure. Attenuation of the cell, neglecting window losses, was obtained from the following expression

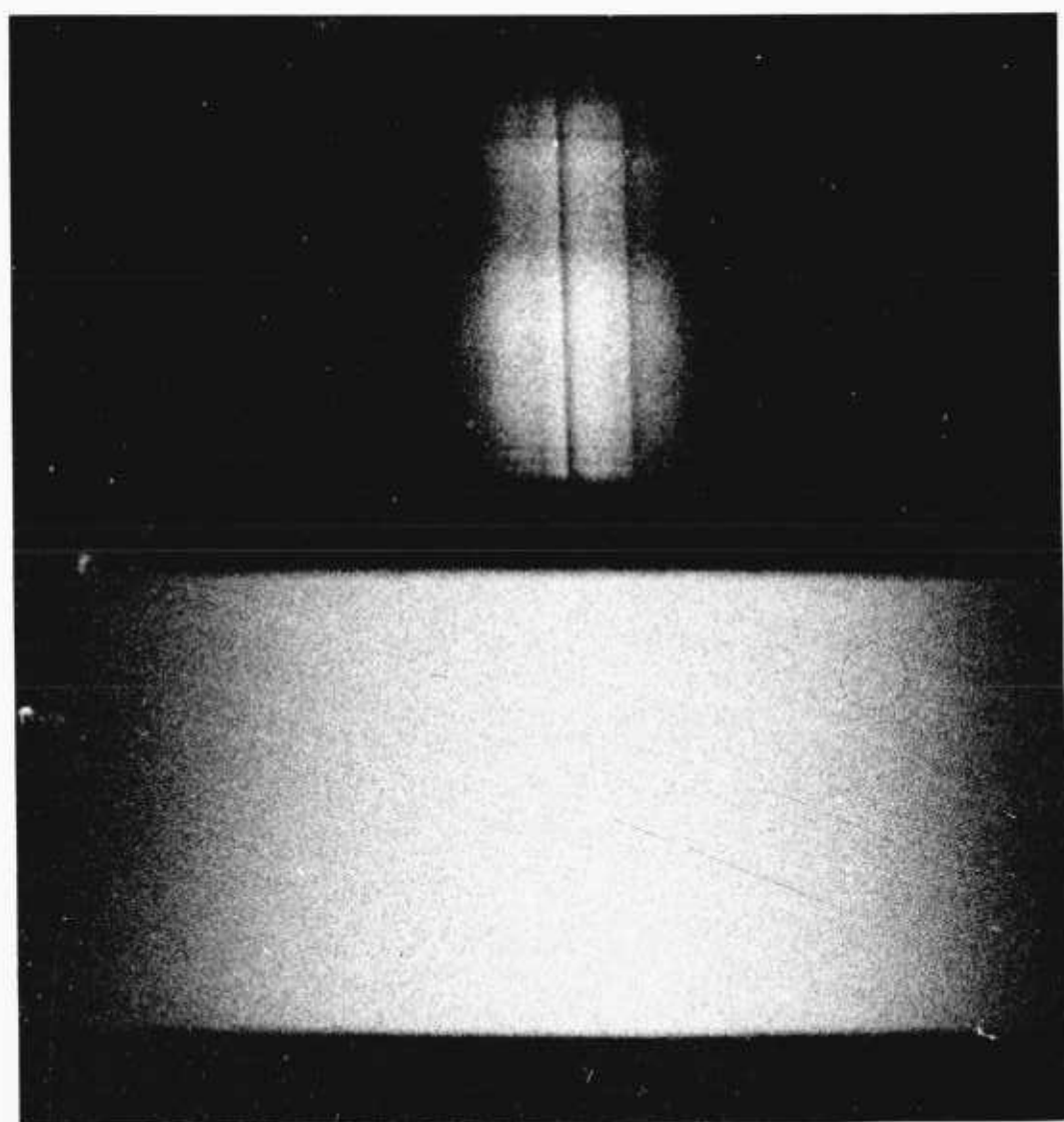
PLATE 9

Spectrum of the Laser Output

(a) laser output at 10 ktorr

(b) fluorescence output at 10 ktorr

wavelength increasing from left to right



$$\frac{I}{I_0} = \exp \left(-\frac{\alpha p l}{760} \right) \quad (5.1)$$

where α = absorption coefficient (cm^{-1})

l = cell length (cm)

p = oxygen pressure (torr)

From analysis of the film data, the increase in the signal coupled into the spectrograph, as compared with the case when no mirrors were used, was estimated to be of the order of 100 times.

Output power and pulse duration were determined using an ITT F4115 photodiode together with a Tektronix 519 oscilloscope, which gave a combined time resolution of about 0.5 ns. The photodiode had a cesium telluride photocathode and a magnesium fluoride window and was only sensitive to radiation in the wavelength range 320 to 113 nm⁽⁷⁴⁾. It was calibrated, by the manufacturer, at 230 nm and it was assumed that the sensitivity did not vary with wavelength, down to 170 nm. In all calculations of power, a value of $30 \text{ mA}\cdot\text{W}^{-1}$ was assumed. The signal was again attenuated using oxygen and using an absorption coefficient of 14 cm^{-1} for oxygen, the peak power obtained with this arrangement was 1 kW, which is equivalent to an output power density of $0.5 \text{ MW}\cdot\text{cm}^{-2}$. The pulse duration decreased to 3.5 ns (FWHM) from the fluorescence half width of approximately 7 ns.

The beam spread was measured by placing SC7 film at the end of a 1 metre long blackened pipe. A well defined spot was observed which was surrounded by scattered radiation. From the spot size, a beam divergence of about 5 mrad was estimated.

When the output mirror was examined, the coating was found to be damaged over a region of 1.5 mm radius from the output coupling hole but there was no damage to the prism. On replacing the damaged mirror by a

similar one, and leaving the system misaligned, the power output was only a few watts and no damage to the coating was observed. This indicated that the damage was due to the high intracavity energy.

The combination of spectral narrowing, change in temporal profile, low beam divergence and the increase in power achieved when the cavity was aligned, was taken as conclusive evidence of laser action.

The hole coupling technique was improved by replacing the prism by a concave mirror. Optimal values of a 0.9 m mirror radius and a 0.6 mm hole radius were determined by ray optics (75). Experimentally an aluminium:magnesium fluoride (Al : MgF₂) mirror with a 1 metre radius of curvature was used. Combination of this mirror with a plane mirror which had a 0.55 mm radius hole, resulted in the power output increasing to about 160 kW. Increasing the hole size to 0.71 mm radius further increased the power output to about 500 kW. In both cases the pulse duration was about 3.5 ns, as shown in plate 10. The output signal was again attenuated using oxygen. Both mirrors in the cavity were damaged and after about ten shots the laser signal decreased. The output beam had an annular profile as shown in fig 22 and the beam divergence was estimated to be about 5 mrad.

The most efficient cavity configuration used consisted of a plane mirror as the back reflector and a partially transmitting plane Al : MgF₂ output mirror, (supplied by "Acton Research Corporation"). The transmission and reflection coefficients were given as 0.03 and 0.76, respectively. The output energy was measured 20 cm from the output window using a calorimeter (Laser Instrumentation Model 142 LR Thermopile) which was mounted inside an evacuated cylinder. The output energy recorded at 10 ktorr of xenon was about 3 mJ which was equivalent to a power of about 1MW. Since the mirror coatings were removed in a single shot, it was not possible to measure the beam divergence or to obtain

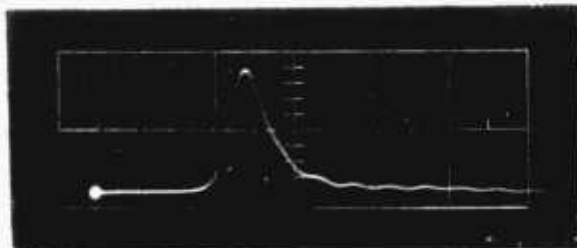
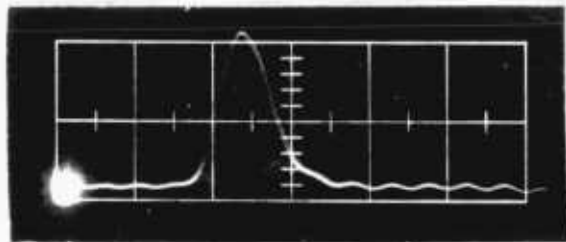
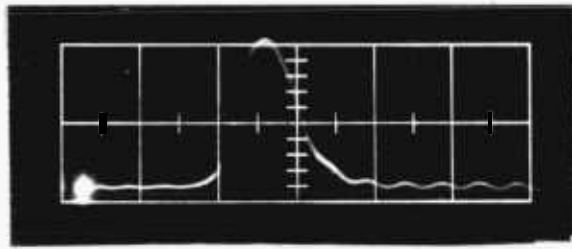
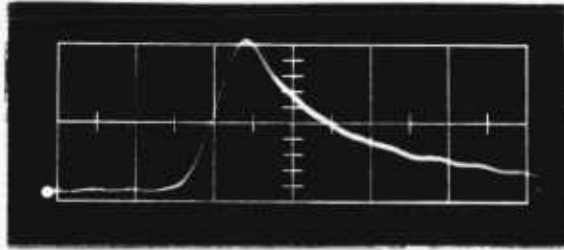
PLATE 10

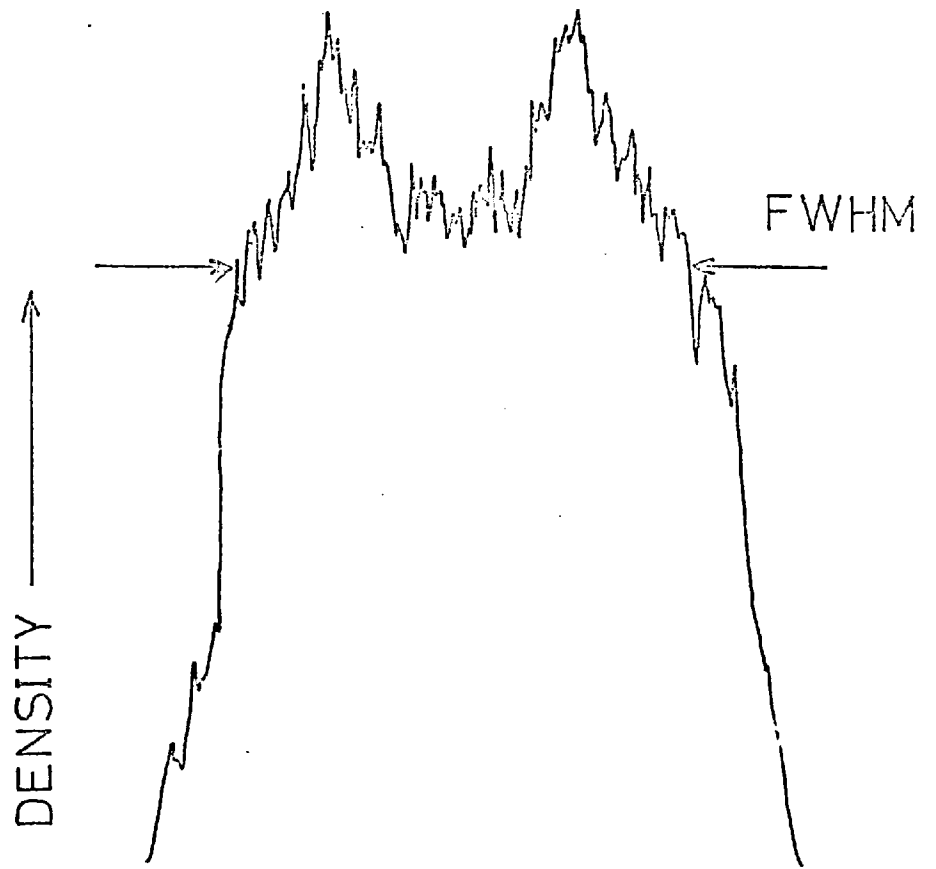
Temporal Dependence of the Laser Output

- (a) fluorescence
- (b) Mark 1 laser
- (c) Mark 2 laser
- (d) Mark 2 laser with extended Blumlein

xenon pressure : 10 ktorr

timescale : 5 ns per major division





HALF-WIDTH = 5mrads

Densitometer trace of beam profile.

Fig 22

spectral information.

In order to look at the variation of output power with pressure, it was necessary to reduce the intracavity laser energy to prevent mirror damage. A stainless steel coil was inserted inside the anode tube, this reduced the number of electrons entering the gas by about 10% and also reduced the effective tube diameter to 3.5 mm. The maximum output power recorded was then about 100 mW when using a plane-parallel cavity with the partially transmitting Acton mirror as the output reflector. The signal incident on the photodiode was attenuated using a barium fluoride (BaF_2) diffuser and wire gauges placed in front of the diode. Each gauge attenuated by a factor of about 4, for up to 3 gauges. This was measured by removing one gauge and attenuating the diode signal using a calibrated electrical attenuator and comparing the peak intensities.

Fig 23 shows the variation of output power with pressure. The laser threshold occurred at about 7.5 kTorr with the optimum pressure at 12.5 kTorr. At higher pressures the signal began to decrease. A similar pressure dependence has been observed by other workers (60) (76) (59). This decrease in the laser output at high pressures is considered to be due to increased photoattenuation of the radiation, leading to a reduction in the gain. Both ground state absorption and scattering processes have to be considered (77) each of which are temperature and pressure dependent. Further discussion of the photoattenuation processes is given in Section 5.3.

5.2 MEASUREMENT OF THE GAIN

In order to obtain an estimate for the gain of the Mark 1 laser, the amplified spontaneous emission (A.S.E.) from the excited medium was

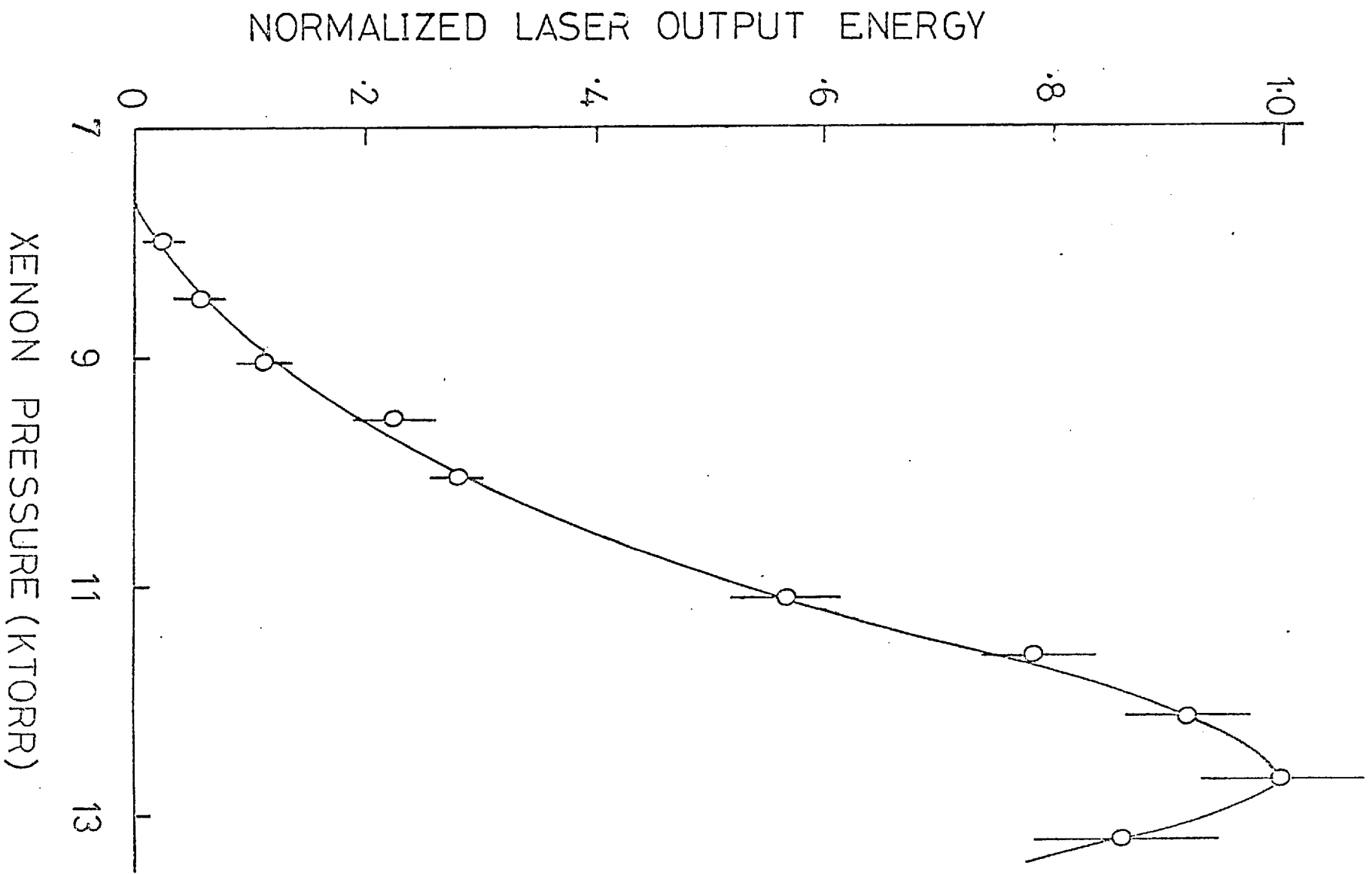


Fig 23

studied spectrally and temporally. The experimental arrangement used was similar to that shown in fig 16 with the output reflector removed.

The output radiation was first observed without the back mirror in position. The intensity was measured using an ITT X4115 photodiode and Tektronix 519 oscilloscope, and spectra were recorded using a 1 metre normal incidence spectrograph and Kodak SC7 film. These results were then repeated with the back mirror in position. This mirror reflected part of the A.S.E. back through the excited medium so that it was further amplified before being detected. In both sets of results the photodiode was placed 1 metre from the excited volume and the light incident on the diode was attenuated by a barium fluoride diffuser placed 15 cm from the diode. It was assumed that the excited volume observed by the photodiode was constant in both cases. Only the relative intensities of the signals was required, so absolute values were not measured. The values of spectral width and the ratio of the intensities are given in Table 5.1.

In order to account for these results, the system was assumed to have a gain coefficient $\alpha(\lambda)$ and a loss coefficient $\gamma(\lambda)$. The intensity incident on the diode without the mirror in position, I_n , is given by

$$I_n = \frac{I_s}{[\alpha(\lambda) - \gamma(\lambda)] l} \left\{ \exp [\alpha(\lambda) - \gamma(\lambda)] l - 1 \right\} \quad (5.2)$$

where I_s = spontaneous emission intensity

l = length of the excited medium

I_n was found by calculating the contribution to the total radiation observed from a small element of the excited volume and then integrating over the excited length. The gain and the losses were assumed to be distributed uniformly throughout the excited region.

With the mirror in position the intensity, I_n , is given by

$$I_m = \frac{I_s}{[\alpha(\lambda) - \gamma(\lambda)]_1} \left\{ R \exp [\alpha(\lambda) - \gamma(\lambda)]_{l+1} \right\} \times \left\{ \exp [\alpha(\lambda) - \gamma(\lambda)]_{l-1} \right\} \quad (5.3)$$

so that

$$\frac{I_m}{I_n} = R \exp [\alpha(\lambda) - \gamma(\lambda)]_{l+1} \quad (5.4)$$

R in this case includes both the mirror reflectivity and a geometrical factor of 0.5. This was included as the area of the mirror was half the cross-sectional area of the tube, so that amplification only occurred over half of the tube area.

The small signal gain coefficient may be estimated ^(7e) using the expression

$$\alpha(\lambda) = \frac{\lambda^2}{8\pi \tau_f} g(\lambda) [N_2 - N_1] \quad (5.5)$$

where λ = wavelength

τ_f = fluorescence decay time

$g(\lambda)$ = normalised line shape function

N_1 = population of the lower level

N_2 = population of the upper level

In the xenon laser $N_1 \simeq 0$, thus $N_2 - N_1 \simeq N_2$.

The population of the upper level, N_2 , was assigned a time dependence similar to that of the fluorescence which was obtained in the absence of appreciable stimulated emission. A good fit to the fluorescence at 10 ktorr was obtained using an equation of the form

$$I(t) = I \exp \left[\left(\frac{-t}{\tau_f} \right) - \exp \left(\frac{-t}{\tau_r} \right) \right] \quad (5.6)$$

where τ_f = fluorescence decay time

τ_r = fluorescence risetime

$I = \frac{\tau_r \tau_f}{\tau_f - \tau_r} \ln \frac{\tau_f}{\tau_r}$ was the normalisation term

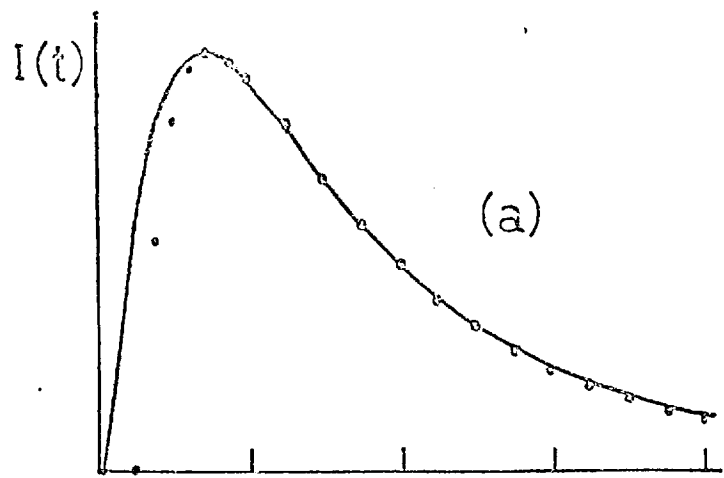
Values of $\tau_f = 5.5$ ns and $\tau_r = 1.0$ ns gave good agreement between the calculated value and the experimental curve, this is shown in fig 24a.

The line shape function, $g(\lambda)$ was assumed to be gaussian with a spectral half width of 14.0 nm. This value of half width was chosen as an average of the values given in the relevant literature (37) (39) (59). The loss term was assumed to be independent of wavelength but to have the same time dependence as $\alpha(\lambda)$. This is considered to be a good approximation when the main loss processes are scattering, photoionization and ground state absorption.

Owing to the complex nature of the gain and loss, equations 5.2 and 5.3 were solved using a Hewlett Packard Series 1000 calculator. A program was designed to allow the time to be varied in steps of 0.5 ns, in the range 0 to 25 ns, and the spectrum to be considered at intervals of 1.0 nm over a 20.0 nm bandwidth. The intensity at each spectral position was calculated for each time step and, by summing all the contributions to each part of the spectrum over all the time steps, the total spectrum was obtained. Also, at each time step, the contribution to the intensity of all the wavelength components at that time, was calculated, and this gave the temporal behaviour of the A.S.E. pulse.

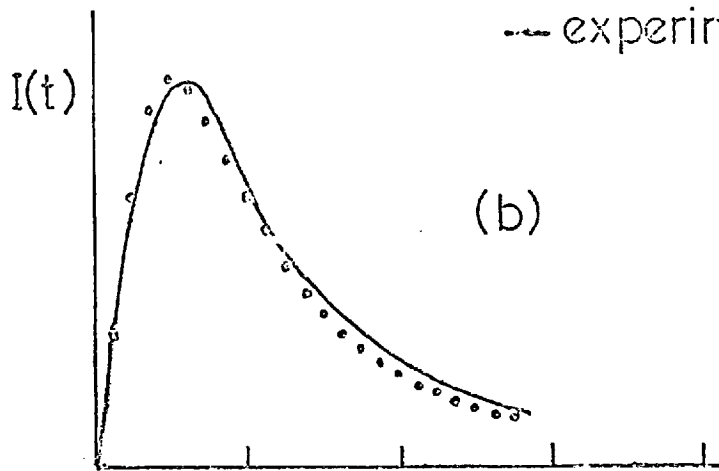
The maximum values of the gain and loss coefficients, α_{\max} and γ_{\max} respectively, were varied until good agreement was obtained between the experimental and calculated values of the spectral half widths and the ratio of the intensities, with and without the mirror.

The optimum values obtained for an excited length, l equal to 8.5 cm and a mirror reflectivity of 0.8 are given in Table 5.1, together with the calculated values of the spectral half width and the ratio of the peak intensities. The excited length of 8.5 cm was chosen from the calorimeter

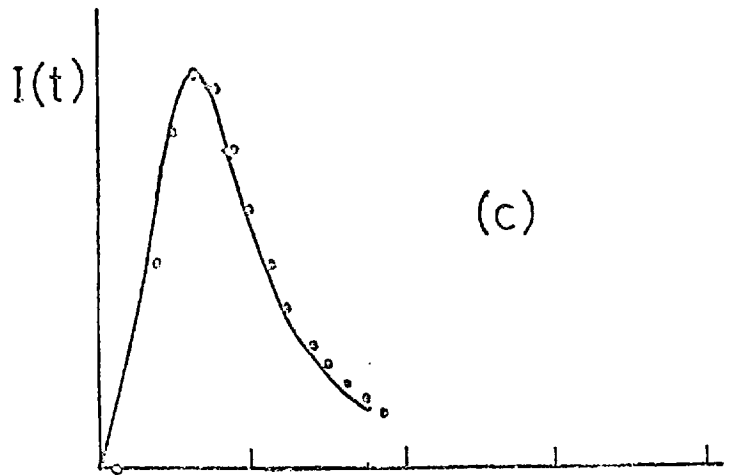


(a)

.... calculation
--- experiment



(b)



(c)

0 4 8 12 16

TIME (NS)

Fig 24

measurement shown in fig 17b. This measurement was less than that which was observed using dye dosimetry, shown in fig 17a, when a 10 cm excited length was measured. It was considered however, that the thermocouple gave a more reliable quantitative result. In order to see the effect of increasing the excited length, the calculations were also carried out for l equal to 10 cm and these results are also given in Table 5.1. α_{\max} decreased by about 20%, whilst the net gain ($\alpha_{\max} - \gamma_{\max}$) changed by only 10%.

The calculated pulse durations were compared with that obtained experimentally, see fig 24b,c. (In both cases the peaks are adjusted to coincide.) Again, there is good agreement between experimental results and calculated values. These results demonstrate that to a first approximation the losses can be considered to be due mainly to a wavelength independent process. It has also been shown that the excited medium has a net gain, with a gain coefficient of the order of 0.3 cm^{-1} .

5.3 THE EFFECTS OF GAS HEATING

When the laser was fired with a frequency of about one shot per minute, the intensities of the second and each subsequent shot were reduced by a factor of greater than 20. It was found that by decreasing the repetition rate, so that the laser was not fired more than once in 15 minutes, the output power was reproducible to within 20% up to about 5 shots, after which a slow decrease, due to mirror damage, was observed. The only factor that was altered by increasing the firing repetition rate was the gas temperature, which rises with each shot that is fired, since the rate of removal of heat from the gas is slow. This can be demonstrated by considering the rate of cooling of the gas after each electron pulse.

Approximately half the electron energy (5 J) was deposited in the 0.06 mm thick stainless steel tube over a length of 8.5 cm. The

temperature rise, ΔT , can be calculated using the expression (79):

$$\text{Energy deposited} = V \delta s \Delta T \quad (5.7)$$

where V = volume

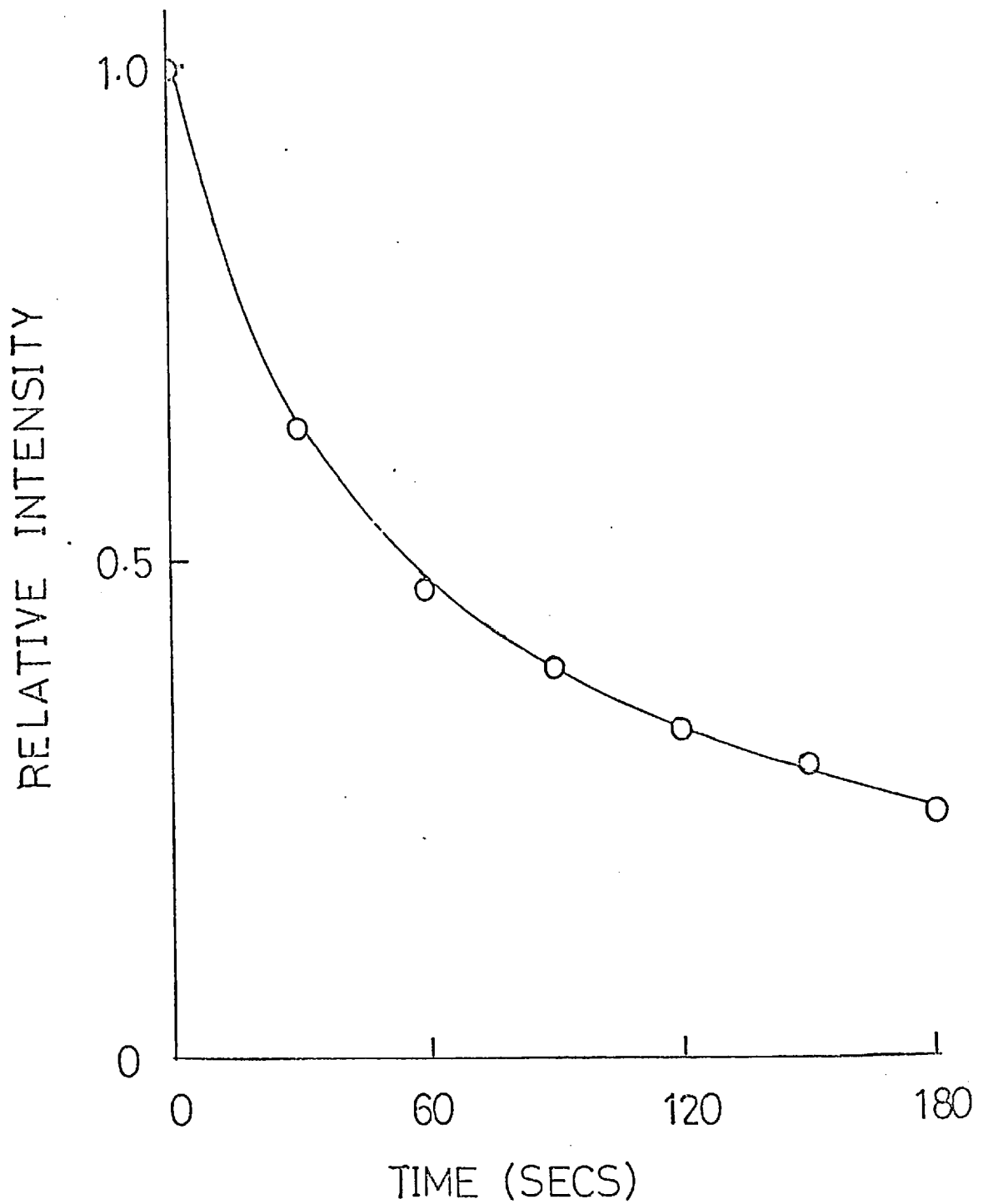
δ = density

s = specific heat of stainless steel

The calculated temperature rise in the walls of the anode tube was about 20°K for each shot that was fired. The remaining 5 J were deposited in the gas and so substituting the relevant values for xenon into equation 5.6 the temperature rise was about 600°K . The gas and walls reached an equilibrium temperature of about 40°K in approximately 20 seconds. As the anode tube was surrounded by vacuum and the thermal conductivity of xenon is low (80), the main method of cooling was by conduction along the length of the tube. Since the cross-sectional area of the tube wall was small (wall thickness = 0.06 mm, tube radius = 2.0 mm), the cooling time was slow. This was measured experimentally by placing a thermocouple in contact with the tube wall and monitoring the change of temperature with time after the electron gun was fired. The temperature was found to return to its original value in about 15 minutes.

The variation of A.S.E. intensity with a repetitive pumping rate of 2 pulses per minute was investigated, this pumping rate being limited by the charging time of the Febetron 706 power supply. The results, which are shown in fig 25, were taken at a xenon pressure of 8 ktorr. In the 30 seconds between shots the equilibrium temperature of the gas and tube did not change significantly, so that in consecutive shots, the gas temperature increased in a linear fashion, with the temperature dependent losses increasing from shot to shot. After a delay of 15 minutes the intensity returned to its original value.

The change of photoattenuation in xenon with temperature, at a



Signal decrease observed at a repetition rate of 2 shots per minute for 8 ktorr xenon.

Fig 25

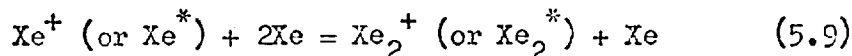
wavelength of 172.0 nm, has been measured by a number of researchers (77) (81) (82), all of whom found an increase with temperature. Kosinskaya et al. (82) measured the photoattenuation in the temperature range 300 to 870^oK; this is the only data at present available for higher temperatures. Gerardo et al. (77) who studied the temperature range of 273 to 373^oK, showed that the major loss is due to resonant Rayleigh scattering, but that other scattering processes are also significant. The scattering occurs from fluctuations of the refractive index of the high pressure gas. Gerardo et al. found that the scattering increased with gas temperature and that by increasing the temperature from 300 to 373^oK, the attenuation coefficient more than doubled. This increase in attenuation with temperature, may account for the reduction in the laser and A.S.E. output signal when shots were taken at 30 second intervals. Although the temperature difference in consecutive shots taken at 30 second intervals was about 40^oK, the absolute temperature rise of the gas during the excitation pulse is expected to be much higher. This is because a number of the formation mechanisms create energetic ground state atoms, which can then collide with other atoms, molecules, etc., so that the overall temperature rises.

In the dissociative recombination reaction:



the ground state xenon atom carries away excess energy of the order of 1 eV, which is the approximate energy difference between Xe_2^+ and Xe^{**} .

Also the two 3-body reactions:



and the vibrational relaxation of these molecules to the lower vibrational states in collision with ground state atoms, causes gas heating. The ground state atoms gain further kinetic energy when the excited molecules radiate and the quasi ground state molecules formed, dissociate.

$$\text{Xe}_2^* = \text{Xe}_2 + h\nu = \text{Xe} + \text{Xe} + \text{K.E.} \quad (5.10)$$

It is estimated that these reactions cause a temperature rise of about 200°K during the laser pulse.

The effect of gas heating has been observed by other workers. It is well illustrated by the experimental results of Hughes et al. (83) who used an electron beam with a pulse of about 50 ns (FWHM) and a total beam energy of 2 kJ deposited in a volume of 30 cm³. The laser pulse duration, however, was only about 6 ns and terminated 20 ns after the start of the electron beam pulse so that the majority of the energy deposited was not used to sustain laser action but went into heating the gas. Termination of the laser pulse was also reported by Gerardo et al. (60) and Koehler et al. (7). In all cases the cut-off was estimated to occur when the energy deposited in the gas was in the range 5 to 6 J.cm⁻³.

If the cut-off is caused by some temperature dependent loss, then reducing the deposited energy density should increase the laser efficiency by reducing the losses, and prevent the premature termination of the pulse. This was verified experimentally by Hunter et al. (84), who constructed a high aspect ratio electron beam with dimensions 50 cm by 5 cm. The electron energy was 850 keV and an energy of between 600 and 800 J, in a pulse of 40 ns, was injected into xenon at a pressure of 5 ktorr, giving a total energy deposited of less than 0.5 J.cm⁻³. The measured laser output energy was 8 J which gave an efficiency of 2% relative to the energy deposited in the gas.

In the calculation of the gain, it was assumed that the losses were wavelength independent and had the same time dependence as the fluorescence and this is probably a reasonable approximation if scattering is the main loss process. At first it was considered that the main loss was due to photoionization (85), but the photoionization cross-section calculated by

Lorents et al. (54) is approximately an order of magnitude less than the stimulated emission cross-section measured by Gerardo et al. (56).

5.3.1 THE ADDITION OF OTHER NOBLE GASES TO XENON

Johnson et al. (86) suggested that one of the lighter noble gases could be added to xenon to reduce the temperature rise or that another gas could be used to absorb part of the electron energy and then transfer this energy to the xenon atoms (18). This second scheme would enable a lower partial pressure of xenon to be used but the energy deposition would remain unchanged.

Both of these approaches have been studied by Johnson et al. using a 50 ns pulse of electrons as an excitation source. They found that a He : Xe mixture improved the efficiency of conversion of electron beam energy into stored laser energy. They also showed that pure xenon was more efficient than an equivalent pressure of Xe : A even though there was energy transfer from excited argon to xenon. (Equivalent pressure is the pressure of the mixture which has the same electron stopping power as pure Xe, and is defined as

$$\text{Equivalent pressure} = P_{\text{Xe}} + \frac{Z_{\text{A}}}{Z_{\text{Xe}}} \cdot P_{\text{A}}$$

where P_{Xe} and P_{A} are the partial pressures of xenon and argon, respectively

Z_{Xe} and Z_{A} are the atomic numbers of xenon and argon, respectively.)

A systematic study of Xe : A mixtures has not been carried out using short electron pulse excitation but a number of readings at 5 and 10 ktorr showed that pure xenon was more efficient than an equivalent pressure of the mixture, in agreement with Johnson et al.

The effect of an addition of helium on the output fluorescence for a fixed xenon pressure of 5.5 ktorr was studied over a range of helium pressures from 0 to 9.5 ktorr. The amount of xenon required to fill the Mark 1 cavity to a pressure of 5.5 ktorr, was frozen in a high pressure cylinder. The system was filled with helium to a given pressure and the xenon was then heated to room temperature. It was found that it took two to three hours for the gases to mix thoroughly even if the electron gun was pulsed every few minutes. Readings were then taken at 15 minute intervals until 3 consecutive shots were constant in both peak and decay time.

The fluorescence was monitored using an ITT F4115 photodiode and a Tektronix 519 or 7904 oscilloscope. The signal incident on the photodiode was attenuated using a barium fluoride diffuser and calibrated wire gauzes. The photodiode signal was further reduced using calibrated electrical attenuators. The total output signal was measured by integrating over the area under the oscilloscope trace and correcting for attenuation. It was assumed that the electron deposition did not change with the addition of helium owing to the much longer range of electrons in helium than in xenon ⁽¹⁹⁾ so that for each set of results the same amount of energy was deposited per unit volume in the field of view of the photodiode. The variation of total energy output with pressure is shown in fig 26; this has been normalized to the value for no helium present. The fluorescence output remained constant for helium pressures in the range 0 to 3 ktorr and then decreased at higher pressures.

The decay time was measured by enlarging the oscillograms and plotting $\log I(t)$ against t . For all helium pressures the decay, τ_d , was accurately described by a single exponential term. The variation of decay rate, τ_d^{-1} , with helium pressure is shown in fig 27.

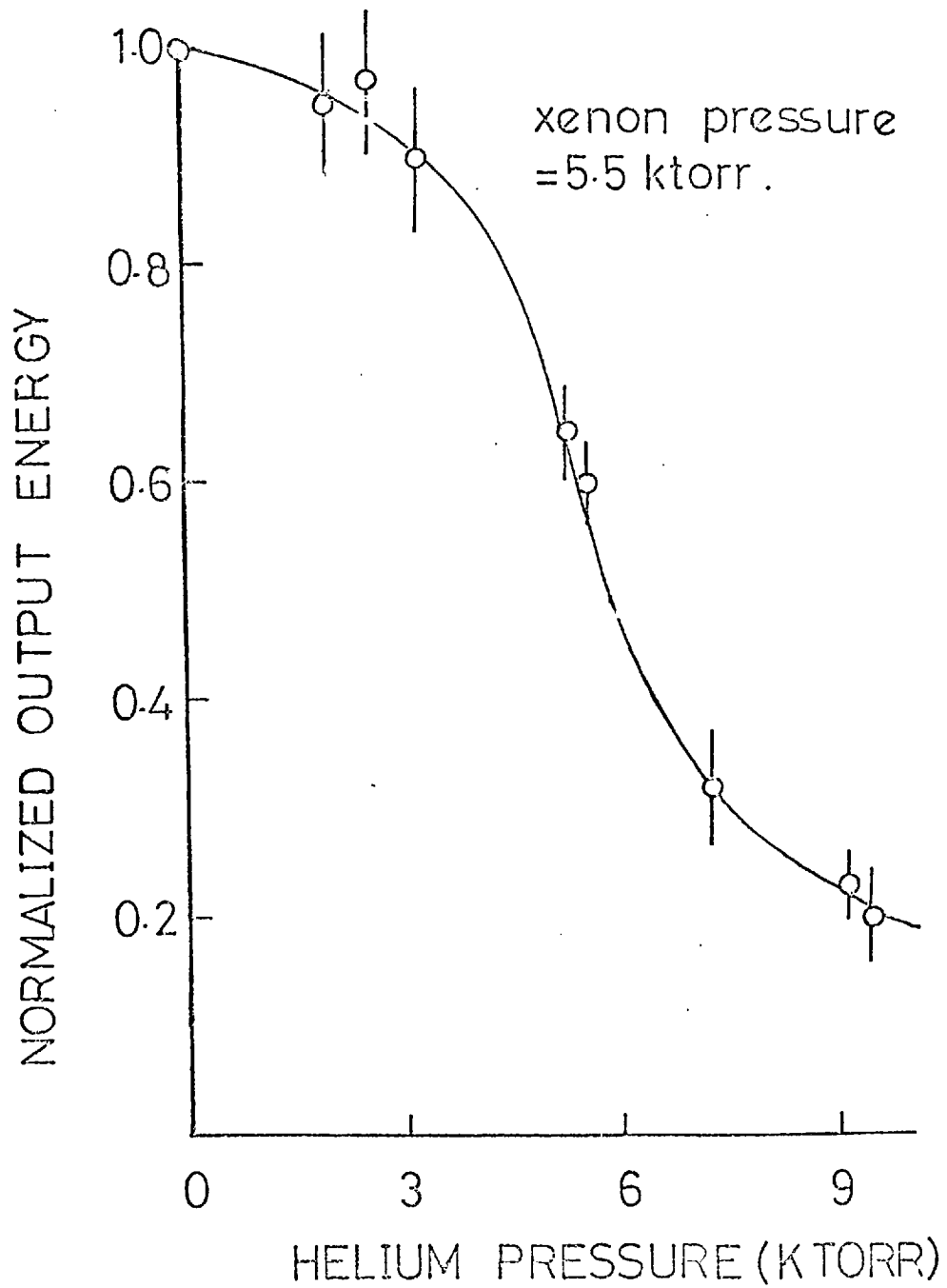


Fig 26

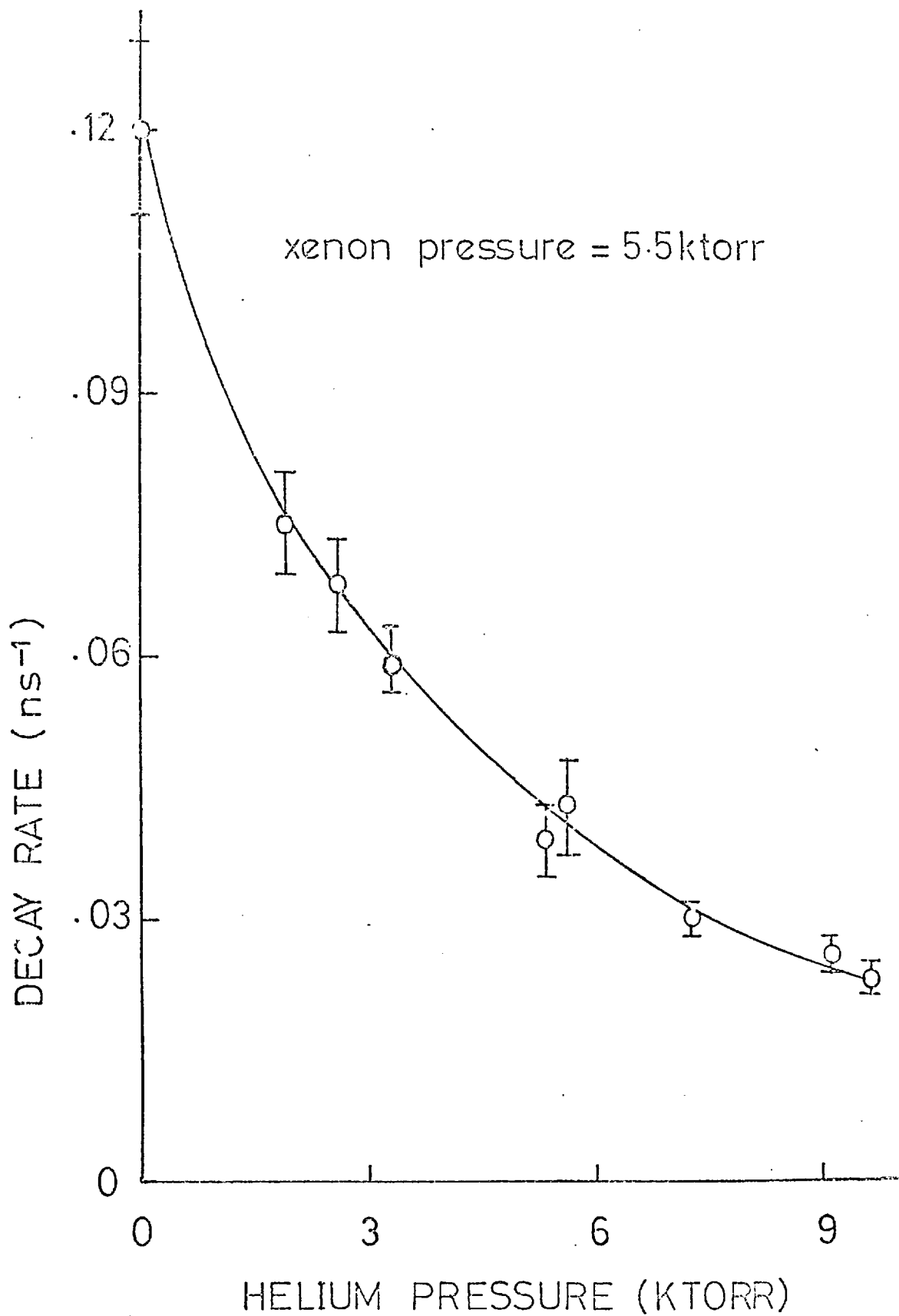


Fig 27

The reason for the decrease in total signal and decay rate with increasing helium pressure is still uncertain. Fournier has proposed (87) that the results are consistent with his theoretical model for electron-beam excited VUV fluorescence from xenon (55). As helium is a much lighter gas than xenon, the rate of thermalisation of the electrons due to elastic collisions with He atoms is much faster than for pure xenon. The rate of thermalisation also increases with helium pressure owing to the higher collision frequency. Fournier suggests that as the main mode of decay of the molecular ion is by dissociative recombination (see Section 2.4) then by reducing the electron temperature the number of atoms in the cascade level builds up rapidly. In dissociative recombination an electron is removed so that the number of electrons remaining to induce reactions from the cascade level to the levels which form Xe_2^* is reduced. So as the helium pressure is increased the main mode of decay will be radiative. This radiative decay time is of the order of tens of nanoseconds (31) so that it will be the rate limiting process, the decay of Xe_2^* will then be a measure of the decay from the cascade level. At very high helium pressures, Fournier predicts that the fluorescence decay will reach an asymptotic value which is the fluorescence decay rate of the cascade level. It appears from fig 27 that the results are tending to an asymptotic value of about 0.02 ns^{-1} . Higher helium pressures were not investigated because of the limitation of the strength of the anode tube.

Fournier's hypothesis also accounts for the results of Gerardo et al., using the 50 ns pulse of electrons. In this case electrons are being continuously supplied by the electron beam during the fluorescence pulse so that there are electrons available to induce transitions from the cascade level.

The decrease in signal with the addition of helium may be attributed to increased photoattenuation due to an increase in temperature during

the fluorescence pulse. The addition of helium to xenon will cause the gas temperature to rise more rapidly although the overall temperature rise will be lower. In the long pulse case the energy is being added over a longer time so that the average temperature is important and as this is reduced the signal will increase.


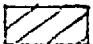
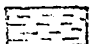
5.5.2 THE GAS CIRCULATING SYSTEM

A similar decrease in the laser signal was observed when the Mark 2 diode (described in section 5.4) was used, so in order to increase the laser repetition rate a gas circulating system was added, the details of which are shown in fig 28. The circulating fan was made from PTFE and a small magnet was firmly fixed to it. The fan was then rotated by a second magnet mounted on an a.c. motor which was separated from the high pressure gas region by a brass cylinder, of wall thickness 0.25 mm. Using a magnetically coupled drive ensured that the gas was not contaminated as the motor was isolated from the gas.

The gas was cooled by passing it through a heat exchanger, which consisted of seven stainless steel tubes with wall thickness of 0.15 mm and diameter of 4 mm. These tubes were fitted into holes drilled in two stainless steel plates and sealed into position with Araldite epoxy resin. Cooling of the gas was then achieved by circulating water around the pipes. Stainless steel pipes with an internal diameter of 6 mm were used to connect the circulating system to the laser cavity in order to obtain a sufficient flow rate. Viton O-rings were used to isolate the high pressure gas from the cooling water, to prevent contamination of xenon by water vapour which absorbs strongly at the laser wavelength (88).

With the gas cooling system in operation the laser output remained constant. In the Mark 2 laser, different reflectors were used from those used in the Mark 1 system and no damage occurred to these mirrors so that

GAS CIRCULATING SYSTEM

-  BRASS
-  STAINLESS STEEL
-  MAGNETS

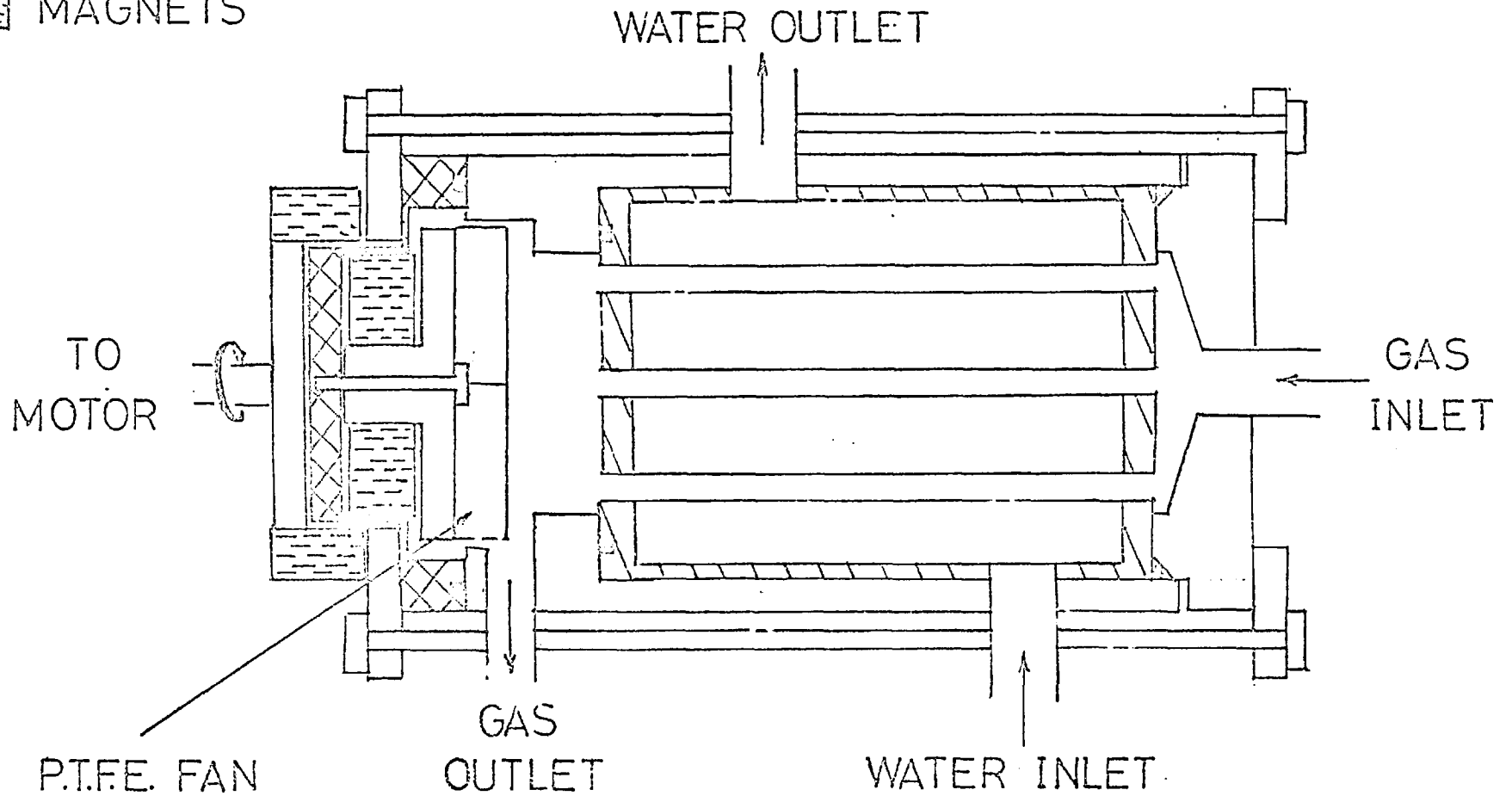


Fig 28

the signal remained constant over tens of shots when the electron gun was pulsed at 30 second intervals. No change in the laser output was observed if the pump was kept running during, or switched off before firing.

5.4 THE COAXIAL XENON LASER (MARK 2)

A major drawback of the Mark 1 system was the difficulty of replacing and aligning a back reflector, as the complete system had to be dismantled. It was also necessary to protect the mirror from the electrons to prevent damage to the magnesium fluoride coating (48).

The Mark 2 system shown in fig 18, was designed to allow access to both ends of the anode tube. A total electron beam energy of about 5 J was deposited in the gas over a 12.0 cm length in a pulse of duration 2.5 ns. A plane-parallel cavity was used, one mirror with a reflectivity, R, of about 80% (supplied by Matra Seavom) and the other with R equal to 76% and transmission, T, equal to 24% (supplied by Acton Research Corporation). Both mirrors had aluminium coatings, which were overcoated with magnesium fluoride. The maximum output energy recorded was 1 mJ in a pulse of duration of about 3.5 ns, and both mirrors were found to be damaged after a few shots.

In order to reduce the intracavity energy, the output transmitting mirror was replaced by a single plate barium fluoride etalon. This consisted of a 1 mm thick disc of barium fluoride with the angle between the faces less than 1 m radian, and both faces flat to $\frac{\lambda}{15}$. The reflectivity was calculated from the following equation (89) (90)

$$R = \left[\frac{n^{2N} - 1}{n^{2N} + 1} \right]^2 \quad (5.11)$$

where n = refractive index

N = number of plates forming the etalon.

For $n = 1.7$ and $N = 1$, R is approximately 0.2. The transmission of barium fluoride is approximately 0.75⁽⁴⁸⁾. With this etalon as the output reflector, the energy output increased to 2.4 mJ and remained constant to within 10% over many shots. No damage was observed to either of the reflectors. The pulse duration was 3.5 ns, as shown in plate 10 and the spectral half width was 1.3 ± 0.2 nm, which was similar to that of the Mark 1 system.

The peak gain was calculated using equation 5.4, comparing the fluorescence intensity with and without the back mirror in position. In this case, R was the mirror reflectivity only, as the area of the mirror used to reflect the pulse back through the medium was the same as that of the anode tube. A value of 0.18 cm^{-1} was found for the net gain, using l equal to 12 cm as taken from the thermocouple measurement, which is shown in fig 19b. (Spectra were not recorded with and without the mirror so that no estimates of the total gain and losses were obtained.) This system was less efficient than the Mark 1, although it was much easier to carry out the alignment.

In order to increase the laser output the Blumlein circuit was extended (this was described in Section 4.5), to increase the pulse duration to 5 ns and the total energy deposited in the gas to 10 J. The energy was distributed over a length of about 13.5 cm so that the energy density was about 6 J.cm^{-3} . The gain of the laser was measured, as described in Section 5.2, by studying the A.S.E. spectrally and temporally and the results are given in Table 5.1. The peak value for net gain of $0.30 \pm 0.01 \text{ cm}^{-1}$ at a pressure of 10 ktorr, was similar to that achieved with the Mark 1 system.

When the 80% reflecting mirror and the single plate etalon were used, the laser output energy was 8.7 mJ. This corresponds to an increase by

a factor of four in the laser output energy, by doubling the input energy. A further increase in laser output to 12 mJ was obtained by replacing the 80% mirror with a 93% reflecting dielectric mirror. In all subsequent experiments, the Mark 2 laser, with extended Blumlein was used.

5.5 OPTIMISATION OF THE LASER OUTPUT

The output of the xenon laser is dependent on both the gas pressure and the reflectivities of the mirrors used in the resonator. In order to get the maximum possible output, both these parameters were optimised experimentally.

The mirror reflectivity was optimised by keeping one mirror fixed with $R_1 = 0.93$ and varying the output reflectivity, R_2 , from 0.07 to 0.93 with corresponding transmission of about 0.9 to 0.06. The fixed mirror had a transmission of about 0.06 but the output from this was not included in the measurement of total energy.

Low reflectivity was achieved by reflection from a single face of a lithium fluoride window. The two faces of the window were wedged by about 5 mrad (measured using a Twyman-Green interferometer) so that only one surface contributed to the reflectivity. Both faces were flat to about $\frac{\lambda}{10}$. The reflectivity, R_1 , from a single surface is given by ⁽⁹⁰⁾

$$R_1 = \left[\frac{n-1}{n+1} \right]^2 \quad (5.12)$$

where n is the refractive index

For $n \approx 1.7$, then $R_1 \approx 0.07$

A single plate and a two plate resonant reflector were also used. These were made up of 1 mm thick barium fluoride plates, the faces of which were parallel to better than 1 mrad and flat to $\frac{\lambda}{15}$. The reflectivities

were calculated using equation 5.1. For the single plate etalon R is approximately 0.2 and for the two plate resonant reflector R is approximately 0.6. In both cases the true values will be slightly less than those calculated owing to absorption of the order of 5% in the barium fluoride.

The two plate resonant reflector was aligned using a helium-neon laser beam. The plates were separated by 3 mm and as the reflector was mounted inside the high pressure gas, the space between the plates was maintained at the same pressure as the surrounding region. Multilayer dielectric mirrors with given coefficients of reflectivity and transmission were obtained from Acton Research Corporation and Matra Seavom.

The change in output energy with mirror reflectivity, R_1, R_2 , is shown in fig 29. The optimum output reflectivity was of the order of 0.1 to 0.2. In all cases the pulse duration remained approximately constant in the range 3.0 to 3.5 ns.

When the optical components were examined there was no visible damage to the dielectric mirrors. The barium fluoride etalon and the lithium fluoride reflector were, however, damaged over a region of the order of 2 mm diameter from the centre, on the surface adjacent to the anode tube. In the case of the barium fluoride the damage did not reduce the output as the laser energy was consistent over tens of shots but with the lithium fluoride the output decreased after a few shots.

The optimum working pressure was measured with $R_1 = 0.93$ and $R_2 = 0.2$. The pressure was increased from 5 ktorr and the output energy recorded using a calorimeter. The results are shown graphically in fig 30. The laser threshold occurred at about 6.7 ktorr and the output energy increased to a maximum of 12 mJ which was recorded at a pressure of 11 ktorr, after

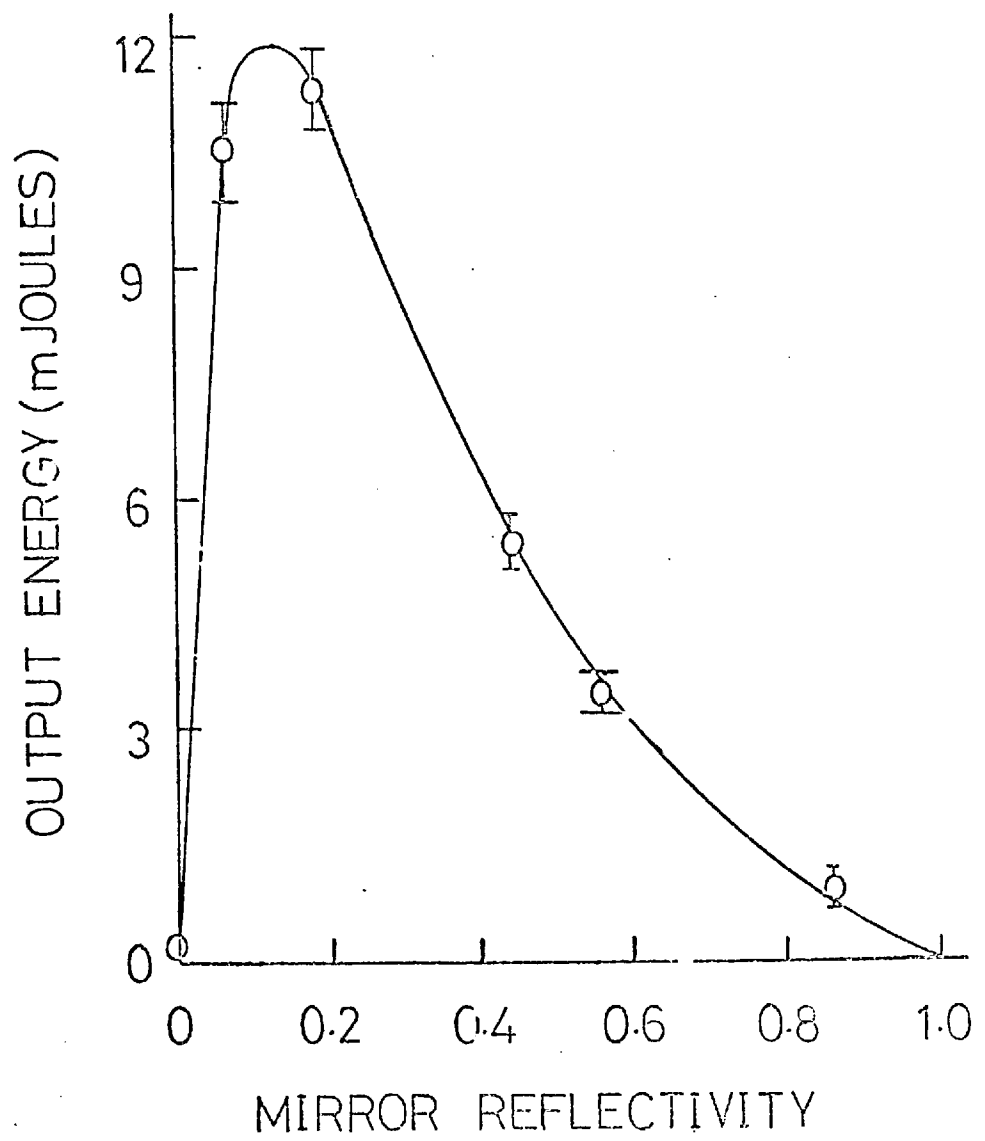


Fig 29

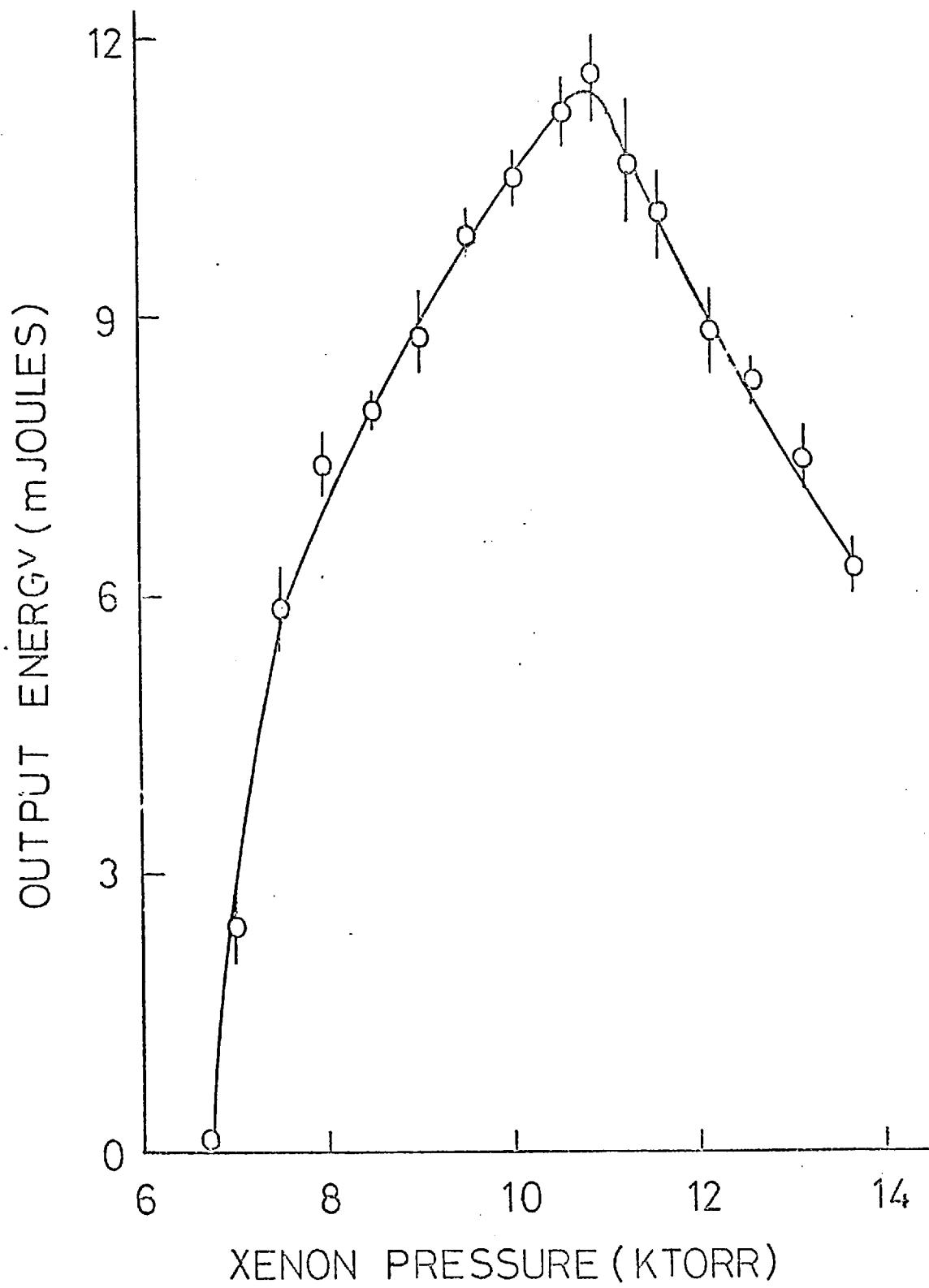


Fig 30

which a decrease was observed. Each point on the graph is an average of at least 3 consecutive shots and the error bar indicates the overall spread in the results. The readings were repeated starting at 14 ktorr and decreasing the pressure, and similar values were obtained.

5.6 SATURATION OF THE LASER

It is evident from plate 10 that when the pumping pulse duration was increased from 2.5 to 5.0 ns, the laser pulse duration decreased from about 3.5 to 3.0 ns. At the same time the total energy increased from the order of 3 to about 12 mJ. This shortening of the laser pulse may be explained by saturation effects. The laser initially builds up from spontaneous emission but with the high gain of the present system the photon flux quickly builds up due to stimulated emission. A stage may be reached when the photons produced deplete the inversion rapidly, until the inversion remaining is not sufficient to maintain the rate of photon creation at the level of the photon loss rate. The photon density then declines and the laser pulse decays at a rate determined by the rate of escape of photons from the laser.

The rate equation for the decay of the upper state population is

$$\frac{dN^*}{dt} = -\sigma N^* F(t) - \frac{N^*}{\tau_f} \quad (5.13)$$

where σ = stimulated emission cross section (cm^2)

$F(t)$ = photon flux ($\text{cm}^{-2}\cdot\text{s}^{-1}$)

τ_f = fluorescence decay time (s)

When the photon flux builds up, the spontaneous term will be small compared with the stimulated emission term so that

$$\begin{aligned}
 N^* &= N_0^* \exp \left[- \sigma \int E(t) dt \right] \\
 &= N_0^* \exp \left[- \sigma E \right]
 \end{aligned}
 \tag{5.14}$$

where N_0^* = initial inversion

The term $\int E(t) dt$ is the accumulated pulse energy, E , in units of photons. cm^{-2} . The saturation energy, E_s , is defined as the energy which reduces the inversion by a factor of $\frac{1}{e}$ (91), so that

$$E_s = \frac{1}{\sigma}$$

The stimulated emission cross section, σ , was measured by Gerardo et al. (56) to be $10^{-25} \tau_f^{-1} \cdot \text{cm}^2$. The measured values of τ_f lie in the range 4×10^{-9} to 20×10^{-9} s, so that σ lies within the range 25×10^{-18} to $5 \times 10^{-18} \text{ cm}^2$. This corresponds to a saturation energy, E_s , of 46 to 230 $\text{mJ} \cdot \text{cm}^{-2}$. In the present laser, the anode tube radius was 2 mm so that the energy density inside the cavity, for a 12 mJ output was of the order of $150 \text{ mJ} \cdot \text{cm}^{-2}$, when allowance was made for both the etalon and window transmission. This indicates that the laser is in the saturation regime.

The value of saturation is consistent with the results of Hunter et al. (84), who found that the sidelight decreased, due to laser action, and the shape of the laser pulse showed that saturation occurred. The total laser output was 8 J and by integrating over the laser pulse up to the time that saturation occurs, it was estimated that the energy density was of the order of $190 \text{ mJ} \cdot \text{cm}^{-2}$. This assumed that the output 2 inch diameter reflector was uniformly illuminated. The total output of 8 joules corresponds to an energy density of about $400 \text{ mJ} \cdot \text{cm}^{-2}$. In the long pulse case, the laser does not terminate so rapidly as the pumping pulse continues to repopulate the upper level.

Because of the high gain of the present system (about 30 per pass) the saturation energy is quickly reached even for a low reflectivity output

reflector. The A.S.E. output for a double transit of the cavity was measured to be about 10^{-2} of the laser output so that if the order of 20% of the A.S.E. is reflected back through the excited medium then after about one further cavity round trip the saturation energy will be reached.

If a higher reflectivity mirror is used then again saturation will be quickly reached, but as the mirror transmission is less, then less energy will be transmitted per transit. For a loss less medium and short pulse excitation, the laser output energy should remain approximately constant if the gain is saturated but the pulse duration should increase as the cavity lifetime increases.

(The cavity lifetime, t_c , is defined as the lifetime of a quantity in the cavity and is related to the mirror reflectivities, R_1 and R_2 , and to the transmission coefficient, T , of the laser medium by (78)

$$t_c = \frac{2L}{c \ln (R_1 R_2 T^2)^{-1}} \quad (5.15)$$

where L is the cavity length

c is the velocity of light.)

It was found, however, that the pulse duration was approximately independent of mirror reflectivity, indicating that when the inversion was depleted and hence the gain reduced, that the scattering losses reduced the output.

The results presented in this chapter have illustrated conclusively the feasibility of constructing a reliable high power xenon laser using short pulse excitation. This was due mainly to the use of a coaxial electron beam diode as the excitation source as it enabled the energy to be coupled efficiently into the laser medium. The laser output was optimised experimentally and the limitations of short pulse excitation were discussed.

TABLE 5.1

	$\Delta\lambda_N$	$\Delta\lambda_W$	Ratio of Intensities	α_{\max}	γ_{\max}	$\alpha_{\max} - \gamma_{\max}$
MARK 1 DIODE						
1. Experimental Results	8.6 ± 0.5	5.0 ± 0.3	4.7 ± 0.1	—	—	—
2. Calculated Values for $l = 8.5$ cm	8.6 ± 0.3	5.0 ± 0.2	4.6 ± 0.2	0.63 ± 0.03	0.33 ± 0.03	0.30 ± 0.01
3. Calculated Values for $l = 10$ cm	8.6 ± 0.3	5.0 ± 0.2	4.6 ± 0.3	0.52 ± 0.03	0.25 ± 0.03	0.27 ± 0.01
MARK 2 DIODE						
1. Experimental Results	5.6 ± 0.4	3.2 ± 0.3	30 ± 2	—	—	—
2. Calculated Values for $l = 13.5$ cm	5.5 ± 0.4	3.2 ± 0.4	30 ± 3	0.63 ± 0.08	0.38 ± 0.08	0.30 ± 0.01

TUNING OF THE XENON LASER

The broad continuous emission spectrum of xenon, which results from transitions between a bound state and a repulsive ground state suggested that it may be possible to obtain a tunable laser. In order to tune the laser continuously, the spectrum must be homogeneously broadened (78) on the time scale of the laser emission. According to the analysis of Mies (61) the spontaneous emission spectrum is a result of the superposition of the spectra of the individual vibrational levels, weighted by the concentrations of the initial states. If the radiative loss is slow compared with the vibrational relaxation time then the population of the vibrational levels will be maintained in a Boltzmann distribution. The data of Fink et al. (43) indicates that vibrational relaxation is fast. Assuming their value of $3 \times 10^{-11} \text{ cm}^3 \text{ s}^{-1}$ for the rate coefficient, then the time for vibrational relaxation to occur is about 90 ps for a number density of atoms of $3.5 \times 10^{20} \text{ cm}^{-3}$ (10 ktorr). For a radiative lifetime of about 4 ns (39) (40) then this relaxation time decreases to approximately 20 ps. Although stimulated emission will deplete particular levels, vibrational relaxation will quickly repopulate these levels so that the spectrum will be quasi homogeneous. The continuous tunability of the xenon laser reported in this chapter is evidence that the spectrum is homogeneous on the timescale of the laser emission.

Most of the work to date on tunable lasers has been with flashlamp or laser-pumped dye lasers (93) which operate over most of the visible region of the spectrum. Most of the techniques devised in these studies may be applied to noble gas lasers when allowance is made for the VUV operating conditions.

Frequency narrowing may be achieved by inserting a dispersive element in the cavity, in order that the normal broad band laser output may be extracted over a smaller frequency band which satisfies the feedback condition. If losses in the dispersive element are ignored, then for a homogeneous transition, the total energy may be extracted in this narrow band.

In this chapter methods of tuning are reviewed and the choice of a tuning element for the xenon laser is discussed. The design of a mount which allows alignment at the He-Ne (helium-neon) laser wavelength is outlined and results for the tuned laser are reported.

6.1 THE SELECTION OF A TUNING ELEMENT

It has been observed experimentally ^{(83) (55)}, that the peak wavelength of the xenon laser shifts to longer wavelengths as the xenon pressure is increased. This pressure tuning is small, of the order of 1 nm for a pressure change from 5 to 15 ktorr.

To obtain a frequency narrowed, tunable output, a wavelength selective element, such as a diffraction grating ^{(94) (95)}, Fabry Perot etalon ⁽⁹⁶⁾, prisms ^{(97) (98)}, or some combination of these elements, may be inserted into the cavity so that only a small frequency range satisfies the feedback condition. These tuning elements were considered, in order to find which was the most suitable for VUV wavelengths.

6.1.1 DIFFRACTION GRATINGS

A diffraction grating was the first dispersive element used for tuning a dye laser ⁽⁹⁴⁾. For a diffraction grating ⁽⁹⁰⁾

$$m\lambda = d (\sin\alpha + \sin\beta) \quad (6.1)$$

where $m =$ order

$\lambda =$ wavelength

$d =$ separation of the grating rulings

$\varphi =$ angle of incidence

$\beta =$ angle of diffraction

For autocollimation, the incident and diffracted beams are collinear ($\varphi = \beta$), so that the angular dispersion, $\frac{d\varphi}{d\lambda}$, is given by

$$\frac{d\varphi}{d\lambda} = \frac{m}{2d \cos\varphi} \quad (6.2)$$

For a first order spectrum and $600 \text{ lines}\cdot\text{mm}^{-1}$ grating, the angular dispersion is approximately $3 \times 10^{-4} \text{ rad}\cdot\text{nm}^{-1}$. The xenon laser has a beam divergence, $\Delta\varphi$, of typically 2 mrad, so substituting this value in equation 6.2, the passive spectral bandwidth is approximately 7 nm. For a diffraction limited beam, the divergence ⁽⁹⁰⁾, $\Delta\varphi_D$, is given by

$$\varphi_D = \frac{1.22 \lambda}{D} \quad (6.3)$$

where $D =$ diameter of the anode tube (3.5 mm)

So with $\lambda = 172 \text{ nm}$, then $\Delta\varphi_D$ is approximately 0.08 mrad and thus the spectral width equals 0.2 nm, which is the minimum passive bandwidth obtainable with this grating.

The reflectivity of a diffraction grating in the vacuum ultraviolet, is less than 50% ⁽⁹⁹⁾, so using a grating as a reflector introduces a large loss into the system. As VUV gratings are normally coated with a thin layer of aluminium and overcoated with magnesium fluoride, the damage which was observed to mirrors with similar coatings (see Chapter 5), is likely to occur to diffraction gratings. To prevent damage to the grating it may be possible to expand the laser beam or to use a partially transparent mirror in front of the grating, as suggested by Bjorkholm et al. ⁽¹⁰⁰⁾. This mirror-grating combination acts as a high reflectivity resonant reflector for the tuned output and at the same time reduces the

power incident on the grating. Owing to the low reflectivity and low damage threshold, a grating was considered to be unsuitable as a dispersive element in the VUV.

6.1.2 FABRY-PEROT ETALONS

Fabry-Perot etalons (FP) have been successfully used to obtain narrow bandwidth tuning in dye lasers ⁽⁹⁶⁾. The wavelength, λ , which has the maximum transmission in the p^{th} order is given by ⁽⁹⁰⁾

$$\lambda = \frac{2nd \cos \alpha}{p} \quad (6.4)$$

where n = refractive index of the material between the FP plates

d = plate separation

α = angle between the beam and the normal to the plates

The angular dispersion, $\frac{d\lambda}{d\alpha} = -\frac{2nd \sin \alpha}{p}$, (6.5)

so for a beam divergence, $\Delta\varphi$, the passive spectral bandwidth, $\Delta\lambda_p$, is given by

$$\Delta\lambda_p = \frac{2nd}{p} \sin \alpha \cdot \Delta\varphi \quad (6.6)$$

The passive spectral bandwidth is therefore dependent on the angle of incidence. If however, α is small then the bandwidth is determined by the finesse of the etalon and not the beam divergence. In this case the spectral width of the output is given by

$$\Delta\lambda_p = \frac{\text{FSR}}{F} \quad (6.7)$$

where $\text{FSR} = \frac{\lambda^2}{2d}$ is the free spectral range

$F = \frac{\pi R^2}{1 - R}$ is the finesse of an FP with plates of reflectivity, R .

At present, low loss, high reflectivity coatings are not readily available, so that a high finesse FP can not be obtained. Using uncoated plates, reflectivities of about 0.2 may be obtained giving an F of the order of 1.3.

The above analysis relates to the passive bandwidth but in the case

of a laser the bandwidth of the output decreases in successive transits through the dispersive element (101) (102). In the experiments described in this Chapter using short pulse excitation, there are only a few transits through the dispersive element, so that little narrowing occurs using uncoated plates.

The output coupling element used in the untuned laser was an uncoated single plate etalon consisting of a 1 mm thick disc of barium fluoride, so that FSR is equal to 9×10^{-3} nm for $\lambda = 172$ nm and $n = 1.6$. Any structure on the laser spectrum of this order of magnitude could not be resolved in the spectrographs which were available.

Whilst tuning of the short pulse xenon laser using a Fabry-Perot etalon is not feasible at the present time, with the development of longer pumping pulses and improvement in VUV coatings this method may become practical. Furthermore the requirement for a second dispersive element to prevent overlapping of successive orders introduces additional losses in the cavity.

6.1.3 PRISMS

At visible wavelengths, the dispersion of most transmitting materials is small so that single prisms are not used as tuning elements when narrow bandwidth outputs are required. They can be used to select one of the several sharp lines which occur in gas lasers, such as the argon ion, or as a predisperser in conjunction with a second dispersive element (103). Prisms have the advantage over other tuning elements in that losses can be made very small, and the damage threshold is much higher (97). In order to increase the dispersion in lasers operating at visible wavelengths, multiple prism arrangements have been used (97) (98).

At the xenon laser wavelength (172 nm), however, the dispersion, $\frac{dn}{d\lambda}$,

of many transmitting materials, such as barium fluoride, sapphire and fused silica, is high (greater than 10^{-3} nm^{-1}), as the bandgap is close to the wavelength of interest. Because of the high dispersion and the good transmission, a fused silica prism was chosen as the dispersive element. The transmission of a 3 mm disc of the material (Thermal Syndicate Spectrosil 'B'), was measured to be 85% at 170 nm, although at this wavelength the absorption was beginning to increase. The refractive index was estimated to be about 1.62 by extrapolating from values given in 'Handbook of Chemistry and Physics' (80), and the dispersion $\frac{dn}{d\lambda}$, of about $3 \times 10^{-3} \text{ nm}^{-1}$ was estimated from the slope of the graph of n vs. λ .

In order to reduce reflection losses at the prism surfaces, a prism with angles close to Brewster's angle was used (90). The geometry of a beam passing through such a prism, at minimum deviation, is shown in fig 31 below.

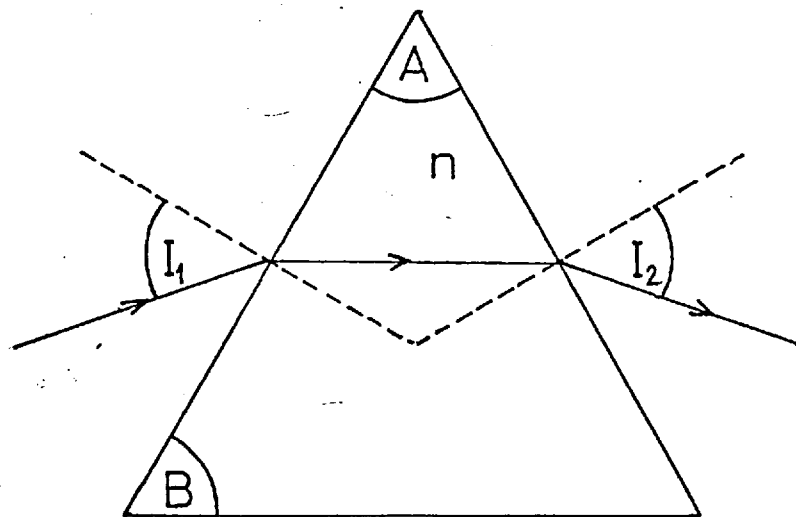


Fig 31

Now $\tan I_1 = \tan I_2 = n = \tan B$ (6.8)

where n = refractive index

B = Brewster's angle

For n equal to 1.62, B is approximately 58.3° . In practice a 60° prism was used.

For a prism at or near Brewster's angle, the following relationship holds (90)

$$\frac{d\phi}{d\lambda} \approx 2 \frac{dn}{d\lambda} \quad (6.9)$$

so for a fused silica prism, the angular dispersion is about 6×10^{-3} rads.nm⁻¹. For a beam divergence of 2 mrad, then from equation 6.9, the passive spectral width is 0.3 nm and for a diffraction limited beam divergence of about 0.08 mrad, the passive spectral width is approximately 0.013 nm.

A separate mirror and prism were used, as shown in fig 32, in preference to using a coated prism (104), as twice the dispersion was achieved per transit. This increased the difficulty of alignment, (described in the next section), but if the mirror was damaged it was not necessary to realign the complete system as the mirror could be rotated in its mount to expose an undamaged part of the coating.

6.2 THE DESIGN OF A MOUNT FOR THE TUNING ELEMENT

The tuning element mount was designed to enable

- (i) the refracting edge of the prism to be adjusted so that it was parallel to the axis of rotation of the table,
- (ii) the plane of the mirror to be aligned independently, so that it too was parallel to the axis of rotation of the table,
- (iii) the prism and mirror to be adjusted together, so that a He-Ne laser beam aligned along the anode tube was reflected back along its own path,

TUNING ARRANGEMENT

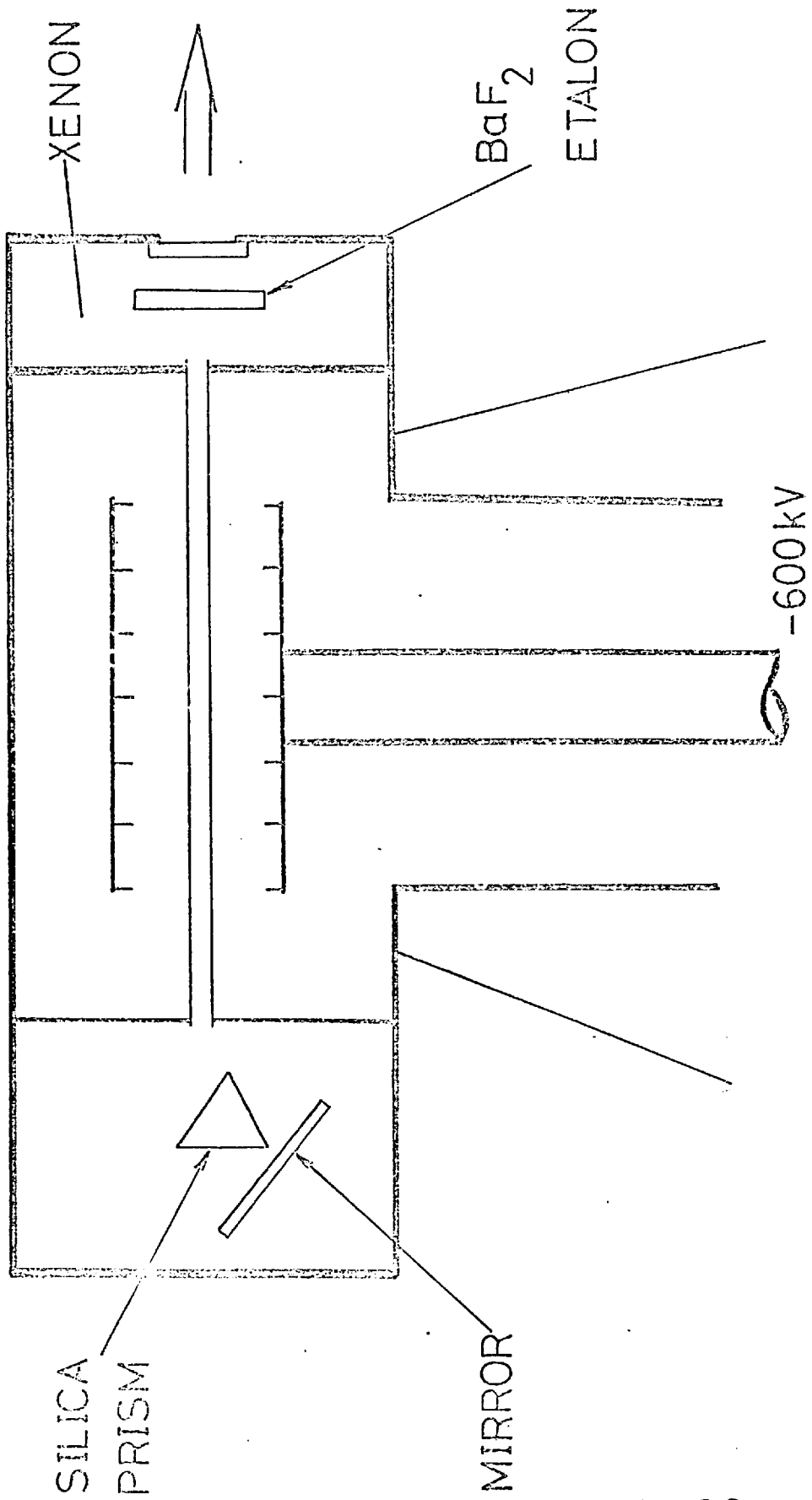
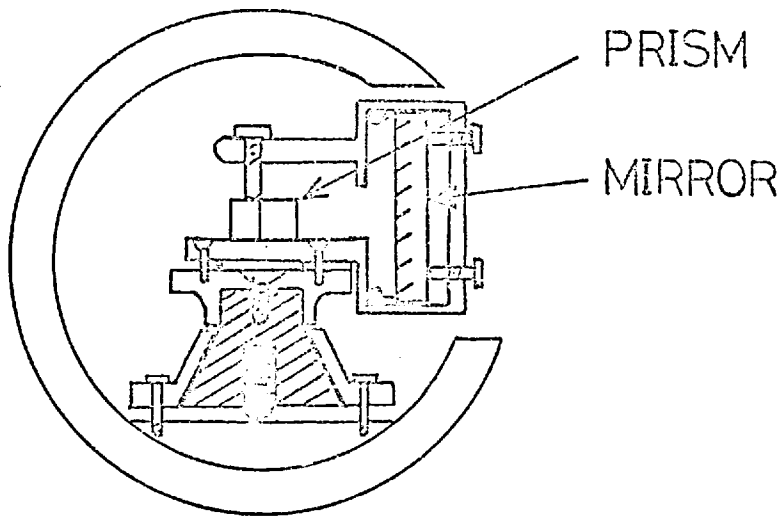


Fig 32

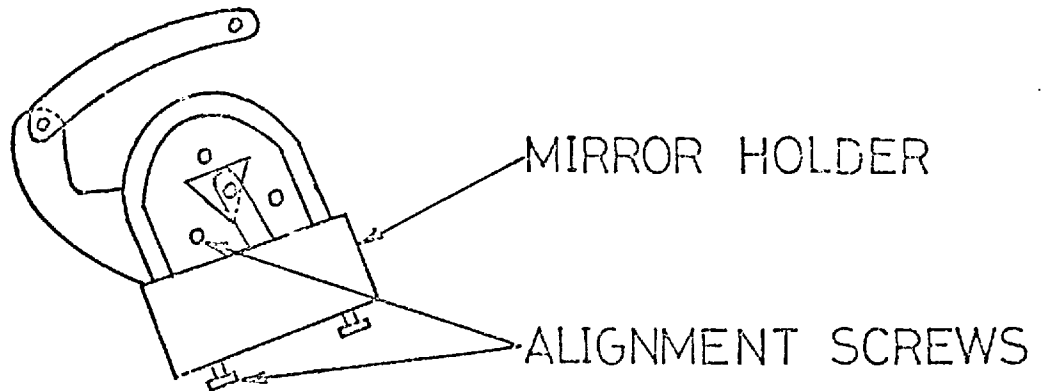
- (iv) the prism and mirror to be rotated from the 632.8 nm position to the region of 170 nm, and
- (v) the prism and mirror to be rotated with sufficient accuracy to tune across the xenon wavelength; this fine adjustment was made through a high pressure seal.

The mount that was constructed to satisfy these conditions, is shown in fig 33. The complete mount was firmly fixed inside a cylinder, which could be inserted into the laser cavity. This enabled the initial alignment of the system to be carried out before inserting the element into the cavity. A spring and bearing arrangement was used to maintain firm contact between the stainless steel cone and the brass retaining plate, both of which had been accurately machined to give rotation about a fixed axis. In order to define this axis the prism table was removed and replaced by a polished rod, the surface of which was parallel to the axis of rotation. The axis of rotation was defined by noting the position of three reflections from a helium-neon laser off the rod. To facilitate final alignment the rod axis was adjusted so that it was approximately perpendicular to the alignment beam.

The mirror and prism were mounted on a common table, but each had separate fine adjustments. The prism was positioned so that the beam passed close to the refracting edge, to reduce the path length traversed in the fused silica. As the prism and mirror were mounted on a common table, the angle, I_1 , between them (see fig 31) remained constant so that the prism was adjusted to give $I_1 \simeq 58^\circ$, and then fixed rigidly in position. The next step was to adjust the prism so that its refracting edge was parallel to the axis of rotation. The prism was adjusted using the screws on its kinematic mount until the He-Ne laser reflections from the refracting faces were coincident with those observed from the polished rod. Alignment was made much easier if reflections from both faces were observed and adjusted simultaneously. The mirror was placed



//// STAINLESS STEEL
(Other material was
brass)



TUNING ELEMENT MOUNT

Fig 33

in position and adjusted so that the refracted beam was reflected back along its own path. At the wavelength 632.8 nm, the refractive index of fused silica is about 1.46⁽⁸⁰⁾, so that the angle of deviation is different from that at 172 nm. For a fixed angle $I_1 \simeq 58^\circ$ the angle of deviation at the wavelength of 632.8 nm was calculated to be about 37° compared with 50.5° at 172 nm, so that after alignment the table had to be rotated by about 13° to the tuning position.

The cylinder containing the tuning element was firmly bolted to the inside of the cavity and a final adjustment made, using the screws on the base of the brass retaining plate so that the beam was reflected along the tube axis. This adjustment enabled the axis of rotation to be varied while keeping the prism and mirror axis parallel to it.

Rotation of the table through a high pressure seal was possible using two arrangements. In the first, a screw was pressed against a plate which was attached to the table and the force required to rotate the table was provided by a compressed spring. The second arrangement had a direct drive between the table and a micrometer and provided a more reproducible arrangement. When the first method of adjustment was used the wavelength of the laser was reproducible to within ± 0.2 nm for a given position of the adjusting screw whereas with the second arrangement the wavelength could be reproduced to within 0.1 nm for a given micrometer reading. In order to obtain reproducible results it was necessary in both cases to take all readings when rotating the adjusting screw in the same direction.

The output reflector used, was a single plate barium fluoride etalon and this was aligned using the He-Ne laser. The prism table was rotated to the helium-neon wavelength and then the cavity evacuated before filling with high pressure xenon. As the xenon pressure increased the reflected laser spot was observed to move along a line perpendicular to the axis of

rotation. This was due to the change in pressure in the wedges of gas between the prism and the mirrors. As the pressure of the gas increases, the refractive index, n , changes such that (105)

$$\frac{n - 1}{D} \approx \text{constant} \quad (6.10)$$

where D = gas density

For xenon at a pressure of 11 ktorr, the refractive index is about 1.01. With this change in refractive index, the deviation from the zero pressure position is, therefore, about 2° , for the helium-neon wavelength. The deviation will be larger at shorter wavelengths, so in practice it was easier to find the tuning position experimentally rather than by calculation, since the gas refractive index is unknown in the VUV. It was also observed that if the helium-neon laser was not aligned accurately along the anode tube axis, then there was a deviation of the reflected beam along the axis of rotation. If the etalon was aligned with the beam which was reflected by the mirror when the system was evacuated, then the resonator appeared to move out of alignment as the xenon pressure increased. This was corrected by adjusting the helium-neon laser, while the system was under pressure, until the beam reflected from the tuning element was collinear with the incident beam. The etalon could then be aligned correctly.

6.3 THE OUTPUT OBTAINED FROM THE TUNED LASER

The Mark 2 diode, with the extended Blumlein circuit was used to obtain the tuning results. The resonator length was 25 cm and the output reflector was a 1 mm thick, single plate barium fluoride resonant reflector with reflectivity of about 0.2 while the mirror mounted in the tuning element had a multilayer dielectric coating with reflectivity of 0.93. A xenon pressure of 11 ktorr was used for all readings.

Output spectra were recorded on Kodak SC7 film using a 1 metre normal incidence vacuum spectrograph in first order. With a slit width of 0.05 mm

spectra were not recorded unless the feed back condition was satisfied. The film holder was modified so that it was possible to place the film in the same position for consecutive shots thus enabling one edge to be calibrated absolutely. This edge was calibrated using the 184.9 nm line of mercury and the known dispersion of the spectrograph. For calibration the mercury lamp was mounted in a T-piece, one arm of which was connected to the spectrograph input slit, but isolated from it using a barium fluoride window. Helium was allowed to flow continuously around the lamp to keep it cool, and to remove oxygen and ozone which are strongly absorbent at 184.9 nm.

Plate 11 shows spectra of the tuned and narrowed output of the xenon laser, the film being displaced vertically between consecutive shots. The spectral half width was measured by taking a densitometer of the spectra as shown in fig 34 and then using the measured value of the film γ . The recorded bandwidth, λ_m , was 0.16 nm and the instrumental resolution, λ_r , was 0.08 nm so that the true bandwidth, λ_t , calculated from

$$\lambda_t^2 = \lambda_m^2 - \lambda_r^2 \quad (6.11)$$

was 0.13 ± 0.03 nm.

There is spectral narrowing by a factor of 100 from the fluorescence bandwidth and by a factor of 10 from the untuned laser. The total tuning range extended from 169.2 ± 0.2 nm to 176.5 ± 0.2 nm and it was possible to tune continuously over the entire range. The spectral bandwidth at all wavelengths was less than 0.2 nm, but small variations could not be measured accurately due to the uncertainty in the γ of the film. When the spectrally narrowed output was observed only about 4 mm of the slit was illuminated although a much lower intensity scattered component was seen to fill the complete slit, this indicated the low divergence of the beam.

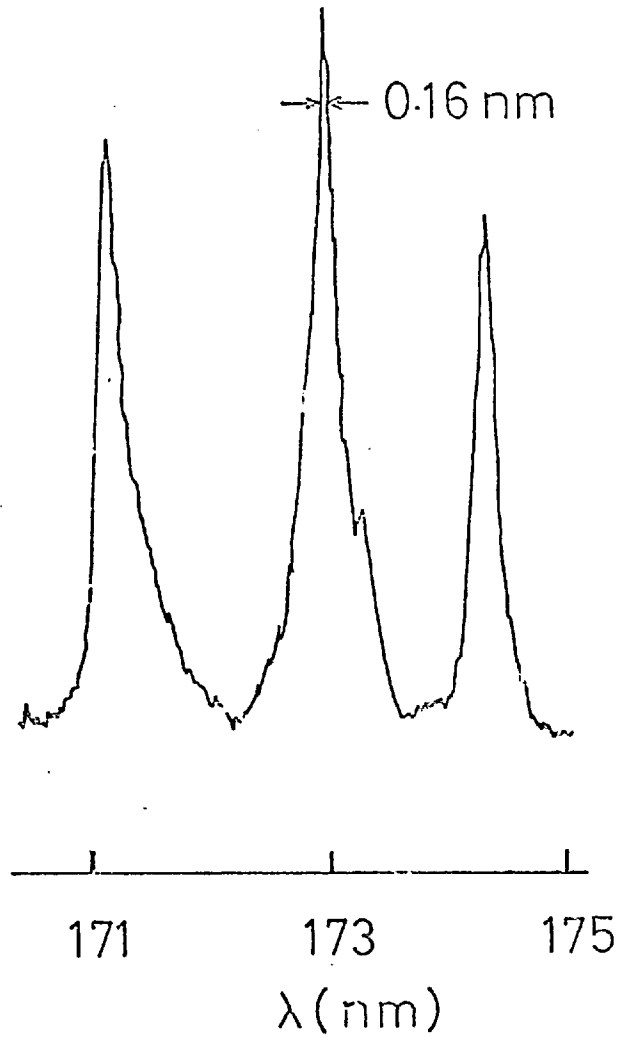
PLATE 11

Output Spectra of the Tuned Laser

Wavelengths from left to right :

171.4, 173.0 and 174.4 nm



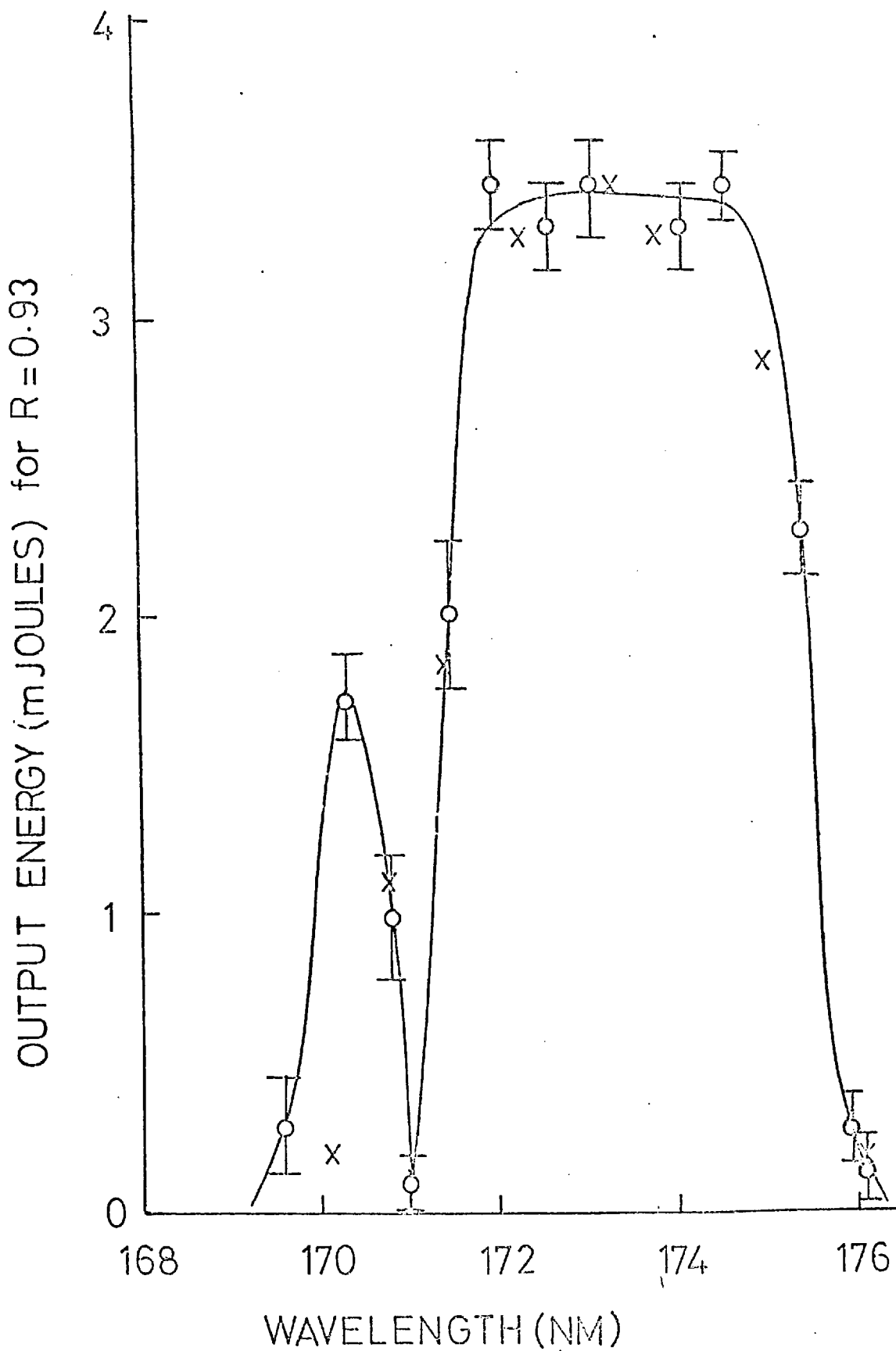


Microdensitometer trace of tuned spectra showing discrete lines.

Fig 34

The micrometer used to rotate the prism table was calibrated for wavelength and the output energy was then measured at different wavelengths using a calorimeter (Laser Instrumentation Model 142 LR Thermopile). The variation of output energy with wavelength is shown in fig 35. Each point is the average of at least three shots and in most cases the reproducibility was better than 20%. The maximum energy recorded was 3.6 mJ and the energy remained within the range 3.3 ± 0.3 mJ over the wavelength interval 172 to 175 nm. A series of results taken when the 93% reflectivity mirror was replaced by an Al : MgF₂ 80% reflectivity mirror, are also shown in fig 35 for comparison. In this case the peak output obtained was 1.9 mJ. (The two sets of results were normalized at 173.0 nm.) The tuning range was increased slightly by using the higher reflectivity mirror. The tuning range measured spectrally was about 0.5 nm greater than that shown in fig 35, as the calorimeter only measured energies greater than about 0.2 mJ.

Narrowing of the laser output was only possible if reflections from the walls of the anode tube were eliminated, because at angles near grazing incidence, the reflectivity of metals is high ⁽⁸⁸⁾ (greater than 90%). If the prism and mirror are set up for tuning at a particular wavelength then longer and shorter wavelengths will be diverging, relative to the tuning axis, on leaving the prism. Any wavelengths which enter the anode tube will be amplified as they will be guided along the tube by wall reflections. The separation between the prism and the anode tube was about 20 mm so that any wavelength which diverges by less than about 15 mrad from the axis will enter the tube. For an angular dispersion of about 6×10^{-3} rads. nm⁻¹ the passive bandwidth for a double transit through the prism would be of the order of ± 1.2 nm about the wavelength satisfying the feedback condition. When the wall reflections were not eliminated, the recorded bandwidth was 1.8 ± 0.2 nm and the total tuning range, taken as the separation of the peaks at the extremes of tuning, was



o-R=0.93, x-R=0.8 (R=mirror reflectivity)

Fig 35

only 1.5 nm.

Wall reflections were eliminated by inserting a spiral of nichrome wire inside the tube. When the spiral was inserted the energy of the untuned laser decreased to about 8 mJ. The tube diameter was also decreased from about 4 mm to 3.5 mm so that the output energy density remained unchanged at approximately 85 mJ. cm^{-2} . The peak tuned energy density of about 37 mJ. cm^{-2} was thus about 45% of the untuned output. This decrease may be attributed mainly to losses in the prism due to both absorption in the fused silica and reflection losses at the prism surfaces.

The pulse duration of the tuned output was measured using an ITT F4115 photodiode and Tektronix 519 oscilloscope. Three typical results are shown in plate 12. In all cases the pulse duration (FWHM) was approximately 5 ns and this remained unchanged at any wavelength observed. This is to be compared with the untuned pulse duration of 3 ns.

6.4 A DISCUSSION OF THE TUNING RESULTS

It was found that the total tuning range of the xenon laser was about 7.5 nm, compared with the fluorescence bandwidth of about 14 nm. The wavelength dependence of the gain could not be measured so a rough estimate was obtained from the calculations carried out in Section 5.2 to find the laser gain. In these calculations the temporal dependence and the spectral profile of the A.S.E. output, with and without one mirror aligned in the cavity, were obtained. The fluorescence spectrum in the absence of gain was assumed to be gaussian with a half-width of 14 nm. The values of peak gain and loss were varied until good agreement was obtained between the experimental and calculated values of the spectral half-width and the ratio of peak intensities.

The calculated spectral profiles, with and without a mirror aligned,

PLATE 12

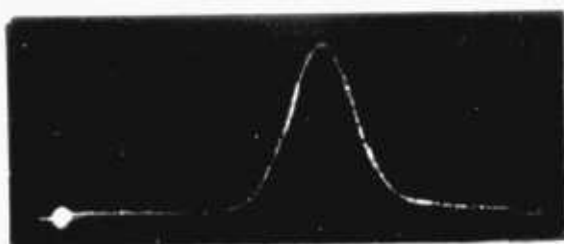
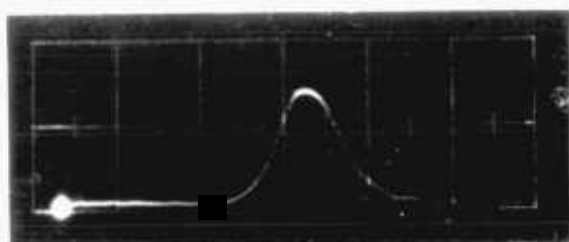
Temporal Dependence of the Tuned Laser

(a) 171.4 nm

(b) 173.0 nm

(c) 174.4 nm

timescale : 5 ns per major division



are shown in fig 36a: these have been normalised at the peak values. By measuring the relative intensities of the 2 spectra at different wavelengths, an estimate of the wavelength dependence of the gain, $e^{\alpha l}$, was obtained, as shown in fig 36b. This curve is for $\alpha_{\max} = 0.7$ and $\gamma_{\max} = 0.4$, which gave good agreement between experimental values of both spectral half-width and peak intensity. It can be seen that the gain falls off rapidly from the peak value and is reduced by about a factor of five at about 4 nm from the peak. When a tuning element is inserted, further losses are introduced in the cavity due to reflections at the surfaces of and absorption losses in the fused silica prism. From fig 36b it is reasonable to expect that the bandwidth over which net gain occurs, that is the tuning range, will be of the order of 8 nm when the additional tuning losses are included.

The graph of output energy against wavelength, fig 35, does not follow the calculated gain curve. The output of the tuned laser remained in the range 3.3 ± 0.3 mJ in the wavelength region 172 to 175 nm and this may be explained by saturation. Saturation effects were discussed in Section 5.6, with regard to the untuned laser, where a saturation energy density of about 87 mJ. cm^{-2} was estimated. The lower saturation energy density of about 37 mJ. cm^{-2} in the tuned laser may be attributed to the slower build up due to increased losses caused by the insertion of the prism. This slower build up is evident by comparing the pulse shapes of the tuned and untuned laser shown in plates 10 and 12, respectively. During the build up time the inversion is being continuously depleted by spontaneous emission, so by the time the laser pulse has reached its maximum the inversion has been reduced to a value less than that for the untuned case. The saturation condition may again be defined as the energy density required to reduce the inversion by $1/e$, so a lower inversion results in a lower saturation energy.

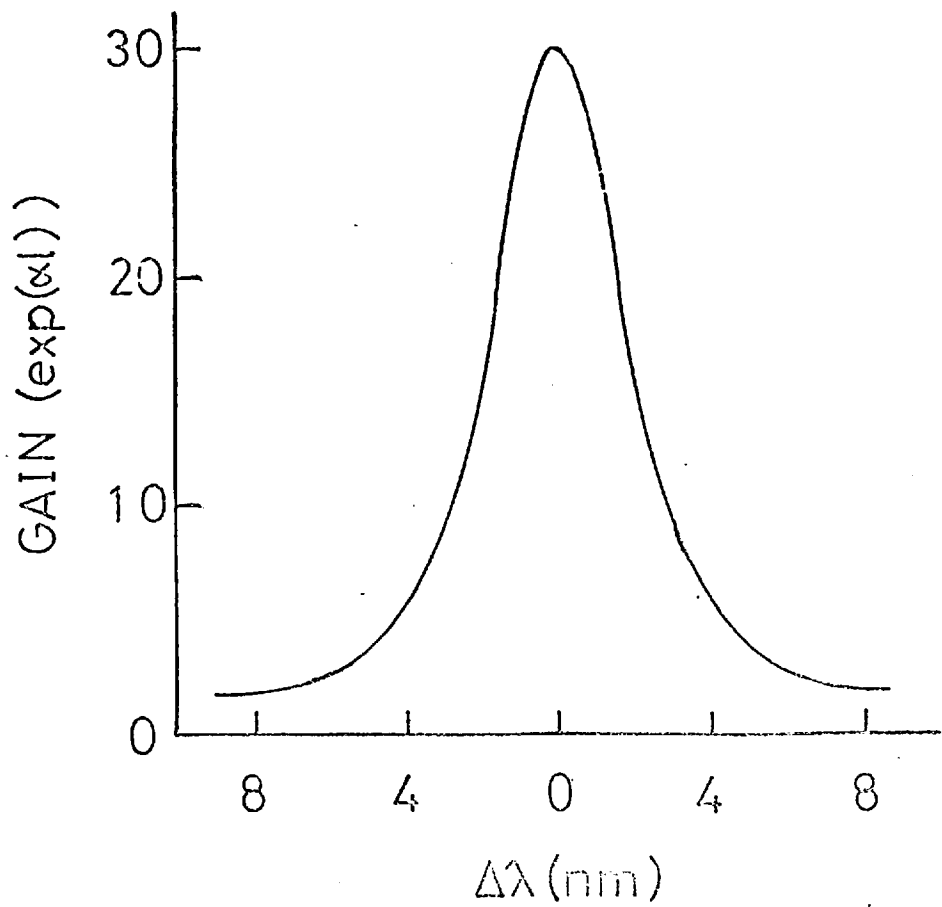
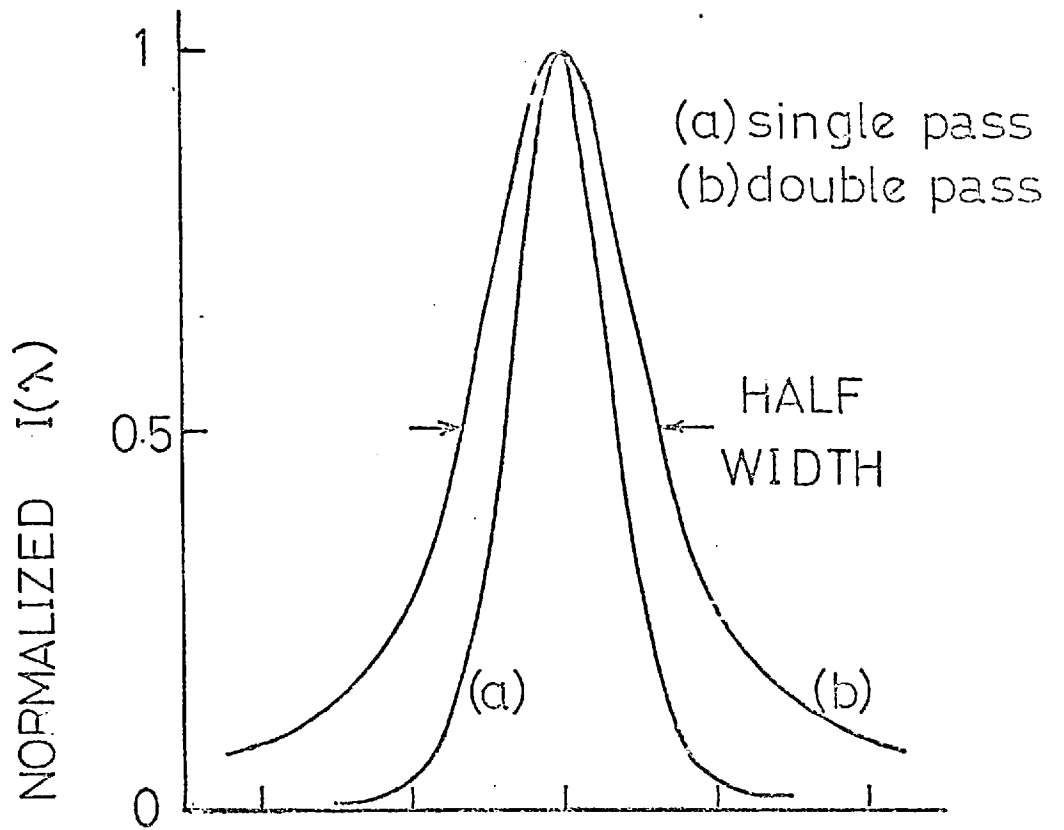


Fig 36

The results obtained without placing the spiral of wire in the anode tube in order to reduce wall reflections, indicate that the gain is wavelength dependent. When the tuning element was set up for feedback at 169 nm and 175 nm the peaks of the output spectra occurred at about 171 and 173 nm, respectively. This shows that although the feedback was less at these wavelengths, the gain was much higher thus allowing the laser flux to build up.

From the experimental results it appears that the peak gain occurs at 172.5 ± 0.5 nm. The short wavelength dependence of the tunable output was not obtained accurately owing to the strong impurity absorption at about 171.2 nm and also the increasing absorption in the prism at wavelengths less than 170 nm.

In the spectrum of the untuned laser shown in plate 9 two absorption bands at about 171.2 and 172.9 are evident, but the 172.9 band does not appear in the tuned spectrum. The microdensitometer trace shown in fig 21 indicates that this absorption band is less strong than that at 172.9 nm. Although in the tuned laser the total intensity is reduced, the intensity per unit wavelength is increased so that the transition leading to the absorption at 172.9 may be saturated or "bleached". The gain at this wavelength will be reduced but it is still sufficient to allow the laser to build up to saturation.

The results presented in this chapter illustrate conclusively the continuous tunability of the xenon laser over the range 169.2 to 176.5 nm. Tuning of the laser over a range of 5 nm has also been reported by Wallace et al. (104) using a BaF_2 prism as a dispersive element. The spectral half-width of 1 nm obtained by them was about a factor of 10 greater than that reported here and the peak power was less by a factor of 10^3 . The energy tuning range of 2500 cm^{-1} for the xenon laser is the largest range of any laser which has been reported.

CONCLUSIONS

The output fluorescence from xenon, which was emitted mainly in the spectral region of 170 nm, was studied over a range of pressures from 0.6 to 14 ktorr and found to have a pressure dependence. As the pressure increased the rates of rise and decay increased, and by analysing these results values of 16 ± 2 ns for the true fluorescence decay-time and $(3.0 \pm 0.3) \times 10^{-32} \text{ cm}^6 \cdot \text{s}^{-1}$ for the three body formation rate of the excited xenon molecule were obtained. The measured decay rate was found to increase linearly with pressure above 3 ktorr so a quenching of the excited molecule in collision with a ground state atom was postulated. However the experimental results differed from those obtained at other laboratories in which a similar excitation source was used, indicating that this simple approach was not adequate. A number of theoretical explanations have been put forward to account for the pressure dependent decay and the discrepancies in experimental results. As with all solutions of 'many body' problems each model makes a number of assumptions and there is not as yet enough experimental evidence to assess fully the validity of each theoretical approach. All theories include contributions from both the $1\sum_u^+$ and $3\sum_u^+$ levels to the total output radiation. These two levels are always given different radiative lifetimes but the values used vary widely. The results of each of the theoretical approaches lead to the conclusion that the observed pressure dependent decay is actually an electron density dependent decay, so that the discrepancy in the results obtained at different laboratories may be attributed to different pumping geometries and electron beam characteristics.

Experiments aimed at building a xenon laser using standard commercial electron beam diodes were not successful owing to the difficulty of efficiently coupling the energy into the gas. A laser was successfully

built after designing and constructing a novel electron beam diode employing a coaxial pumping geometry. Electrons were emitted from a cylindrical cathode which was concentric with an anode consisting of a thin walled stainless steel tube, which also acted as the container for the high pressure gas. When the -600 kV pulse was applied to the cathode electrons were emitted by field emission, from an array of spikes, and accelerated towards and passed through the anode tube which was maintained at earth potential. This arrangement had the advantage of using the radial focussing inherent in the cylindrical geometry to help overcome the beam scattering introduced by the beam foil and the gas. The anode tube had a wall thickness of 0.06 mm so that about 50% of the electrons were stopped in the tube walls. This fraction could have been reduced by decreasing the wall thickness or using another metal such as titanium, which has equivalent strength but about half the stopping power. The radius of the anode was chosen to give uniform electron deposition in the gas at about 10 ktorr which in most experiments that were reported was the region of optimum pressure for laser energy. The dimensions of the cathode were then calculated from the space charge equations for current flow between concentric cylinders.

Using the coaxial diode, laser powers of the order of 1 MW were produced. This was increased to 4 MW (12 mJ) when both the energy deposited in the gas and the pumping pulse duration were doubled, by modifying the Blumlein circuit. Initially the reliability of the laser was limited by the quality of the laser optics as the coatings on the Al : MgF₂ mirrors were damaged after a few shots by the high intracavity laser energy. The use of multilayer dielectric mirrors with low absorption and high reflectivity, together with a single plate BaF₂ etalon, enabled the laser output to be consistent as no damage was observed to the optics after several hundred shots had been fired.

The gain of the laser was obtained by comparing the spectral widths and the ratio of the intensities of the amplified spontaneous emission with and without a high reflectivity mirror aligned in the cavity. The total gain of the laser was calculated to be about 0.7 cm^{-1} with a net gain of about 0.3 cm^{-1} . The main loss mechanisms are thought to be due to scattering in the laser medium and ground state absorption, both of which are temperature dependent. The temperature dependence of the loss mechanisms was illustrated by the marked decrease in the laser output when the laser was fired repetitively, so that the gas was not allowed to cool between shots. If, however, the gas was cooled by allowing it to flow through a heat exchanger then the laser output remained constant when fired repetitively. Johnson et al. ⁽⁸⁶⁾ suggested the addition of helium to reduce the gas temperature but with the short pulse excitation this was found to have a detrimental effect unlike the case using a 50 ns excitation pulse. Gas heating by the electron beam will be one of the important considerations in building an efficient xenon laser, especially when excitation pulses of tens of nanoseconds are used. In the case of short pulse excitation the high energy density is required to create the inversion quickly so that the laser builds up before the upper level is depleted by spontaneous emission.

The present limit on the output energy of 12 mJ is considered to be due to saturation effects. It was shown that the saturation energy density, E_s , which is the energy density that reduces the inversion by $1/e$, is equal to $1/\sigma$ where σ , the stimulated emission cross section, is approximately equal to 10^{-17} cm^2 . In short pulse excitation, E_s may be taken as the upper limit because when the inversion is depleted repopulation does not occur as the pumping pulse has terminated.

The spectral bandwidth of the untuned laser was about 1.3 nm, centred at 172 nm, so in order to obtain a narrower bandwidth tunable laser, a dispersive element was inserted in the cavity. A fused silica prism was

selected as the dispersive element because of its high dispersion and transmission in the VUV. The prism and mirror were mounted on a common table which could be rotated about the prism axis while the system was at the working pressure. The laser output was continuously tunable over the range 169.2 to 176.5 nm and the spectral bandwidth of about 0.13 nm was a factor of ten less than the untuned laser and a factor of one hundred less than the fluorescence bandwidth. Narrower bandwidths could be obtained using longer pumping pulses, thereby increasing the number of transits through the dispersive element, or by using a multiple prism arrangement. In the short pulse case the additional losses due to absorption losses in the material and reflections at the surfaces, may prevent the laser reaching threshold.

The maximum tuned output laser energy of 3.6 mJ was about 45% of the untuned laser under similar experimental conditions. It was necessary to insert a spiral of wire in the cavity to prevent wall reflections from the anode tube, otherwise the laser was only tunable over about 1.5 nm with a bandwidth of 1.8 nm. The decrease in the tuned output energy was due mainly to the increased cavity losses caused by the insertion of the prism. This was illustrated by the longer build up time of 3.5 ns in the tuned laser compared with about 2.0 ns in the untuned case. The output energy remained approximately constant over the wavelength range of 172 to 174.5 nm and this was taken as an indication of saturation.

The laser system described in this thesis has proved to be a reliable compact system, providing an intense source of tunable VUV radiation. One important application for the laser may be in the field of photofragmentation spectroscopy. The photons have an energy of the order of 7 eV and this is sufficient to break the bonds in many large organic molecules such as are found in plant and human tissue. The fragments produced may then be analysed and the structures of many of these molecules determined.

As the laser is tunable over a large range it may be possible to use it for selective excitation of both inner and outer shell electrons. A second photon of a different wavelength may then be used to ionize the atom (106). If a narrower bandwidth could be obtained from the xenon laser then this method of selective ionization could be investigated for use in isotope separation as it may be both cheaper and more efficient than existing techniques.

Since the xenon laser has a short wavelength, it could also be employed for diagnostics of high density plasmas. A photon cannot propagate in a plasma unless its frequency is greater than the plasma frequency, ω_p (72), which is proportional to the (electron density) $^{1/2}$. The ω_p corresponding to the wavelength of the xenon laser, occurs at an electron density of about $3 \times 10^{22} \text{ cm}^{-2}$, approximately solid density. This should enable scattering measurements to be made on very high density plasmas which occur in laser compression experiments.

At present there is a great deal of interest in any efficient laser system that might be used to study the interaction of high power laser radiation with solid targets, with a view to laser fusion experiments (107). In order to obtain output energies of hundreds of joules in pulses in the range of 100 ps to 1 ns from a xenon laser, it would be necessary to build xenon amplifiers and to obtain short pulses from an oscillator by mode locking or some other method. Xenon does not however, have the properties of an efficient amplifier medium, because of its high stimulated emission cross section ($\sim 10^{-17} \text{ cm}^2$) and low storage time ($\sim 10^{-8}$ ns). The oscillator pulse would have to be synchronised with the gain of the amplifier, so that the pulse arrived when the inversion was at its maximum. When a short pulse is amplified, only the energy stored in the period of approximately 10 ns before the passage of the pulse will be used in amplification and so in this case it would not be

efficient to use long pulse electron beams for amplifier excitation. To date a method for mode locking the laser has not been found. Work is being carried out however, to obtain mode locked pulses at the xenon laser wavelength from the fourth harmonic of a mode locked ruby laser (103). This is generated by a 4 wave parametric process where two fundamental photons are added to a second harmonic photon in phase-matched magnesium vapour. These pulses may then be amplified and this should provide information on the vibrational relaxation times of the excited molecules.

Before any large amplifier system can be designed, it will be necessary to determine a number of important parameters in both the gas and the optical materials. At the xenon wavelength, most transmitting materials absorb a few per cent of the radiation so that at high energy densities the mirror and window materials may be damaged. Two photon absorption from valence to conduction bands may also occur in the optical materials so that a knowledge of two photon cross sections is necessary. The fluxes should be less than the damage limits of the materials. To reduce the fluxes the beam would have to be expanded and thus it would be necessary to uniformly pump large volumes of high pressure xenon, as any non-uniformity in pumping would degrade the beam quality of the laser output. To obtain uniform pumping of large volumes it may be necessary to use lower pressures of gas together with very high energy electrons. The coaxial electron beam diode which has been described, will be important in such amplifiers as it effectively irradiates the gas from all sides. It is possible to build much longer diodes than those used in the construction of the oscillator; a 50 cm long diode has been designed to operate with a Febetron 705 electron beam generator. In order to make a long diode, the impedance of the excitation source should be low as the diode impedance is inversely proportional to the length of the diode.

The successful operation of the xenon laser has shown the feasibility

of using molecular transitions from stable states to dissociative levels and the possibility of direct pumping using relativistic electrons. Effort is now being concentrated on the search for dissociative transitions which will lead to efficient laser action in the visible region. The coaxial beam diode will probably become a widely used excitation source in the search for these new media, since although direct electron beam pumping is theoretically less efficient than sustained discharges (109) it will probably continue to be widely used in pumping high pressure gases, as discharges have not been successfully used for excitation of lasers which involve electronic transitions.

ACKNOWLEDGEMENTS

I wish to thank my supervisor Professor D. J. Bradley for his encouragement and guidance during the past three years.

I also want to acknowledge the help of Drs. H. H. R. Hutchinson and H. W. McGeogh for their helpful advice in many aspects of this work and Dr. E. G. Arthurs and Mr. G. R. Fournier for many useful discussions.

I must thank Mr. A. Johnston and the other members of the workshop staff for their assistance in constructing much of the apparatus used in this research.

I wish to thank my wife for her encouragement and help in the preparation of this thesis and my mother for her skill and care in typing the thesis.

This work was supported by a post graduate studentship from the Department of Education, N. Ireland.

REFERENCES

1. HOUTERMANS F. G., *Helvetica Physica Acta.*, 33, 933 (1960).
2. BASOV N. G., *IEEE Journal of Quantum Electronics*, QE-2, 354 (1966).
3. MULLIKEN R. S., *Journal of Chemical Physics*, 52, 5170 (1970).
4. TANAKA Y. and ZELIKOFF H., *Journal of the Optical Society of America*, 44, 254 (1954).
5. SCHANLOW A. L. and TOWNES C. H., *Physical Review*, 112, 1940 (1958).
6. BASOV N. G., DANILYCHEV V. A., POPOV Yu. M. and KHODKEVICH D. D., *J.E.T.P. Letters*, 12, 329 (1970).
7. KOEHLER H. A., FERDERBER L. J., REDHEAD D. L., and EBERT P. J., *Applied Physics Letters*, 21, 198 (1972).
8. HOFF P. W., SWINGLE J. C. and RHODES C. K., *Applied Physics Letters*, 23, 245 (1973).
9. HUGHES W. M., SHANNON J. and HUNTER R., *Applied Physics Letters*, 24, 488 (1974).
10. JOHNSON A. W. and GERARDO J. B., *Journal of Applied Physics*, 45, 867 (1974).
11. WILKINSON P. G. and TANAKA Y., *Journal of the Optical Society of America*, 45, 344 (1955).
12. TANAKA Y., *Journal of the Optical Society of America*, 45, 710 (1955).
13. TANAKA Y., JURSA A.S. and LeBLANC F. J., *Journal of the Optical Society of America*, 47, 105 (1957).
14. ANDERSON D. K., *Physical Review*, 137A, 21 (1965).
15. HUFFMAN R. E., LARABEE J. C. and TANAKA Y., *Applied Optics*, 4, 1581 (1965).
16. HERZBERG G., 'Spectra of Diatomic Molecules' published by D. van Nostrand Company Inc. (1950).
17. TIMPSON P. R. and ANDERSON J. M., *Canadian Journal of Physics*, 48, 1817 (1970).
18. GEDANKEN A., JORTNER J., RAZ B. and SZOKE A., *Journal of Chemical Physics*, 57, 3456 (1972).
19. SPENCER L. V., National Bureau of Standards, Monograph 1.
20. PLATZMANN R. L., *International Journal of Applied Radiation and Isotopes*, 10, 116 (1961).
21. PETERSON L. R. and ALLEN J. E., *Journal of Chemical Physics*, 56, 6068 (1972).
22. SMITH D., DEAN A. G. and PLUMB I. C., *Journal of Physics*, B5, 2134 (1972).

23. BATES D. R., Physical Review, 78, 492 (1950).
24. LENNON J. J. and SEXTON M. C., Journal of Electronics and Control, 1, 123 (1959).
25. OSKAM H. J. and MITTLESTADT V. R., Physical Review, 132, 1445 (1963).
26. BARDSLEY J. F. and BIONDI M. A., 'Advances in Atomic and Molecular Physics', Volume 6, published by Academic Press, New York, (1970).
27. MEHR F. J. and BIONDI M. A., Physical Review, 176, 322 (1968).
28. LORENTS D. C. and OLSEN R. E., Stanford Research Institute Technical Report 1 (1972).
29. DAVIDENKO V. A., DOLGOSHEIN B. A., SOMOV S. V., STAROSEL'TSEV V. N., Soviet Physics J.E.T.P., 30, 49 (1970).
30. FROMMHOLD L. and BIONDI M. A., Physical Review, 185, 244 (1969).
31. ALLEN L., JONES D. G. C. and SCHOFIELD D. G., The Journal of the Optical Society of America, 59, 842 (1969).
32. VEROLAINEN Ya. F. and OSHEROVICH A. L., Optics and Spectroscopy, 27, 14 (1969).
33. PHELPS A. V., Physical Review, 114, 1011 (1959).
34. GEORGE E. V. and RHODES C. K., Applied Physics Letters, 23, 139 (1973).
35. FOURNIER G. R., Optics Communications, 13, 385 (1975).
36. HORNBECK J. A. and MOLNAR J. P., Physical Review, 84, 621 (1973).
37. BRADLEY D. J., HUTCHINSON M. H. R. and KOETSER H., Optics Communications, 7, 187 (1973).
38. WALLACE S. C., HODGSON R. T. and DREYFUS R. W., Applied Physics Letters, 23, 22 (1973).
39. KOEHLER H. A., FERDERBER L. J., REDHEAD D. L. and EBERT P. J., Physical Review, A9, 768 (1973).
40. KETO J. W., GLEASON Jr. R. E. and WALTERS G. K., Physical Review Letters, 33, 1365 (1974).
41. FREEMAN C. J., McEWAN H. J., CLARIDGE R. F. and PHILLIPS L. F., Chemical Physics Letters, 10, 350 (1971).
42. BOUCIQUE R. and MORTIER P., Journal of Physics, D5, 1905 (1970).
43. FINK E. H. and COMES F. J., Chemical Physics Letters, 30, 267 (1975).
44. BRADLEY D. J., HULL D. R., HUTCHINSON M. H. R. and McGEOGH M. W., Optics Communications, 14, 1 (1975).
45. FIELD EMISSION CORPORATION, McMinnville, Oregon.
46. BLUMLEIN A. D., Patent Application 589127 (October 1941).
47. MARTIN J. C., A.W.R.E. Report (1970).

48. HEATH D. F. and SACHER P. A., Applied Optics, 5, 937 (1966).
49. 'HARSHAW OPTICAL CRYSTALS', published by Harshaw Chemical Co. (1967).
50. HOLSTEIN T., Physical Review, 83, 1159 (1951).
51. BROCKLEHURST B., Radiation Research Review, 1, 223 (1968).
52. DOLGOSHEIN B. A., LEBEDENKO V. N., ROGOZHIN A. M., RODIONOV B. V. and SHUVALOVA E. N., Soviet Physics, J.E.T.P., 29, 619 (1969).
53. JOHNSON A. W. and GERARDO J. B., Journal of Chemical Physics, 59, 1738 (1973).
54. LORENTS D. C., ECKSTROM D. J. and HUESTIS D. L., Stanford Research Institute Report (1973).
55. WERNER C. W., GEORGE E. V., HOFF P. W. and RHODES C. K., Applied Physics Letters, 25, 235 (1974).
56. GERARDO J. B. and JOHNSON A. W., Applied Physics Letters, 26, 582 (1975).
57. BURTON W. H., HATTER A. T. and RIDGELEY A., Applied Optics, 12, 1851 (1973).
58. FOWLER W. K., RENSE W. A. and SIMMONS R., Applied Optics, 4, 1596 (1965).
59. LAGARDE F. and NOVARO M., L'Onde Électrique, 54, 463 (1974).
60. GERARDO J. B. and JOHNSON A. W., IEEE Journal of Quantum Electronics, QE9, 748 (1973).
61. MIES F. H., Molecular Physics, 26, 1233 (1973).
62. 'ATOMIC AND MOLECULAR PROCESSES', Edited by D. R. Bates, published by Academic Press (1972).
63. OLSEN C. L., Physics of Fluids, 16, 529 (1973).
64. GOODMAN H. J., A.W.R.E. Report (1968).
65. LORRAIN P. and CORSON D. R., 'Electromagnetic Fields and Waves', published by W. H. Freeman and Co. (1970).
66. MILLER P. A. and GERARDO J. B., Journal of Applied Physics, 43, 3008 (1972).
67. U.K. Patent Application No. 14102 (1974).
68. HENLEY E. and RICHMAN D., Analytical Chemistry, 28, 1850 (1956).
69. LANGMUIR I. and COMPTON K. T., Review of Modern Physics, 3, 191 (1931).
70. LANGMUIR I. and BLODGETT K. B., Physical Review, 22, 347 (1923).
71. BURCHAM W. E., 'Nuclear Physics', published by Longmans (1970).
72. SPITZER L., 'Physics of Fully Ionized Gases', published by Wiley, New York (1967).

73. WATANABE E., *Advances in Geophysics*, 5, 153 (1958).
74. FISHER G. B., SPICER W. E., MCKERNAN P. C., PERESKOK V. F., and WANNER S. J., *Applied Optics*, 12, 799 (1973).
75. MCGEOGH M. W., Private Communication.
76. WALLACE S. C., HODGSON R. T. and DREYFUS R. W., *Applied Physics Letters*, 23, 672 (1973).
77. GERARDO J. B. and JOHNSON A. W., *Physical Review*, A10, 1204 (1974).
78. YARIV A., 'Quantum Electronics', Published by John Wiley and Sons (1975).
79. TABOR D., 'Gases, Liquids and Solids', published by Penguin (1969).
80. 'HANDBOOK OF CHEMISTRY AND PHYSICS', Chemical Rubber Publishing Co.
81. EMMONS D. A., *Optics Communications*, 11, 257 (1974).
82. KOSINKAYA I. V. and POLOZOVA L. P., *Optics and Spectroscopy (USSR)*, 30, 458 (1971).
83. HUGHES W. H., SHANNON J., KOLB A., AULT E. and BHANMIK M., *Applied Physics Letters*, 23, 385 (1973).
84. HUNTER R. O., SHANNON J. and HUGHES W., Maxwell Laboratories Inc., Report MLR-378 (1975).
85. BRADLEY D. J., HULL D. R., HUTCHINSON M. H. R. and MCGEOGH M. W., *Optics Communications*, 11, 335 (1974).
86. JOHNSON A. W. and GERARDO J. B., *Journal of Applied Physics*, 45, 867 (1974).
87. FOURNIER G. R., Private Communication.
88. SAMSON J. A. R., 'Techniques of Vacuum Ultraviolet Spectroscopy', published by John Wiley (1965).
89. WATTS J. K., *Applied Optics* 7, 1621 (1968).
90. BORN M. and WOLFF E., 'Principles of Optics', published by The Macmillan Co. (1964).
91. KRIUKOV P. G. and LETOKHOV V. S., 'Laser Handbook', Vol. 1, North Holland Publishing Co. (1972).
92. KOPP I., LINDGREN R. and RYDA B., 'Tables Internationales de Constants', Paris.
93. SOROKIN P. P. and LANKARD J. R., *I.B.M. Journal of Research and Development* 11, 148 (1967).
94. SOFFER B. H. and MCFARLAND B. B., *Applied Physics Letters*, 10, 226 (1967)
95. BRADLEY D. J., DURRANT A. J. F., GALE G. M., MOORE M. and SMITH P. D., *IEEE Journal of Quantum Electronics*, QE4, 707 (1968).
96. BRADLEY D. J., GALE G. M., MOORE M. and SMITH P. D., *Physics Letters*, 26A, 378 (1968).

97. STROME Jr. F. C. and WEBB J. P., Applied Optics, 10, 1348 (1971).
98. SCHAFER F. P. and HULLER H. Optics Communications, 2, 407 (1971).
99. GARTON W. R. S. 'Advances in Atomic and Molecular Physics' (1966).
100. BJORKHOLM J. E., DAMEN F. C. and SHAH J., Optics Communications, 4, 283 (1971).
101. GALE G. M., PhD. Thesis, The Queen's University of Belfast (1971).
102. ARTHURS E. G., PhD. Thesis, The Queen's University of Belfast (1972).
103. SCHAFER F. P., 'Laser Handbook', Vol. 1, North Holland Publishing Co. (1972).
104. WALLACE S. C. and DREYFUS R. W., Applied Physics Letters, 25, 498 (1974).
105. JENKINS F. A. and WHITE H. E., 'Fundamentals of Optics', published by McGraw Hill Book Co. Inc. (1957).
106. BRADLEY D. J., EWART P., NICHOLAS J. V. and SHAW J. R. D., Journal of Physics, B6, 1594 (1973).
107. MUCKOLLS J., WOOD L., THIESSEN A. and ZIMMERMAN G., Nature, 239, 139 (1972).
108. ARTHURS E. G., BRADLEY D. J., EDWARDS C. B., HULL D. R., HUTCHINSON M. H. R. and LING C. C., Paper presented at 2nd National Quantum Electronics Conference, St. Catherines College, Oxford (1975).
109. BASOV N. G., DANILYCHEV V. A., DOLGIKH V. A., KERIMOV O. H., LOBANOV A. H., PODSOSONNYI A. S. and SUCHKOV A. F., Soviet Journal of Quantum Electronics 5, 13 (1975).

MEGAWATT VUV XENON LASER EMPLOYING COAXIAL ELECTRON-BEAM EXCITATION

D.J. BRADLEY, D.R. HULL, M.H.R. HUTCHINSON and M.W. McGEACH

*Optics Section, Physics Department, Imperial College,
London SW7 2BZ, UK*

Received 11 June 1974

3 nsec laser pulses, of bandwidth 1.3 nm, are obtained from a 10 J, 600 keV coaxial diode electron-beam pumping arrangement. Uniform pumping, with a well defined cylindrical geometry, facilitates experimental investigation of the laser parameters. Gas heating limits the laser repetition rate. While mirror damage at present limits the peak power to ~ 1 MW, higher powers seem available. The addition of helium results in a drastic reduction of peak molecular xenon fluorescence.

To date quasi-molecular vacuum ultraviolet lasers have employed transverse pumping of high-pressure xenon [1-5], krypton [6], argon [7] or noble gas mixture [6,8] by relativistic electron beams. Apart from the work described in [5], the electron-beam sources employed for laser pumping delivered several hundreds of joules in pulses of duration ~ 50 nsec, or longer. With such long pulse excitation premature termination of laser action occurs [2,3] and the overall laser efficiency is $\ll 1\%$ despite a potential fluorescence efficiency of ~ 10% [1,9]. To obtain an efficient and convenient laser system with short duration, low energy pumping and capable of peak powers exceeding 1 MW, we have designed and constructed a coaxial diode, electron-beam arrangement. Also with uniform pumping of a well-defined cylindrical geometry, investigations of the laser parameters are more easily carried out than in the case of transverse pumping systems. In particular, because the pumping pulse duration (2.5 nsec) is shorter than the fluorescence lifetime of the xenon molecular dimer, at the gas pressures employed [9], laser and fluorescence kinetics can be studied.

The experimental arrangement is shown in fig. 1. The coaxial field emission diode consists of a thin-walled (~ 70 μm) stainless steel tubular anode, of ~ 4 mm internal diameter, maintained at earth poten-

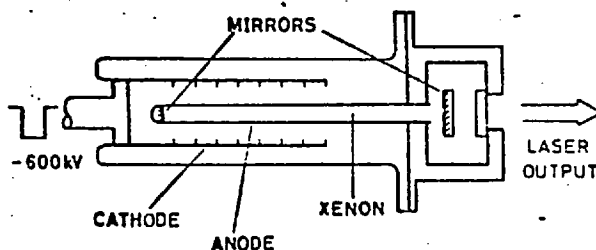


Fig. 1. Details of coaxial diode construction.

tial. The anode, which is also the container for the high pressure laser gas, is concentric with a cylindrical field emission cathode. 10 J, 600 keV, 2.5 nsec pulses are produced by a Marx bank and Blumlein switch circuit. Both electrodes are contained in a glass envelope, which is evacuated by continuous pumping to a pressure of $\sim 2 \times 10^{-5}$ torr. One laser mirror is sealed into the unsupported end of the anode tube and the output mirror, on a kinematic mount, is supported inside the xenon reservoir. The output beam is transmitted through a BaF_2 window into a vacuum for intensity and spectral measurements.

The diode was designed for use with a Febetron 706 pulse generator (Field Emission Corp) which has a load impedance of 60 Ω (10 kA, 600 kV). The tube radius is determined by the range of the electrons and hence by the gas pressure. For 600 keV electrons at

10 ktorr, a tube of ~ 4 mm diameter gives uniform pumping. The cathode which has a diameter of ~ 3 cm and a length of 7 cm, was constructed from titanium sheet, perforated to produce an array of spikes. The distribution of pumping energy over the inner surface of the anode tube was measured using cellophane dye dosimetry [10]. The microdensitometer trace of fig. 2 shows a variation of less than 10% in dose along the tube. Because of end effects, the pumped length exceeds the physical length of the cathode. The energy entering the gas was measured calorimetrically with a thermopile and found to be ~ 5 J.

The anode tube was evacuated to 10^{-4} torr by a mercury diffusion pump. Liquid-nitrogen cold traps were used on both the diffusion pump and the rotary backing pump. The xenon (B.O.C. Research Grade) was frozen in a high-pressure bomb by liquid nitrogen and pumped to $< 10^{-4}$ torr to ensure that impurity concentrations were < 1 ppm. The bomb temperature was maintained $< 0^\circ\text{C}$ while the tube was filled to the working pressure of 10 ktorr. This helped to reduce the water vapour partial pressure. With these procedures stimulated emission intensity measurements could be reproduced to $\pm 5\%$ and laser output was maximum.

Two combinations of mirrors were employed in the optical cavity. Megawatt powers were obtained with a spherical mirror of one metre radius of curvature and a plane mirror with a 1.4 mm diameter hole for output coupling. Both mirrors had Al:MgF₂ maximum reflectivity coatings. Better results were obtained with two plane mirrors, one of which had a transmission of $\sim 8\%$. In both cases the mirror separation was 22.5 cm. Mirror damage at present limits the peak power to ~ 1 MW. By employing multilayer dielectric mirror coatings [11] or prisms, higher working powers should be possible.

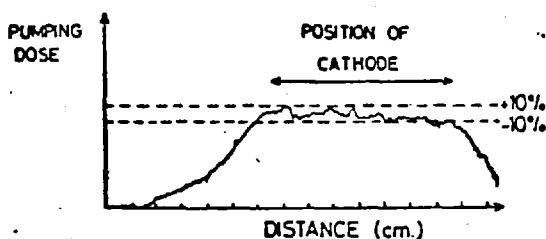


Fig. 2. Microdensitometer trace of cellophane recording of electron energy deposition, showing uniformity along anode.

The laser spectrum was recorded in a 1 metre normal incidence vacuum spectrograph, with a 600 lines/mm grating. The microdensitometer traces of fig. 3 clearly show the considerable spectral narrowing produced by the mirrors. The laser linewidth is $\sim 13 \text{ \AA}$ when account is taken of the absorption lines on either side of the peak. The full height of the spectro-

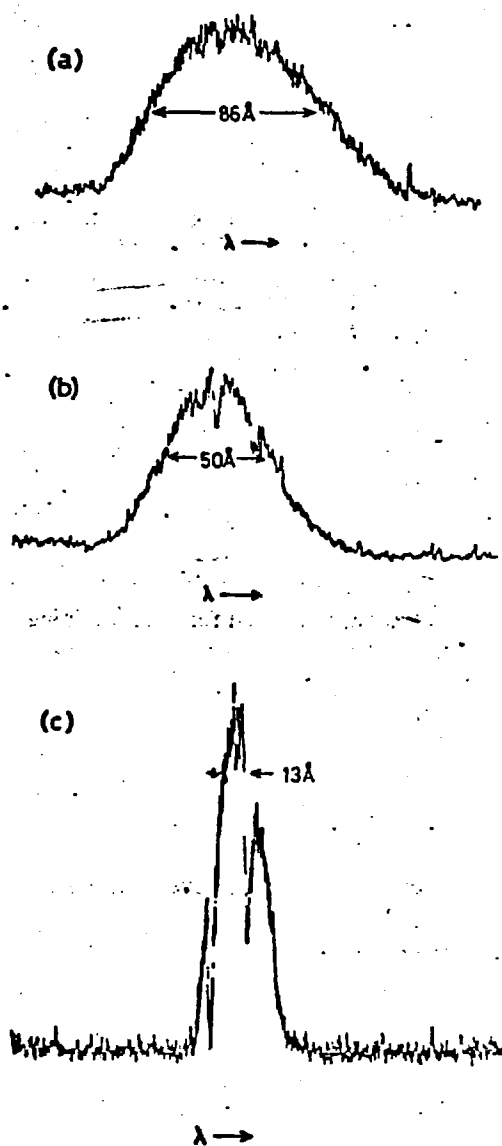


Fig. 3. Microdensitometer traces of spectra (1 metre normal incidence spectrograph) recorded with (a) no mirrors, (b) single high reflectivity plane mirror (double transit), and (c) 1 metre radius of curvature mirror and output plane mirror with 1.4 mm diameter coupling aperture (both mirrors high reflectivity). Spectral resolution of (c) is $< 1 \text{ \AA}$.

graph slit is illuminated when only one mirror is employed or when the output mirror of the laser resonator is misaligned but only a 1 mm length of the slit (placed 35 cm from the output mirror) is illuminated by the laser beam. The beam cross section was recorded on SC7 film (Kodak--Pathe) at a distance of 1 metre. With the hole-coupled resonator an annular beam of 6 mm diameter was obtained, corresponding to a beam divergence of ~ 5 mrad. As expected, a circular beam of slightly better divergence was produced with the semi-transparent mirror.

Pulse duration and output power were measured using a solar-blind ITT FW 4115 photodiode and a Tektronix 519 oscilloscope. A typical oscillogram obtained at a xenon gas pressure of 10 ktorr is shown in fig. 4. The pulse duration is 3.5 nsec. At this pressure the fluorescence lifetime is ~ 7 nsec [9]. Output powers in excess of 1 MW were measured using the manufacturer's calibration of the diode, assuming that the quantum efficiency is constant at wavelengths shorter than 230 nm. These powers corresponded with the output energies obtained from a thermopile (Laser Instrumentation Ltd) enclosed in a vacuum chamber. To eliminate errors arising from electrical noise, the thermopile readings were compared with those recorded when the vacuum chamber was at atmospheric pressure. To prevent saturation of the photodiode, the laser radiation was attenuated by a known pressure of oxygen contained in a 14 cm long cell. Since at megawatt powers saturation is beginning to occur and could influence the observed laser intensity profile, we confirmed that the oscillograms did not change in shape with a variation of $\times 10$ in laser power.

To maintain high laser powers it was necessary to allow ~ 20 minutes to elapse between firings. We have investigated possible reasons for this effect. Fig.

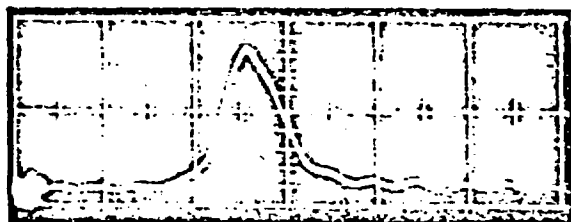


Fig. 4. Oscillogram of laser output. Time-scale 5 nsec per major division.

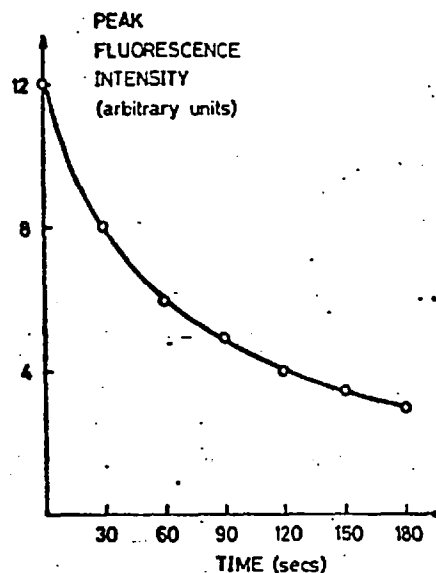


Fig. 5. Variation of fluorescence intensity from coaxially excited xenon at 6 ktorr pressure. Points on graph represent consecutive firings of the electron beam source.

5 shows how the fluorescence intensity changes with repetitive pumping at the maximum rate (permitted by the power supply) of 2 pulses per minute. If the delay between the first and second firings was increased to 5 minutes, the intensity reduction was $\sim 10\%$. We have calculated that the instantaneous rise in temperature of the xenon is $\sim 700^\circ\text{C}$ and that the steel tube temperature increases by $\sim 30^\circ\text{C}$ after thermalization with the xenon gas which occurs after a few seconds. Absorption by unbound ground-state xenon molecules increases rapidly with increasing temperature [12], and consequently gas heating would be expected to strongly affect both fluorescence and laser intensities. The thermal time constant of the anode tube is estimated to be ~ 10 minutes, which would explain the long recovery time of the laser.

An increase in xenon fluorescence efficiency by the addition of helium was attributed to cooling effects, by the authors of [8]. However, adding partial pressures of 4 ktorr and 8 ktorr of helium (B.O.C. Research Grade) to 5 ktorr of xenon in our system, resulted in both cases in a reduction of peak fluorescence by an order of magnitude. Since the results quoted in [8] were obtained with a Febetron 705 which produces a 50 nsec pulse, we repeated our measurements with the same type of electron beam source. In this case,

with partial pressures of 5 ktorr xenon and 4 ktorr helium, and increase of $\sim 10\%$ in fluorescence was recorded, in agreement with [8]. We are investigating further the role of helium.

Finally, we measured the amplified spontaneous emission when the high reflectivity mirror at the end of the coaxial anode tube was covered and the output mirror was removed. By comparing this intensity with that produced with one mirror we obtained a value of $\sim 0.25 \text{ cm}^{-1}$ for the net gain. The spectral narrowing would indicate a gain coefficient of $\sim 0.7 \text{ cm}^{-1}$, if absorption is ignored.

With its low pumping threshold, this coaxial electron-beam design provides in a compact form a high power VUV laser. The gain is sufficient to allow prism tuning and by employing other gases convenient tunable lasers covering the near VUV spectral region should be possible. Because of its well defined geometry the system has advantages for studying kinetics, and the atomic and molecular processes involved in quasi-molecular dissociative ground-state lasers.

Financial support from the Science Research Council and UK AEA Culham Laboratory is also acknowledged.

References

- [1] H.A. Koehler, L.J. Ferderber, R.L. Redhead and P.J. Ebert, *Appl. Phys. Letters* 21 (1972) 198.
- [2] W.M. Hughes, J. Shannon, A. Kolb, E. Ault and M. Bhaumik, *Appl. Phys. Letters* 23 (1973) 385.
- [3] J.B. Gerardo and A. Wayne Johnson, *IEEE J. Quantum Electron.* QE-9 (1973) 748.
- [4] P.W. Hoff, J.C. Swingle and C.K. Rhodes, *Opt. Commun.* 8 (1973) 128.
- [5] S.C. Wallace, R.T. Hodgson and R.W. Dreyfus, *Appl. Phys. Letters* 23 (1973) 672.
- [6] P.W. Hoff, J.C. Swingle and C.K. Rhodes, *Appl. Phys. Letters* 23 (1973) 245.
- [7] W.M. Hughes, J. Shannon and R. Hunter, *Appl. Phys. Letters* 24 (1974) 488.
- [8] A. Wayne Johnson and J.B. Gerardo, *J. Appl. Phys.* 45 (1974) 867.
- [9] D.J. Bradley, M.H.R. Hutchinson and H. Koetser, *Opt. Commun.* 7 (1973) 187.
- [10] E.J. Henley and D. Richman, *Analytical Chemistry* 28 (1956) 1850.
- [11] A. Malherbe, *Applied Optics* 13 (1974) 1276.
- [12] L.V. Kosinskaya and L.P. Polozova, *Opt. Spectrosc. (USSR)* 30 (1971) 458.

CO-AXIALLY PUMPED, NARROW BAND, CONTINUOUSLY TUNABLE, HIGH POWER VUV XENON LASER

D.J. BRADLEY, D.R. HULL, M.H.R. HUTCHINSON and M.W. McGEOCH

Optics Section, Physics Department, Imperial College, London SW7 2BZ, UK

Received 4 February 1975

High efficiency spectral narrowing to 0.13 nm and frequency tuning from 169 nm to 176 nm has been produced with a new design of coaxial-pumped xenon laser employing a single intra-cavity prism. The laser peak power is 3 MW (9 mJ) and becomes 0.7 MW (power density 10 MW cm^{-2}) when frequency narrowed.

We recently reported the achievement of megawatt power from a high-pressure VUV xenon gas laser pumped by a 10 J pulse of 500 keV electrons in a new coaxial-diode arrangement [1]. It was pointed out that in this system the laser gain was sufficient to allow intra-cavity prism tuning. We now wish to report efficient spectral narrowing to a bandwidth of 0.13 nm and continuous tuning from 169 nm to 176 nm, with an increased overall efficiency. To produce this first narrow-band tunable VUV laser it was necessary to redesign the laser diode and the associated high-voltage power supply.

The coaxial diode arrangement is shown in fig. 1. Compared with the first design [1], both ends of the thin-walled stainless steel tubular anode open into high-pressure chambers which contain the laser optical elements. The concentric cathode was extended to a length of 10 cm with an internal diameter of 3.5 cm. The Blumlein circuit of the Febetron 706 pulse generator was modified to produce a 5 ns pulse of 500 kV electrons. When the anode and the end chambers were filled with xenon at a pressure of 10 ktorr uniform pumping was obtained over a 14 cm length. Calorimeter measurements showed that a total energy of 10 J was transmitted through the $70 \mu\text{m}$ thick anode walls corresponding to the deposition of 5.5 J/cm^3 . (Anode internal diameter was 4 mm.) A minimum interval of 15 minutes between shots was necessary to allow the gas to cool to room temperature. The procedures for purifying the gas and filling the system were the same

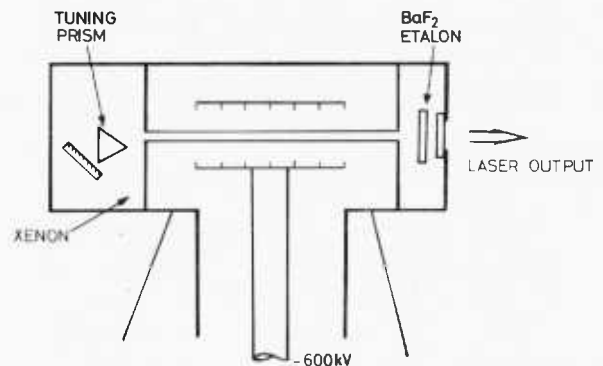


Fig. 1. Coaxial diode with tuning elements.

as reported in ref. [1].

The laser resonator reflectors consisted of an Al: MgF_2 coated plane mirror* with $\sim 85\%$ reflectors and a BaF_2 single-plate resonant-reflector with an effective reflectivity of $\sim 20\%$. The optical cavity length was 25 cm. When these two reflectors only were employed an output laser energy of 9 mJ in a 3 ns pulse was obtained, corresponding to a peak power of 3 MW and an efficiency of $\sim 0.1\%$. The pulse duration was measured with a solar-blind ITT FW4115 photodiode and a Tektronix 519 oscilloscope and the pulse energy with an evacuated thermopile (Laser Instrumentation Ltd). The measurements were reproducible to 10%

* Supplied by Matra Seavom.



Fig. 2. Output spectra of VUV xenon laser showing frequency narrowing and tuning. The spectrograph plate was moved vertically between recordings and the tuning prism rotated.

over many shots showing the excellent reliability of the laser. At these high output powers the surface of the BaF_2 etalon suffered damage but the Al:MgF_2 mirror appeared to be unaffected. (In the first coaxial laser the high reflectivity Al:MgF_2 mirror was damaged at a peak power of ~ 1 MW. The use of a low reflectivity resonant reflector for output coupling reduced the peak power inside the cavity). Beam divergence was determined from burn patterns on exposed SC7 (Kodak-Pathe) film. A half-angle divergence of ~ 1 mrad was calculated. The amplified spontaneous emission was measured when the resonant reflector was removed. By comparing the intensities when the high reflectivity mirror was aligned and misaligned, respectively, a value of $0.25 \pm 0.02 \text{ cm}^{-1}$ was obtained for the net gain, in good agreement with the measurements reported in ref. [1]. In the coaxial system of (1) ~ 5 J of pumping energy was deposited in 2.5 ns in an anode length of ~ 8 cm, so the pumping energy density was practically the same in both cases. The increase in laser output energy from 3 mJ to 9 mJ, corresponding to an increase in efficiency of 50%, then arises mainly from the increased length of the active medium and the doubling of the electron-beam pulse duration to 5 ns.

With this increase in total gain considerable frequency-narrowing would be expected. A fused quartz prism (Spectrasil B) was employed as the intra-cavity dispersing element. At the operating wavelength of the xenon laser (~ 172 nm) the angular dispersion of a prism is comparable to that of a grating of the same area [2]. Also a prism is less susceptible to damage and has smaller losses. The 60° prism (dispersion $\sim 3 \times 10^{-3} \text{ nm}^{-1}$) was mounted with the Al:MgF_2 mirror on a common base on a rotating table. The prism edge was adjusted parallel to the mirror surface and the axis of rotation was in the same direction. Alignment was carried out with a He-He laser at 632.8 nm and the table was rotated through the calculated angle necessary to produce a resonator operating at the VUV wavelength with the same output reflector. Rotation of the prism was obtained by a drive operated through a seal capable of operating under both high pressure and vacuum conditions.

The laser spectra were recorded on SC7 film in a 1 metre normal incidence vacuum spectrograph. Fig. 2 shows 3 typical spectra at 170.0, 172.3 and 174.1 nm. Microdensitometer measurements (fig. 3) showed a

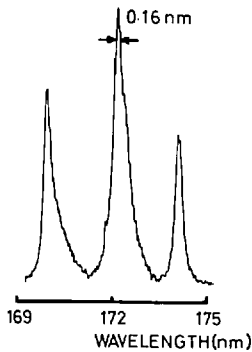


Fig. 3. Microdensitometer trace of spectra of fig. 2 showing a recorded linewidth of 0.16 nm. After allowing for the spectrograph resolution a laser linewidth of 0.13 nm is calculated.

recorded bandwidth of 0.16 nm. Deconvolving the instrumental resolution of 0.08 nm gave a laser bandwidth of 0.13 nm. There is thus a spectral narrowing by a factor of 100 from the ~ 15 nm fluorescence bandwidth [3] and by a factor of 10 from the untuned laser bandwidths of 1.3 nm [1].

The complete tuning range is shown in fig. 4. The wavelength scale was calibrated employing the 184.9 nm line of Hg I and the known dispersion of the spectrograph. The laser energy at each of the marked points on the curve was measured with the thermopile. Each point is an average of 3 shots and the variation between shots was $\sim 10\%$. The peak power, at the centre of the tuning range, was 0.7 MW giving an output power density of 10 MW cm^{-2} . The tuning range was also confirmed by photographing the spectra. It was possible to tune continuously over the entire range of 7.3 nm from 169.2 nm to 176.5 nm. No damage to the laser components was observed after more than 100 shots.

This high-efficiency spectral narrowing and wide tuning range was only achieved when near grazing incidence reflection at the inner walls of the anode was eliminated by inserting a wire spiral of the same diameter as the tube. The grazing incidence reflectivity of metals is high and wall reflection will increase the beam divergence and prevent frequency narrowing by the prism. When the spiral was removed the laser bandwidth broadened to 1.3 nm and it was only possible to tune over ~ 2 nm centred at 172 nm.

Prism tuning of a low power-density (10 kW cm^{-2}), transversely pumped xenon laser over a range of 5 nm has recently been reported [4]. However, the laser

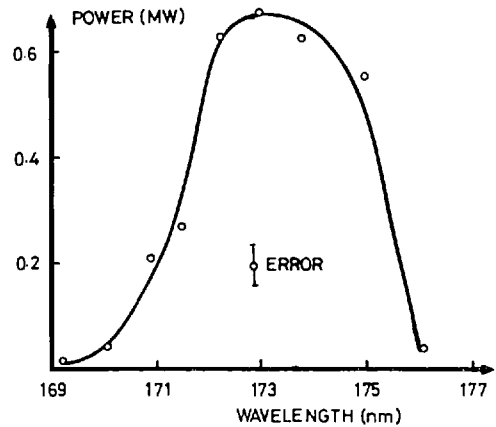


Fig. 4. Tuning efficiency curve of xenon laser.

bandwidth of 1 nm was only a factor of X 2 narrower than that produced by the untuned laser and the overall efficiency of the laser was low.

The peak power of the coaxial xenon laser is comparable to that obtained from high-power flashlamp pumped dye-lasers [5] while the tuning range ($>2500 \text{ cm}^{-1}$) is considerably greater. There seems no reason to prevent narrower bandwidths being achieved with multiple-prism arrangements. It is likely that these new tunable-frequency VUV lasers will play a revolutionary role in VUV spectroscopy and photochemistry similar to that which dye lasers are now playing at longer wavelengths, particularly if frequency narrowing and tuning is obtained with krypton [6] and argon [7] operating at even shorter wavelengths.

We are pleased to acknowledge the skilled technical assistance of Mr. A. Johnson in the construction of the laser cavity.

References

- [1] D.J. Bradley, D.R. Hull, M.H.R. Hutchinson and M.W. McGeoch, *Opt. Commun.* 11 (1974) 335 (UK Patent Application No. 14102/74).
- [2] P. Jacquinot, *J. Opt. Soc. Amer.* 44 (1954) 761.
- [3] D.J. Bradley, M.H.R. Hutchinson and H. Koetser, *Opt. Commun.* 7 (1963) 187.
- [4] S.C. Wallace and R.W. Dreyfus, *Appl. Phys. Lett.* 25 (1974) 498.
- [5] D.J. Bradley, W.G.I. Caughey and J.I. Vukusic, *Opt. Commun.* 4 (1971) 150.
- [6] P.W. Hoff, J.C. Swingle and C.K. Rhodes, *Appl. Phys. Lett.* 23 (1973) 246.
- [7] W.M. Hughes, J. Shannon and R. Hunter, *Appl. Phys. Lett.* 24 (1974) 488.